Fluid-dynamic description of heavy quarks in the quark-gluon plasma

Doctoral Dissertation
Heidelberg University

Doctoral Candidate: Federica Capellino

PhD Advisor: Prof. Dr. Silvia Masciocchi

Dissertation
submitted to the
Combined Faculty of Mathematics, Engineering and Natural Sciences
of Heidelberg University, Germany
for the degree of
Doctor of Natural Sciences

Put forward by
Federica Capellino
born in Savigliano
Oral examination: 22.05.2024

Fluid-dynamic description of heavy quarks in the quark-gluon plasma

Referees:

Prof. Dr. Silvia Masciocchi

Prof. Dr. Carlo Ewerz

Abstract

Heavy quarks (i.e. charm and beauty) are powerful tools to characterize the quark-gluon plasma (QGP) produced in heavy-ion collisions. Although they are initially produced out of kinetic equilibrium via hard partonic scattering processes, recent measurements of anisotropic flow of charmed hadrons pose the question regarding the possible thermalization of heavy quarks in the medium. In this work, we provide new insights into the level of thermalization of charm and beauty quarks in the QGP. In particular, exploiting a mapping between transport theory and fluid dynamics, we show how a fluid-dynamic description of charm diffusion in the QCD plasma is feasible. Inspired by recent Lattice-QCD calculations, we show that fluid dynamics seems to be applicable also for beauty quarks in the latest stages of the expanding QGP. We present results for transverse momentum distribution and integrated yields of charmed hadrons in central Pb–Pb collisions at $\sqrt{s_{\mathrm{NN}}}$ = 5.02 TeV at the LHC obtained with a fluid-dynamic code coupled with the conservation of a heavy-quark – antiquark current in the QGP. Our calculations are in agreement with the available experimental measurements in the low transverse momentum region, indicating an effective hydrodynamization of charm quarks in the QGP.

Zusammenfassung

Schwere Quarks (d. h. Charm und Beauty) sind mächtige Werkzeuge zur Charakterisierung des Quark-Gluon-Plasmas (QGP), das bei Kollisionen von schweren Ionen erzeugt wird. Obwohl sie anfangs in harten partonischen Streuprozessen außerhalb des kinetischen Gleichgewichts erzeugt werden, werfen aktuelle Messungen des anisotropen Flusses von Charm-Hadronen die Frage nach der möglichen Thermalisierung von schweren Quarks im Medium auf. In dieser Arbeit liefern wir neue Einblicke in das Level der Thermalisierung von Charm- und Beauty-Quarks im QGP. Insbesondere zeigen wir anhand eines Zusammenhangs zwischen Transporttheorie und Fluiddynamik, wie eine fluiddynamische Beschreibung der Charm-Diffusion im QCD-Plasma realisierbar ist. Inspiriert durch aktuelle Lattice-QCD-Berechnungen zeigen wir, dass die Fluiddynamik auch für Beauty-Quarks in den letzten Stadien des expandierenden QGP anwendbar zu sein scheint. Wir präsentieren Ergebnisse für die Transversalimpulsverteilung und die integrierten Erträge von Charm-Hadronen in zentralen Pb–Pb-Kollisionen bei $\sqrt{s_{\mathrm{NN}}}$ = 5.02 TeV am LHC, die mit einem Fluiddynamik-Code in Verbindung mit der Annahme der Erhaltung eines Quark-Antiquark-Stroms für schwere Quarks und Antiquarks im QGP berechnet wurden. Unsere Berechnungen stimmen mit den verfügbaren experimentellen Messungen im Bereich kleiner Transversalimpulse überein und deuten auf eine effektive Hydrodynamisierung von Charm-Quarks im QGP hin.

Contents

Chapter 1

Introduction

This chapter is mostly inspired by [1, 2].

Notation

In the course of this thesis, we will often adopt natural units,

$$c = \hbar = k_{\mathrm{B}} = 1 \,,$$

where c is the speed of light in the vacuum, $\hbar$ is the Planck constant divided by 2π, and k_{B} is the Boltzmann constant.

We use Greek indexes for four-vectors' components $\mu = 0, 1, 2, 3$, while the Latin index for the spatial coordinates $i = 1, 2, 3$. We adopt the Einstein summation convention to sum over indexes that appear at least once in the upper and once in the lower position.

We refer at the pseudo-critical temperature of the QCD chiral phase transition as T_{pc}. In the literature, however, it is sometimes referred to as T_{c}.

1.1 High-energy nuclear physics

High-energy nuclear physics is a field of study that explores the behavior, properties, and interactions of nuclear matter under extreme conditions of temperature, density, and energy. This branch of physics often investigates nuclear matter in the context of high-energy particle accelerators, where two accelerated nuclei collide with each other creating extreme energy conditions. It

is an interdisciplinary topic, involving elements of nuclear physics, particle physics, astrophysics, and cosmology.

High-energy physics is ultimately devoted to studying the fundamental forces that define the Standard Model of particle physics, namely the electromagnetic, weak, and strong interaction. High-energy nuclear collisions, such as proton-proton (pp) or heavy-ion collisions, allow us to deepen our understanding of Quantum-Chromodynamics (QCD), the quantum field theory associated with the strong interaction. In particular, with heavy-ion collisions, one probes the nature of QCD interactions in extended systems. When colliding heavy ions such as lead (Pb) or gold (Au) nuclei at high energies, a new state of matter is created, that is, the quark-gluon plasma (QGP). At the time of impact, the nucleons that compose the colliding nuclei lose their identity of "protons" and "neutrons". For a fraction of microseconds ($\sim 10^{-22}$ s), the elementary components of the nucleons, i.e. quarks and gluons, exist unconfined. The produced system undergoes a rapid expansion and cools down until the quarks and gluons combine to form more complex objects in which they are confined, the hadrons.

The main objective of high-energy nuclear physics and heavy-ion collisions is to produce and characterize the QGP. This characterization spans from pinning down the transport properties of the plasma – such as its shear and bulk viscosity, heat and electric conductivity, and so on – to its Equation of State (EoS). From a broader point of view, heavy-ion collisions help in describing the QCD phase diagram by providing information on the low-baryon chemical potential/high-temperature region. An additional motivation behind the heavy-ion collision program is given by its deep connection with the Big Bang. In fact, it is vastly agreed upon in the scientific community that a QGP phase has taken place in the first few microseconds of our Universe. Its expansion – due to gravitational forces – gave rise to the formation of the elements and large-scale structures that we observe today. Heavy-ion collisions allow to re-create, for shorter timescales, a hot and dense system sharing similar features, therefore providing insights into the early stages of the Universe.

In recent years, dramatic progress has been achieved in the field, leading to a whole set of new, still unanswered questions. Because of the success of relativistic viscous hydrodynamics in modeling the QGP phase of a heavy-ion collision (see e.g. Ref. [3] for a recent review), a lot of interest has been devoted to the QGP as a collectively expanding system. In particular, physicists have been focusing on understanding what properties of the hadrons measured in the heavy-ion collision experiments stem from such collective expansion. More fundamentally, the mere fact of the fast emergence of the collective behavior of the QGP, given the far-out-of-equilibrium initial condition of two colliding nuclei, has already been thoroughly investigated [4–7]. In a similar direction, the question about the formation of a QGP phase in small systems has also been raised (see e.g. Refs. [8, 9] for recent reviews). While the build-up of a collective expansion is now unquestioned in ultrarelativistic collisions of heavy nuclei such as Pb or Au, it remains

under debate whether the same happens for smaller systems, such as proton-lead (p–Pb), until the extreme case of pp collisions. In particular, it is still ambiguous if the available experimental data hint at the emergence of a collective phase in the collision.

Some of the most recent advancements in the field regard interdisciplinary pioneering studies. As an example, a paradigm on how to probe the nuclear structure of the colliding nuclei by exploiting heavy-ion collisions has been recently established. The joint effort between the low- and high-energy nuclear physics communities allowed for a fast improvement in the knowledge of the geometry of the colliding nuclei and how the latter impacts the subsequent QGP phase [1, 10–12]. To the set of these new approaches belongs also the mapping of the collective dynamics developed in heavy-ion collisions onto cold atom systems made out of only a few particles [13, 14]. The striking question here is how many particles are needed to observe a fluid-like behavior, with the goal of understanding better the interplay between microscopic and mesoscopic physics scales. One of the driving ideas is to employ tools and knowledge from the heavy-ion field to assess the manifestation of collective behavior in cold atom systems.

The heavy-ion physics program has been extremely successful. A large amount of high-precision measurements has been (and is currently being) collected. At the same time, the theoretical understanding of the dynamics of the collision has strongly improved. A solid comprehensive theoretical framework has been developed, allowing to quantitatively describe the experimental data as well as pointing out significant deviations between the modeling and the observations. Thanks to this thorough effort, we are now able to constrain fundamental properties of QCD with unprecedented precision.

1.2 Relativistic heavy-ion collisions

1.2.1 Theoretical framework: QCD

QCD is the quantum field theory describing the strong interaction. Together with the theory of electromagnetic and weak interactions, it is a fundamental pillar of the Standard Model of particle physics.

QCD is a non-abelian field theory that is symmetric under local $SU(3)$ gauge transformations. The conserved charge associated with the $SU(3)$ symmetry is *color*, which can appear in 3 states (usually identified with red, green and blue). The color charge is carried by the spin-1/2 fermions of the theory, the quarks, that are distinguished according to their *flavor* (up, down, strange, charm, beauty, and top). The symmetry under local gauge transformations requires eight gauge fields, which correspond to eight massless gauge bosons, the gluons, mediating the strong interaction and connecting quark states of different colors. Due to color conservation at the QCD interaction vertex, gluons must carry color and anticolor charge. The non-abelian nature of the theory allows for the gluons to self-interact with 3- or 4-gluon vertices.

A striking feature of QCD is the running behavior of the strong coupling constant α_s. In quantum field theory, the quantity describing the interaction between two particles is an effective constant which depends on the energy scale Q^2 of the interaction. The running of the coupling constant in QCD defines two phenomena, namely *asymptotic freedom* and *color confinement*. The larger Q^2, the weaker the interaction between quarks and gluons. In this regime, quarks and gluons are quasi-free particles (asymptotic freedom) and one can rely on perturbative QCD (pQCD) calculations to expand the amplitudes of the scattering matrix in a controlled fashion in terms of powers of α_s. At low Q^2, on the other hand, the coupling diverges, causing the breakdown of the perturbative approach. In this regime, confinement dictates that quarks and gluons cannot exist in isolation and, consequently, are not directly observable. The quarks and gluons form therefore color-neutral bound states – the hadrons – divided, in turn, into *mesons* (2-quark bound state) and *baryons* (3-quark bound state). The study of QCD under these conditions is tackled with Lattice QCD (LQCD), which employs a discretized spacetime lattice in order to evaluate physically relevant quantities. LQCD has become one of the most prominent tools in high-energy physics to determine the thermodynamic properties of QCD, such as its EoS [15, 16]. Alternatively, functional methods, such as the functional Renormalization Group (fRG [17, 18]), also provide a robust mathematical framework to compute QCD properties in the non-perturbative regime.

1.2.2   The QCD phase diagram

The complete understanding of the phase structure of QCD is one of the ultimate goals in physics (see e.g. Refs. [19, 20]). In the attempt to study the various features of the theory, one aims at reconstructing the full QCD phase diagram, which is sketched in Fig. 1.1. A standard way of depicting the phase diagram is as a function of temperature T and baryon chemical potential μ_B or – equivalently – net baryon density.

LQCD calculations and chiral effective models have shown that the QCD phase diagram is non-trivial and displays at least two phases, namely a high-temperature QGP phase – where the active degrees of freedom are quarks and gluons, due to asymptotic freedom – and a low-temperature hadronic phase in which the quarks and gluons are confined. In particular, theoretical calculations on the lattice in the low-baryon chemical potential region predict a smooth crossover associated with the chiral symmetry breaking of the QCD Lagrangian. Shifting to non-zero chemical potential, effective models suggest the presence of a first-order transition, separated from the crossover line by a second-order critical end-point. The exact value at which this should occur is currently under debate.

To explore different regions of the phase diagram, the most direct tool is provided by heavy-ion collisions. By performing experiments at different center-of-mass energies $\sqrt{s}$, a different amount of energy and net-baryon density is deposited in the collision. This allows to explore
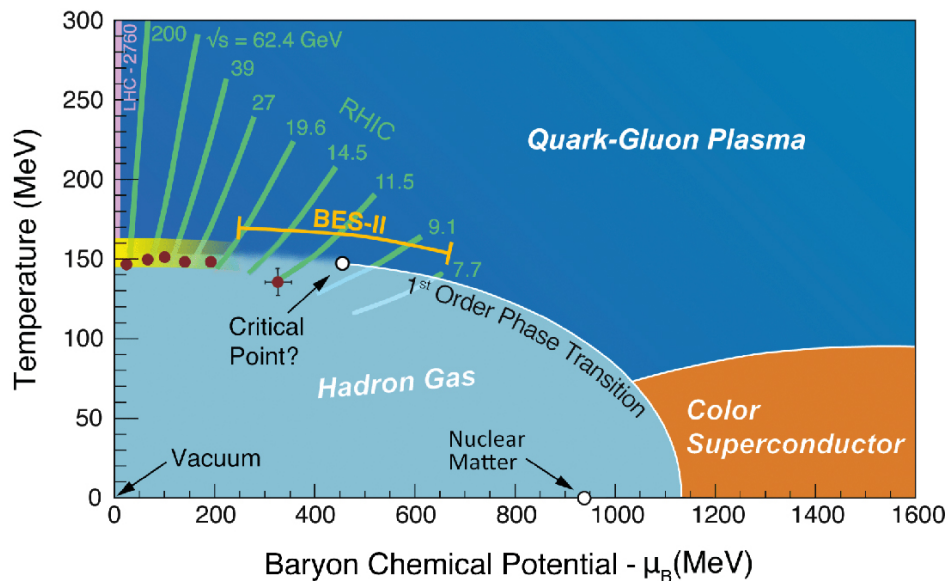
Figure 1.1: Sketch of the QCD phase diagram in the temperature-baryon chemical potential plane. The colored areas identify the different phases, while the white lines indicate the phase transitions. Straight pink and green lines with different slopes show the different regions of the phase diagram probed by collider experiments at various center-of-mass energies.

the QCD phase diagram along straight lines with different slopes (as shown by the pink and light green lines in Fig. 1.1). The highest-energy experiments (LHC at CERN, RHIC at BNL at top energies – see the Sec. 1.2.3 for more details on these facilities) allow us to explore the region of the phase diagram near the temperature axis, that is, at $\mu_B \sim 0$. This regime is of special interest since it corresponds to the conditions of the early Universe. Furthermore, this is the region where the theoretical framework is more under control, also in the non-perturbative regime.

At extremely high baryon densities and low temperatures, a color-superconductor phase is conjectured [21]. In conventional superconductors, electrons form Cooper pairs and condense into a state with zero electrical resistance. In the context of QCD, a similar phenomenon is expected to occur among quarks. At extremely high densities, such as those found in the cores of neutron stars, it is theorized that quark matter undergoes a phase transition to a color superconducting state. In this state, quarks form Cooper pairs and condense, leading to the spontaneous breaking of $SU(3)$ color symmetry.

To approach higher baryon densities, experiments were carried out at SPS, in the Beam Energy Scan (BES) at RHIC, and are planned for the near future at FAIR and NICA. The study of this region of the phase diagram is relevant for the understanding of the nature of quark matter inside neutron stars, which constitute the perfect benchmark for cold and almost infinite nuclear matter. The densities inside a neutron star exceed by far anything found on Earth and a detailed

understanding of the physics phenomena in its core is still absent. Experiments covering this region of the phase diagram are the probes to test the validity of the present theoretical models.

In this thesis, we will focus on the QGP phase at high temperatures and zero baryon chemical potential, such as the ones realized at the LHC.

1.2.3   Collider experiments

Heavy-ion collisions are the experimental tool employed to study the QGP. In order for this state of matter to be created, nuclear matter has to be compressed to extremely high energies and temperatures. Only two experimental facilities in the world can create such conditions, namely the Large Hadron Collider (LHC) at European Center for Nuclear Research (CERN) in Geneva, Switzerland, and the Relativistic Heavy Ion Collider (RHIC) at the Brookhaven National Laboratory (BNL) in Uptown, New York, USA.

The Large Hadron Collider (LHC) is the world's largest and most powerful particle accelerator. It consists of a 27-kilometer ring of superconducting magnets with several accelerating structures to boost the energy of the particles along the way. Inside the accelerator, two high-energy particle beams travel at close to the speed of light before they are made to collide. The beams travel in opposite directions in separate beam pipes – two tubes kept at ultrahigh vacuum. They are guided around the accelerator ring by a strong magnetic field maintained by superconducting electromagnets. The LHC is designed to accelerate protons at a maximum center-of-mass energy $\sqrt{s} = 14$ TeV and lead nuclei at a maximum center-of-mass energy per nucleon pair of $\sqrt{s_{\mathrm{NN}}} = 5.02$ TeV. Collisions in the LHC generate temperatures of the order of 10^{12} K, more than 10^5 times hotter than the center of the Sun. During runtime, for about one month per year, the LHC provides collisions between lead ions, recreating in laboratory conditions similar to those just after the Big Bang. The ALICE Collaboration, one of the four large collaborations working at the LHC, is entirely dedicated to the heavy-ion collision program. Additionally, part of the ATLAS and CMS collaboration are also devoted to the heavy-ion data taking. The LHC is currently in the Run 3 period, providing data for pp and Pb–Pb collisions with unprecedented precision. Oxygen-oxygen (O–O) collisions are also scheduled, with the goal of deepening our knowledge of collectivity and QGP formation in small systems. Nuclear collisions at LHC are foreseen until about 2040. The program for the future years (Run 5 and Run 6) is currently under discussion.

RHIC consists of an accelerator ring with a diameter of about 1.2 kilometers. It can perform pp collisions at center-of-mass energy up to 500 GeV, and nuclear collisions at nucleon-nucleon center-of-mass energy up to 200 GeV. This machine is entirely devoted to studies of high-energy nuclear physics. RHIC is a versatile machine and, since the start of operations in 2000, it collected a large amount of data for several colliding nuclear species (Au, Zr, Ru, etc.). The two main collaborations performing the data taking and analysis are STAR and PHENIX. One

of the main physics goals at RHIC is pursued by the BES program, which focuses on the study of the QCD phase diagram. The STAR experiment at BNL has recently completed the second phase of the beam energy scan (BES-II) program. The center-of-mass energy per nucleon pair of the Au–Au collisions from the collider mode ranges from 7.7 to 54.4 GeV, while the fixed target collisions included in BES-II extend the energy reach down to 3.0 GeV. These studies constitute an opportunity to probe the medium properties of QCD matter at high baryon densities. In the future, RHIC will be reused as the infrastructure on which the Electron-Ion Collider (EIC) will be built. A new electron source, electron accelerator and storage rings will be added inside the existing collider tunnel so that collisions will take place at points where the stored ion and electron beams cross.

Each collision releases a large number of particles. Each (charged) particle leaves a signal in the detector that allows for the particle's track to be reconstructed. All measurements are performed in momentum space. The final reconstructed object corresponds to a given particle's 4-momentum vector, $p^\mu = (p^0, \vec{p})$, where $\vec{p} = (p_x, p_y, p_z)$ and $p^0 = \gamma m$, m is the rest mass of the particle and γ is the Lorentz factor. Often, the spatial momentum components are parametrized as $\vec{p} = (p_\mathrm{T}, \phi, y)$, namely transverse momentum, azimuthal angle and rapidity, defined as

$$p_\mathrm{T} = \sqrt{p_x^2 + p_y^2}, \tag{1.1}$$

$$\phi = \arctan\left(\frac{p_y}{p_x}\right), \tag{1.2}$$

$$y = \operatorname{arctanh}\left(\frac{p_z}{p^0}\right). \tag{1.3}$$

When the emitted particle is not known, the pseudo-rapidity $\eta = \operatorname{arctanh}\left(\frac{z}{t}\right)$ is used instead. The definitions of y and η coincide when the particle energy is much larger than its mass. In a typical Pb–Pb collision at the LHC, about 2000 tracks per collision event are reconstructed at mid-rapidity ($y \sim 0$), of which the most abundant are pions, protons, kaons and their correspondent charge conjugates.

1.2.4 Stages of a heavy-ion collision

Since the heavy-ion program at collider facilities has started, a "Standard Model" of heavy-ion collisions has been developed through the years. The joint effort between theoreticians and experimentalists allowed in fact to distinguish the main stages of a collision, from the time of impact of the nuclei until the hadrons fly into the detectors. This scheme is depicted in Fig. 1.2. The time scan is parametrized by the longitudinal proper time $\tau = \sqrt{t^2 - z^2}$.

Before the collision: $\tau < 0$. The starting point of a heavy-ion collision consists of two heavy nuclei flying into each other at a speed comparable to the speed of light. We often refer to
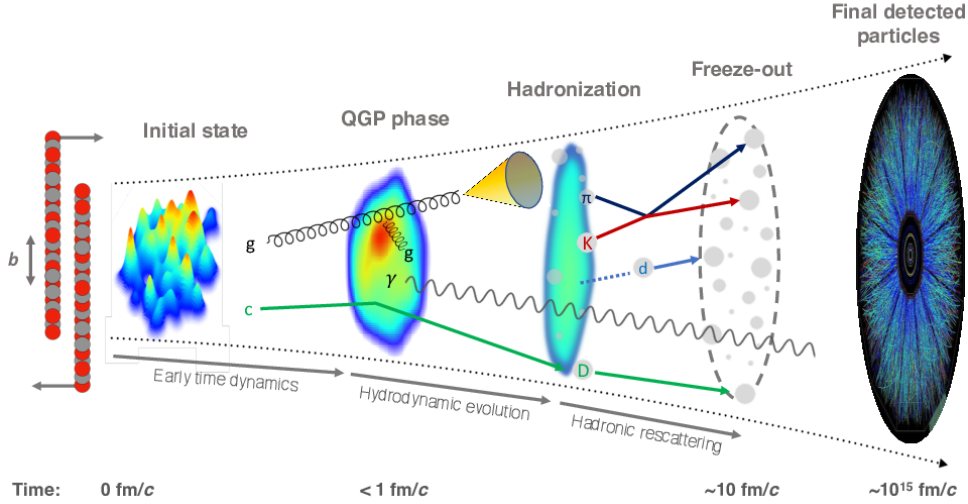
Figure 1.2: An illustration of different stages in a heavy-ion collision. The event display at the final stage is from the STAR experiment at RHIC.

these nuclei as A and B, or projectile and target[1]. We identify the beam axis with the longitudinal z axis and the transverse plane as the orthogonal $x - y$ plane. The colliding nuclei are Lorentz contracted in the z direction.

Initial state: $\tau = 0$. At $\tau = 0$ an amount of energy (entropy) density is deposited by the colliding heavy nuclei. This density is often described by employing the Glauber model[2] [30], a semi-classical approach based on a geometrical description of the incoming nuclei. The interaction between the nuclei is portrayed as an incoherent overlap of nucleon-nucleon collisions, therefore it can be modeled with the theory of probability. The Glauber model allows to give quantitative predictions for the interaction probability of the nucleons, the number of elementary nucleon-nucleon collisions N_{coll}, the number of nucleons which are "wounded" by the interaction (number of *participants* N_{part}) and the ones that are not (number of *spectators* N_{spec}), the size of the overlap region, and so on.

The key ingredients of the Glauber model are the following:

- *Optical limit.* The nucleons in the nucleus are considered like point-like objects[3]. Each nucleon is considered to be independent of the others. This represents a good approximation at high collision energies where the De Broglie wavelength of a nucleon with momentum p from the projectile, $\lambda \sim \hbar c/(pc)$, is much smaller than the typical distance between two

---

[1]Even though the collision is often symmetric, as in Pb–Pb or Au–Au collisions, it is useful to identify one nucleus as a target and the other as a projectile when isolating the effect that a nucleon from nucleus A has on the nucleons in nucleus B.

[2]Alternatives or extensions to the Glauber model have been developed through the years. Some examples are the Color Glass Condensate (CGC) [22–25] and the IP-Glasma model [26–29], that will not be employed in this work.

[3]In certain initial condition models, such as T_RENTo [31], the nucleons can be considered as complex objects with their own size and substructure. This more detailed description plays a role in the study of observables which strongly depend on the initial nucleon fluctuations.

nucleons in the target, $d \sim 1$ fm. Furthermore, the nucleus travels on a straight line along the z axis and it is not deviated by the interaction. Protons and neutrons are considered indistinguishable.

- *Interaction cross section.* The interaction cross section σ depends on the center-of-mass energy of the collision $\sqrt{s}$ and is assumed to be the same for each collision, therefore neglecting modifications due to nucleon excitations in the collision. This is justified since the formation time of a resonant state is much larger than the time between two subsequent interactions. Only the inelastic component of the cross section σ_{in} is considered.

- *Nucleon position.* The incoming nuclei are described according to a density $\rho(r)$, usually provided by a Woods-Saxon curve or a more general n-point Fermi function. The parameters of these distributions, such as average nuclear radius or the density in the center of the nucleus, are taken from independent electron-nucleus or neutron-nucleus scattering experiments.

  On an event-by-event basis, this distribution is used to determine the positions of the nucleons inside the nucleus. While in the optical limit, the density distribution is assumed to be smooth, in numerical approaches known as Glauber Monte Carlo local density fluctuations are included. The two calculations coincide in the limit of large number of nucleons or small inelastic cross section [30]. In general, however, they predict slightly different collision geometries.

- *Impact parameter.* The distance between the centers of the two colliding nuclei is called impact parameter b. The total energy of the system created at the time of the collision $\tau = 0$ fm depends on the overlap between the colliding nuclei, therefore reflects the impact parameter. One can classify different collision events based on the impact parameter as *central* ($b \to 0$), *semi-central* and *semi-peripheral* ($b \sim R_{\mathrm{A}}$), and *peripheral* ($b \to 2R_{\mathrm{A}}$) collisions. The impact parameter can not be measured directly in the experiment; however, the number of produced particles detected at the end of collision evolution can be used as a proxy to estimate it.

- *Participants and spectators.* The number of participants N_{part} is defined as the number of nucleons that have at least one interaction with another nucleon during the collision. The number of spectators N_{spec} is, on the contrary, the number of nucleons that do not participate in any interaction. They are strongly dependent on the impact parameter. For $b \to 0$, meaning full overlap between A and B, N_{part} coincides with the sum of the number of nucleons in the colliding nuclei. A related concept is the number of collisions N_{coll}, which identifies the number of times in which a nucleon-nucleon interaction takes place. The latter is directly proportional to the interaction cross section.

a   **b**
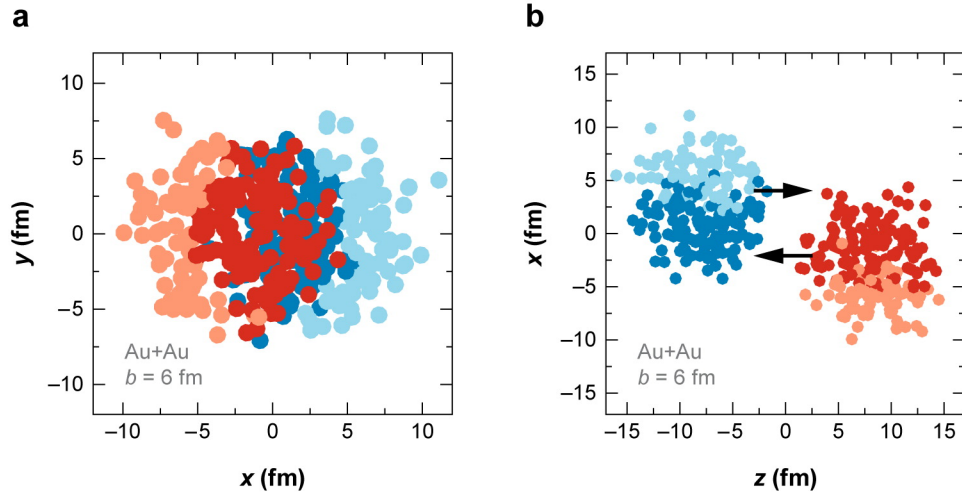
Figure 1.3: A Glauber Monte Carlo simulation of a Au–Au event with impact parameter $b = 6$ fm seen in the transverse plane (a) and along the beam axis (b). Darker circles represent participant nucleons, and lighter circles represent spectators. Figure taken from Ref. [30].

An example of Glauber Monte Carlo simulation is pictured in Fig. 1.3, where a Au–Au event with impact parameter $b = 6$ fm is displayed in the transverse plane (a) and along the beam axis (b). Darker circles represent participant nucleons, and lighter circles represent spectators. The figure is taken from Ref. [30].

Pre-equilibrium phase: $0 < \tau \lesssim 1$ **fm/c.** It is the time frame between the collision time and the *thermalization time* $\tau_0 \sim 1$ fm/c, that is, the beginning of the QGP phase. In many phenomenological descriptions of heavy-ion collisions, the description of this phase is omitted and the initial state is assumed to remain unchanged or to undergo a simple free streaming dynamics in the first fm/c [32, 33]. In recent years, however, the question of how the transition between an out-of-equilibrium system such as one of the colliding nuclei, and a thermalized quark-gluon medium takes place has gained a lot of interest (see e.g. [7] for a recent review).

QGP phase: $1 \lesssim \tau \lesssim 10$ **fm/c.** The QGP phase consists of a thermalized system of free quarks and gluons. Its formation is associated with a phase transition from the hadronic phase to the deconfined phase, which can be reached only under extremely high temperatures and energy densities – such as the ones achieved at the LHC and top RHIC energies. The duration of the QGP phase depends on the energy of the collision as well as on its geometry (at higher energies and in more central collisions the QGP phase is expected to last longer). Due to pressure gradients with respect to the surrounding vacuum, the QGP undergoes a rapid expansion often described as a *fireball*, with a subsequent cooling of the system. This evolution is successfully described by relativistic viscous fluid dynamics – which will be described in detail

in Chapter 2. In particular, fluid dynamics is able to describe some of the most characteristic aspects of the QGP, such as *radial* (isotropic) and *anisotropic flow*. The term "flow" refers to the collective motion of the particles composing the fluid superimposed to their thermal motion. It manifests as an angular modulation in the distribution of the final-state particles (see the Sec. 1.3 for further details). The initial conditions for the hydrodynamic expansion are provided by the initial state model. Examples of state-of-the-art models and code packages that describe the evolution of the QGP are Trajectum [34], MUSIC [35] and FluiduM [36]. The key points which determine the evolution of the QGP system can be synthesized as:

- *Transport coefficients.* Transport coefficients, such as viscosities and conductivities, regulate how the fluid variables (temperature, pressure, fluid velocity, and dissipative currents) evolve in spacetime. Determining these coefficients is one of the main goals of the heavy-ion collision program. They admit a first-principle description in QCD, but their analytical calculation is only possible under certain approximations. From the theoretical point of view, LQCD and functional approaches play a crucial role, granting a numerical treatment of these non-perturbative quantities. Another way to extract transport coefficients of the QGP is through phenomenological studies. A systematic comparison between theoretical calculations and experimental measurements is nowadays an established paradigm for learning information on such quantities.

- *Equation of State.* The Equation of State is a thermodynamic relation between state variables, usually expressed by the pressure or energy density as a function of temperature and chemical potential. It contains the microscopic information on the QCD medium. In the case of ultra-relativistic heavy-ion collision, where the colliding nuclei get scarcely stopped, one can assume that the net baryon chemical potential is roughly zero. In this limit, the EoS can be computed in LQCD [15, 16]. In Fig. 1.4 the results for pressure, energy density, and entropy density are shown as a function of temperature [15]. The lines are the predictions of the Hadron Resonance Gas (HRG) model. LQCD predicts a crossover at the pseudo-critical temperature $T_{\mathrm{pc}} = 154 \pm 9$ MeV, marked by the yellow vertical band. At low temperatures, where confinement sets in, the calculations coincide with the HRG description. At high temperatures, the dominant degrees of freedom are quarks and gluons and the HRG approximation is no longer applicable. The dashed horizontal line shows the asymptotic limit of a non-interacting gas of quarks and gluons. As shown in the figure, however, the non-interacting limit is never reached within the temperature range covered by the experimental conditions. The EoS is a necessary ingredient in heavy-ion collision simulations. It is needed to have a closed system of equations in the hydrodynamic treatment of the QGP.

Hadronization and freeze-out $\tau \sim 10$ **fm/c.** The concept of hadronization is strictly
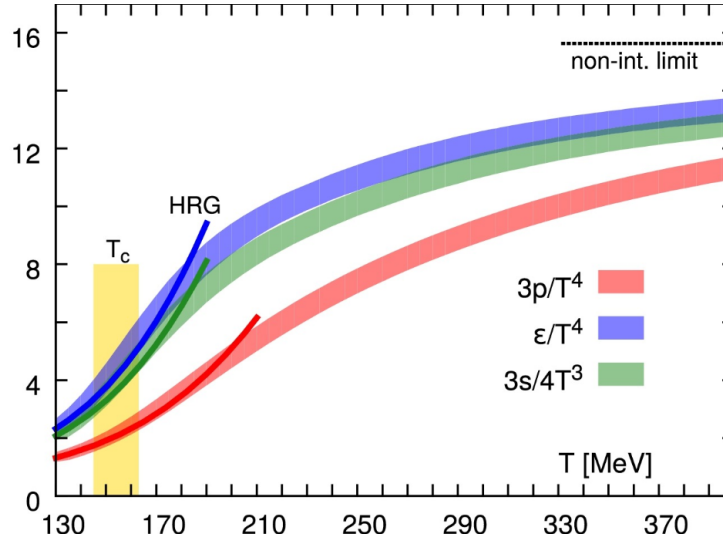
Figure 1.4: Pressure, energy density, and entropy density as a function of the temperature. The lines are the predictions of the HRG model. The vertical band marks the crossover region, at the pseudo-critical temperature $T_{\mathrm{pc}} = 154 \pm 9$ MeV. Figure taken from Ref. [15].
.

related to the one of the phase transition of QCD. The fluid expansion decreases the temperature of the fluid elements until at T_{pc} the QGP description is no longer applicable, and the system enters the hadron-gas phase (*hadronization*). In heavy-ion simulations, when a fluid cell reaches T_{pc} the hydrodynamic evolution is stopped. The freeze-out temperature identifies a *freeze-out hypersurface* in spacetime, from which the hadrons are emitted. An established way of implementing hadronization is to apply the Cooper-Frye prescription [37], that assumes a sudden decoupling of the medium at $T_{\mathrm{FO}} \equiv T_{\mathrm{pc}}$. The momentum distribution of the emitted hadron h is given by the flux of particles through the freeze-out hypersurface Σ_μ,

$$E_h \frac{d^3N}{dp^3} = g_h \int d\Sigma_\mu p^\mu f_h \,, \tag{1.4}$$

which provides the number density of the particle three-momentum scaled by the particle energy E_h. Here, g_h is the number of internal degrees of freedom, and f_h is the momentum distribution of the hadron at T_{FO}. The latter contains the information on the fluid fields on the freeze-out hypersurface. Through the Cooper-Frye formula, one maps the information on the fluid fields from coordinate space onto momentum space.

There exists a distinction between *chemical* (T_{chem}) and *kinetic* (T_{kin}) freeze-out temperature. T_{chem} indicates the temperature under which the chemical composition of the hadrons is fixed – up to feed-down from resonance decays. In this regime, also known as *partial chemical equilibrium* [38, 39], the mean free time for elastic collisions is still smaller than the characteristic expansion time of the expanding system, thereby keeping the gas in a state of local kinetic equilibrium. The chemical equilibrium is not maintained since the mean free path of the inelastic

collisions exceeds this threshold. The hadrons can still interact and exchange momentum until the temperature reaches T_{kin}, when the system falls out of kinetic equilibrium and the momentum distributions are fixed.

In the heavy-ion collision modeling, some approaches consider an intermediate phase between the QGP and the gas of free-streaming hadrons, where scattering processes that occur in the hadron gas are computed. Codes devoted to this task are, e.g., SMASH [40] or UrQMD [41].

Final detected particles $\tau \gg 10$ fm/c. In this stage, the long-lived hadrons (mostly pions, kaons and protons) reach the detector. To correctly reproduce the momentum distribution of the hadrons measured by the experiment, one needs to take into account feed-down contributions from resonance decays. In fact, some of the produced hadrons will strongly decay and will not be observed in the detector. The effect of resonance decays is very significant. For instance, the number of stable light hadrons (pions, kaons, protons) emitted thermally at freeze-out is only half its actual value after all unstable resonances have decayed. An efficient way to compute this is provided by the FastReso code package [42].

1.3   Heavy-flavor observables in heavy-ion collisions

Heavy quarks are produced in the earliest times of the collision via hard scattering processes, namely with high momentum transfer, even before the QGP is formed. They are considered optimal probes of the QGP since they witness all the stages of the heavy-ion collision. In particular, their diffusion through the QGP becomes a tool to infer transport properties of the plasma. In this Section, we present a (selected) class of heavy-flavor observables that can be experimentally measured. Each of them grants indirect access to different features of the QGP.

A fundamental quantity for many of these probes is the Lorentz-invariant differential yield of final state particles, given by

$$E\frac{d^3N}{dp^3} = \frac{1}{2\pi}\frac{d^2N}{p_{\text{T}}dp_{\text{T}}dy}\ .\tag{1.5}$$

By integrating Eq. (1.5) over transverse-momentum and rapidity, one obtains the total number of produced particles in a single collision event (*multiplicity*). It strongly depends on the impact parameter. Since the impact parameter cannot be directly measured, a way to classify different collision events is through the *centrality classes*. The events can be sorted according to the total charged-particle multiplicity in percentiles. The $0-5\%$ centrality class corresponds to the 5% of events with the highest multiplicity, and so on.

From Eq. (1.5) one can construct the *nuclear modification factor* R_{AA}. This observable quantifies a change in the dynamics of heavy quarks in heavy-ion collisions with respect to elementary pp collisions. The R_{AA} as a function of transverse momentum is defined as

$$R_{\text{AA}} = \frac{1}{\langle N_{\text{coll}}\rangle}\frac{dN_{\text{AA}}(p_{\text{T}})/dp_{\text{T}}}{d\sigma_{\text{pp}}(p_{\text{T}})/dp_{\text{T}}}\ ,\tag{1.6}$$

where $dN_{\mathrm{AA}}/dp_{\mathrm{T}}$ is the p_{T} distribution of a hadron in the heavy-ion collision and $d\sigma_{\mathrm{pp}}/dp_{\mathrm{T}}$ is the correspondent one in a pp collision. If the absence of a QGP phase, the dynamics of heavy quarks in a heavy-ion collision would not differ from the one in pp collisions, up to a factor accounting for the total number of binary nucleon-nucleon collisions, and the R_{AA} would be 1. The deviation from unity observed in the experimental measurements is evidence of the presence of the QGP phase. In particular, this observable is sensitive to the radial flow of the plasma. Radial flow is an isotropic boost with velocity $v_{\perp}(r)$ of each fluid cell in the radial direction, whose effect is to push the momentum distribution of hadrons to a larger average p_{T}.

Anisotropic flow, on the other hand, quantifies a correlation between the particles' final angular distribution and the impact parameter. It is observed in non-central collisions, where the impact parameter determines a preferential direction for the emission of the final state hadrons. Anisotropic flow can be studied by looking at the Fourier decomposition of the particle angular distribution,

$$\frac{dN}{d\phi} \propto 1 + \sum_{n=1}^{\infty} v_n \cos[n(\phi - \Psi_{\mathrm{RP}})], \tag{1.7}$$

where v_n are the anisotropic flow coefficients, ϕ is the azimuthal angle and Ψ_{RP} is the reaction plane angle, identified by the azimuthal angle of the impact parameter in the transverse plane. Non-zero v_n coefficients mostly arise from the fluid-dynamic response of the QGP to the initial geometrical anisotropy of the collision system. Their magnitude and distribution as a function of p_{T} are strongly influenced by the EoS and by the viscosities. The most prominent case is the one of the elliptic flow v_2, which quantifies the response to the initial ellipticity in the overlap region of the colliding nuclei. The measurement of heavy-flavor hadrons' elliptic flow quantifies the correlation between the heavy quarks and the underlying medium. In other words, it measures how much the heavy quarks share the collective behavior of the QGP.

.

1.4   This work

This work focuses on the study of the heavy-quark in-medium dynamics. Heavy quarks are canonically treated within kinetic theory approaches due to the energy scale set by their large mass. The new perspective we want to offer regards the *soft* (i.e. low-momentum) aspects of heavy quarks as probes of the QCD medium. While at high transverse momenta the heavy-quark dynamics is dominated by radiative energy loss, soft elastic scattering processes are the most relevant contribution in the low-p_{T} regime. We will concentrate on the soft momentum region and discuss the level of participation of charm and beauty quarks in the collective motion of the QGP. We will do so both from a theoretical and a phenomenological point of view.

1.4.1 Outline

In Sec. 2 an introduction to relativistic viscous fluid dynamics is presented. We will show the main equations needed to study the QGP in the presence of additional conserved currents. We will also define the role of transport coefficients and relaxation times in fluid dynamics. In Sec. 3 we show a theoretical overview of transport approaches to heavy-quark dynamics in heavy-ion collisions. In particular, we will discuss the description of charm and beauty quarks as it is usually treated in the literature, that is, with kinetic theory (e.g. Boltzmann equation). In Sec. 4 the motivation for a fluid-dynamic treatment of charm quarks in the QGP is presented. A preliminary assessment of the situation of beauty quarks will also be shown. In Sec. 5 the fluid-dynamic description of a heavy-quark current is developed. The applicability of such a description to charm and beauty quarks is discussed. In Sec. 6 the results for charmed-hadrons momentum distributions and integrated yields obtained within the fluid-dynamic approach are presented. In Sec. 7 we will outline final remarks and possible extensions of this work.

1.4.2 Research work

In this thesis, I will mainly discuss the results of my research work described in the following publications,

1. F. Capellino, A. Dubla, S. Floerchinger, E. Grossi, A. Kirchner and S. Masciocchi, "Fluid dynamics of charm quarks in the quark-gluon plasma", Phys. Rev. D **108** (2023) no.11, 116011.

2. F. Capellino, A. Beraudo, A. Dubla, S. Floerchinger, S. Masciocchi, J. Pawlowski and I. Selyuzhenkov, "Fluid-dynamic approach to heavy-quark diffusion in the quark-gluon plasma", Phys. Rev. D **106** (2022) no.3, 034021.

I presented this work in two international conferences, Hard Probes 2023, Aschaffenburg (Germany) and Quark Matter 2023, Houston, Texas (USA). The content of the talks is summarized in the following Proceedings,

- F. Capellino, A. Dubla, S. Floerchinger, E. Grossi, A. Kirchner and S. Masciocchi, "Hydrodynamization of charm quarks in heavy-ion collisions" [arXiv:2312.10125 [hep-ph]], Proceedings Quark Matter 2023.

- F. Capellino, A. Dubla, S. Floerchinger, E. Grossi, A. Kirchner and S. Masciocchi, "Momentum distribution of charm hadrons in a fluid-dynamic approach" [arXiv:2307.15580 [hep-ph]], Proceedings Hard Probes 2023.

In all these publications I contributed as the first author. In particular, in 1. I performed all the analytical and numerical calculations. In 2. I co-wrote the code to perform hydrodynamic

simulations of the quark-gluon plasma and extended it to include the heavy-quark degrees of freedom. However, the collaboration with each of the signing authors was of fundamental importance to me, in terms of exchanging ideas, solving problems, writing the manuscript, and promoting our work in the physics community.

Other works in which I participated, but will not be treated in this thesis, are

1. A. Kirchner, F. Capellino, S. Floerchinger, E. Grossi, "Extending the fluid-dynamic description to times before the collision", work in progress.

2. G. Giacalone *et al.*, EMMI Rapid Reaction Task Force (2022), "Nuclear physics confronts relativistic collisions of isobars", soon to appear on Arxiv.

In 1. we explore the feasibility of a fluid-dynamic approach to the initial conditions of a heavy-ion collision. I contributed to the derivation of the equations of motion for the fluid fields in the case of a fluid undergoing a Hubble expansion in the presence of dissipative shear-stress corrections and in the study of the causality bounds on a diffusive equation for the net baryon number evolution.

In 2. I participated actively in the two sections of the RRTF in 2022. Together with Andreas Kirchner, we performed T_RENTo simulations for the initial conditions to Zirconium and Ruthenium nuclear collisions at RHIC studying the impact of various nuclear-structure parameters, such as quadrupole, octupole, and triaxial deformation of the nuclei as well as modification of their nuclear skin thickness. We contributed, together with Farid Tagahavi, to a Section in the RRTF report dedicated to such studies.

Chapter 2

Relativistic fluid dynamics

This chapter is mostly inspired by [43–46].

2.1 Theoretical formulation

Relativistic viscous fluid dynamics is an effective theory used to describe long-distance and long-time dynamics of macroscopic systems. It has applications in high-energy nuclear physics as well as in astrophysics and cosmology [44, 46, 47]. In the context of heavy-ion collisions, fluid dynamics is mainly employed to study the expansion of the QGP medium. Several properties of light hadrons emitted at freeze-out, concerning their momentum and angular distribution, can be successfully predicted by viscous fluid dynamics. In particular, the radial and elliptic flow, mentioned in Chapter 1, are direct consequences of the collective behavior of the medium.

The regime of validity of fluid dynamics is the one where the typical length-scale of the system L is much larger than the mean free path λ_{mfp} of its constituents. This condition can be formulated in terms of Knudsen number, $\mathrm{Kn} \equiv \lambda_{\mathrm{mfp}}/L$. If $\mathrm{Kn} \ll 1$, the microscopic degrees of freedom can be safely integrated out and the whole behavior of the system can be expressed in terms of a few macroscopic fields, such as pressure, temperature, etc. Notice that, if one defines $\lambda_{\mathrm{mfp}} \equiv (\sigma n)^{-1}$, where σ is the interaction cross section among the constituents and n is their number density, the ideal-fluid limit ($\mathrm{Kn} \to 0$) is verified when the system is strongly coupled, corresponding to high particle density and/or large interaction cross section. Fluid dynamics is in fact more general than kinetic theory (presented in Chapter 3) since it does not require the interaction to be small or the system to be diluted. An emblematic example is provided by the AdS/CFT correspondence [48], where hydrodynamics is a valid description of the strongly coupled system.

Fluid-dynamic equations are formulated through a set of conservation laws. They include the conservation of the energy-momentum tensor $T^{\mu\nu}$ and possibly additional currents $\mathcal{J}_i^\mu$,

where each current is associated with a conserved charge Q_i (baryon number, electric charge, strangeness, etc.).

Ideal hydrodynamics. Hydrodynamic equations take the simplest form if local thermal equilibrium is assumed. Let us consider the example of a single conserved charge Q. In this ideal setup, the conserved quantities are described by

$$T^{\mu\nu} \equiv T^{\mu\nu}_{\text{eq}} = \epsilon(T,\mu)u^{\mu}u^{\nu} + P(T,\mu)\Delta^{\mu\nu}\,, \qquad \mathcal{J}^{\mu} \equiv \mathcal{J}^{\mu}_{\text{eq}} = n(T,\mu)u^{\mu}\,. \qquad (2.1)$$

Here we decomposed $T^{\mu\nu}$ and $\mathcal{J}^{\mu}$ along the time-like four-vector u^{μ}, defined as the fluid four-velocity and normalized to $u^{\mu}u_{\mu} = -1$, and $\Delta^{\mu\nu} = u^{\mu}u^{\nu} + g^{\mu\nu}$, the projector selecting the symmetric component orthogonal to the fluid four-velocity, $u_{\mu}\Delta^{\mu\nu} = u_{\nu}\Delta^{\mu\nu} = 0$. The metric tensor $g_{\mu\nu}$ is chosen to follow the mostly plus convention[1]. At this stage, ϵ, P and n are arbitrary functions of the temperature T and chemical potential μ. If we consider the local rest frame (LRF) of the fluid, in which $u^{\mu} = (1,0,0,0)$, the expressions in Eq. (2.1) reduce to

$$T^{\mu\nu} = \text{diag}(\epsilon, P, P, P)\,, \qquad \mathcal{J}^{\mu} = (n, 0, 0, 0)\,. \qquad (2.2)$$

Relating these quantities to the known results for a fluid at rest (energy and charge conservation, absence of pressure gradients), one can identify ϵ as the fluid energy density, P as the fluid equilibrium pressure, and n as the charge density. The set of conservation laws,

$$\nabla_{\mu}T^{\mu\nu} = 0\,, \qquad \nabla_{\mu}\mathcal{J}^{\mu} = 0\,, \qquad (2.3)$$

contains five equations for six unknowns (ϵ, P, the three independent components of the fluid four-velocity u^{i} and n). Therefore, an additional equation is required to close the system. This is provided by the EoS, $P = P(\epsilon, n)$, encoding the entire microscopic information on the medium.

Viscous hydrodynamics from an entropy principle. We discuss here a system that displays dissipative corrections to local thermal equilibrium. To take such effects into account, one can consider small deviations from local equilibrium. Restricting again ourselves to the case of a single conserved charge Q, the conserved quantities can be decomposed as

$$T^{\mu\nu} = T^{\mu\nu}_{\text{eq}} + \Pi^{\mu\nu} + q^{\mu}u^{\nu} + q^{\nu}u^{\mu}\,, \qquad \mathcal{J}^{\mu} = \mathcal{J}^{\mu}_{\text{eq}} + \nu^{\mu}\,, \qquad (2.4)$$

where $T^{\mu\nu}_{\text{eq}}$ and $\mathcal{J}^{\mu}_{\text{eq}}$ correspond to the equilibrium quantities defined in Eq. (2.1). The viscous corrections $\Pi^{\mu\nu}$ are expressed by

$$\Pi^{\mu\nu} = \pi^{\mu\nu} - \Pi\Delta^{\mu\nu}\,. \qquad (2.5)$$

The shear-stress tensor $\pi^{\mu\nu}$ is the viscous correction to the anisotropic energy flow and disfavors the movement of adjacent layers of fluid in opposite directions. It is a symmetric,

---

[1]The metric can in principle be non-Minkowskian, therefore all the derivatives are assumed to be covariant not to lose generality.

traceless tensor, orthogonal to the fluid four-velocity,

$$\pi^{\mu\nu} = \pi^{\nu\mu}, \qquad \pi^{\mu}_{\mu} = 0, \qquad u_{\mu}\pi^{\mu\nu} = u_{\nu}\pi^{\mu\nu} = 0. \qquad (2.6)$$

The bulk viscous pressure Π is the out-of-equilibrium correction to the isotropic pressure and contrasts the radial expansion of the fluid.

Additional corrections, parametrized by q^{μ} and ν^{μ}, account respectively for heat flow and charge diffusion. Both four-vectors are orthogonal to the fluid velocity, therefore satisfying the constraints

$$u_{\mu}q^{\mu} = 0, \qquad u_{\mu}\nu^{\mu} = 0. \qquad (2.7)$$

While ϵ, u^{μ}, and μ are well defined in local thermal equilibrium, out of equilibrium they have no first-principles microscopic definitions and thus should be viewed as merely auxiliary variables used to parametrize the physical observables $T^{\mu\nu}$ and $\mathcal{J}^{\mu}$. Hence, there is some freedom in defining these quantities, as long as all definitions agree in local thermal equilibrium. In the following, we define the fluid four-velocity in the Landau frame [49] as the time-like eigenvector of the energy-momentum tensor,

$$T^{\mu\nu}u_{\mu} = -\epsilon u^{\nu}. \qquad (2.8)$$

In this frame, the heat flow vanishes[2] and the energy density is defined as the eigenvalue of the energy-momentum tensor associated with the eigenvector u^{μ} through Eq. (2.8).

For fluid dynamics to be applicable, dissipative currents shall be much smaller than the equilibrium fields. This condition is often expressed in terms of inverse Reynolds numbers,

$$\mathrm{Re}_{\Pi}^{-1} \equiv \frac{|\Pi|}{P}, \qquad \mathrm{Re}_{\pi}^{-1} \equiv \frac{|\pi^{\mu\nu}|}{P}, \qquad \mathrm{Re}_{\nu}^{-1} \equiv \frac{|\nu^{\mu}|}{n}, \qquad (2.9)$$

being smaller than 1.

In the viscous case, one needs additional relations to determine the bulk viscous pressure, the five independent components of the shear stress, and the three independent components of the diffusion current. The original constructions of relativistic hydrodynamics by Eckart [50], and by Landau and Lifshitz [49] followed from imposing the validity of the second thermodynamic principle, i.e. $\nabla^{\mu}s_{\mu} \geq 0$, where $s^{\mu} = su^{\mu}$ is the entropy current and s is the entropy density. This leads to an expression of the dissipative currents in terms of first-order gradients of the fluid velocity, temperature, and chemical potential to temperature ratio $\alpha \equiv \mu/T$ (*first-order*

---

[2]Another possible choice, for instance, is the Eckart frame [50], where one imposes the charge diffusion current to vanish, $\nu^{\mu} = 0$. The Landau frame is the most natural choice in heavy-ion collisions since usually even if the net-charge density is zero there can be charge diffusion. However, other choices can be made as demanded by the physics problem.

hydrodynamics). These constitutive relations read

$$\Pi = -\zeta \nabla_\mu u^\mu \,, \tag{2.10}$$

$$\pi^{\mu\nu} = 2\eta \sigma^{\mu\nu} \,, \tag{2.11}$$

$$\nu^\mu = \kappa_n \nabla^{\langle\mu\rangle}\alpha \,, \tag{2.12}$$

where $\sigma^{\mu\nu} \equiv \nabla^{\langle\mu}u^{\nu\rangle}$[3]. We identify the coefficients ζ, η, and κ_n with the bulk viscosity, shear viscosity, and charge-diffusion coefficient, respectively. The advantage of first-order hydrodynamics is that all dissipative currents can be expressed in terms of gradients of quantities that are well-defined in local thermal equilibrium. However, this description allows for superluminal propagation, leading to the violation of the relativistic causality principle[4] [52–54].

A causal formulation of relativistic fluid dynamics was proposed by Müller [55] as well as Israel and Stewart [56] (MIS). In this description, the dissipative quantities are promoted to dynamical variables evolving according to an equation of motion (*second-order hydrodynamics*),

$$\dot{\Pi} = -\frac{1}{\tau_\Pi}[\Pi + \zeta\nabla_\mu u^\mu] \,, \tag{2.13}$$

$$\dot{\pi}^{\mu\nu} = -\frac{1}{\tau_\pi}[\pi^{\mu\nu} - 2\eta\sigma^{\mu\nu}] \,, \tag{2.14}$$

$$\dot{\nu}^\mu = -\frac{1}{\tau_n}[\nu^\mu - \kappa_n\nabla^{\langle\mu\rangle}\alpha] \,. \tag{2.15}$$

Their evolution has a characteristic timescale, given by τ_Π, τ_π and τ_n respectively, after which the dissipative fields relax to their asymptotic Navier-Stokes values, represented by Eqs. (2.10),(2.11) and (2.12).

In Ref. [57], a more general structure of second-order hydrodynamic equations was proposed. It was demonstrated that MIS equations do not contain all the allowed second-order terms and, specifically, the ones required by conformal invariance. The general expression for the second order terms for a conformal uncharged fluid in Landau frame in a curved background was found in Ref. [57] using conformal symmetry,

$$\begin{aligned}
\Pi^{\mu\nu} = &- \eta\sigma^{\mu\nu} + \eta\tau_\pi\left[D\sigma^{\mu\nu} + \frac{1}{3}\sigma^{\mu\nu}\nabla\cdot u\right] + \kappa\left[R^{\langle\mu\nu\rangle} - (2u_\alpha R^{\alpha\langle\mu\nu\rangle\beta})u_\beta\right] \\
&+ \lambda_1\sigma^{\langle\mu}_\lambda\sigma^{\nu\rangle\lambda} + \lambda_2\sigma^{\langle\mu}_\lambda\Omega^{\nu\rangle\lambda} + \lambda_3\Omega^{\langle\mu}_\lambda\Omega^{\nu\rangle\lambda}
\end{aligned} \tag{2.16}$$

where $R^{\alpha\mu\nu\beta}$ is the curvature tensor and $R^{\mu\nu}$ is the Ricci tensor. The tensor $\Omega^{\mu\nu} = \frac{1}{2}\Delta^\mu_\alpha\Delta^\nu_\beta(\nabla^\alpha u^\beta -$

---

[3]We define $A^{\langle\mu_1\cdots\mu_n\rangle} = \Delta^{\nu_1\cdots\nu_n}_{\mu_1\cdots\mu_n}A^{\mu_1\cdots\mu_n}$ by using the symmetrized and, for $n > 1$, traceless projection orthogonal to the fluid velocity as in Ref. [45].

[4]Recent theoretical advancements [51] have demonstrated the feasibility of a causal approach to dissipative relativistic fluid dynamics at the first order. This establishes a set of stable frames, from which the Landau frame is excluded. The presence of these stable frames implies that viscous relativistic fluids can be described using temperature, fluid velocity, and chemical potential alone – similar to non-relativistic fluids. This questions the necessity of frameworks like Israel-Stewart and similar constructions in developing a coherent relativistic hydrodynamic theory.

$\nabla^\beta u^\alpha)$ was introduced, together with the second-order transport coefficients κ, λ_1, λ_2, and λ_3. The generic expression for the dissipative tensor in the Landau frame without the assumption of conformal symmetry was derived in Ref. [58].

Viscous hydrodynamics from kinetic theory. From a microscopic point of view, hydrodynamic equations can be derived from the relativistic Boltzmann equation,

$$p^\mu \partial_\mu f(x,p) = \mathcal{C}[f]\,, \tag{2.17}$$

allowing for a direct mapping between the transport coefficients (and correspondent relaxation times) and the collision integral. The energy-momentum tensor and conserved currents can be written in terms of moments of the on-shell single-particle distribution $f(x,p)$,

$$T^{\mu\nu} = \int dP p^\mu p^\nu f(x,p)\,, \qquad \mathcal{J}^\mu = \int dP p^\mu f(x,p)\,, \tag{2.18}$$

where $dP = g d^3p/[(2\pi)^3 p^0]$ is the Lorentz-invariant momentum-space volume, with g accounting for the particle's internal degrees of freedom. The conservation laws can be retrieved by considering the 0th and 1st moments of the Boltzmann equation,

$$\partial_\mu \int dP p^\mu f(x,p) = \int dP \mathcal{C}[f] = 0\,, \tag{2.19}$$

$$\partial_\mu \int dP p^\mu p^\nu f(x,p) = \int dP p^\nu \mathcal{C}[f] = 0\,, \tag{2.20}$$

which vanish due to the microscopic conservation of energy, momentum, and number of particles encoded in the collision integral.

In Ref. [45] a formulation of second-order hydrodynamic equations from a microscopic point of view was derived employing an extension of Grad's method of moments [59]. The *method of irreducible moments* consists of first expanding the single-particle distribution function around its equilibrium value and introducing an out-of-equilibrium component,

$$f(p,x) = f_{\text{eq}}(p,x) + \delta f(p,x)\,. \tag{2.21}$$

The out-of-equilibrium component is projected on a complete orthogonal basis given by tensors k^μ, $k^{\langle\mu}k^{\nu\rangle}$, etc.[5]. Integrating sequentially higher-order moments of the Boltzmann equations, one builds second-order equations of motion for the dissipative currents. The truncation of the infinite series of terms that contribute to the evolution of each variable can be consistently made at fixed order in inverse Reynolds and Knudsen numbers. The approximation derived by Israel

---

[5]The advantage of expanding the distribution function on this basis is that these tensors are irreducible under the Lorentz-transformation Λ^μ_ν that leaves the fluid four-velocity invariant, $\Lambda^\mu_\nu u^\nu = u^\mu$. This implies that they constitute an orthogonal basis. Therefore, the expansion coefficients can be straightforwardly obtained. In a non-orthogonal basis, this requires in general the inversion of an infinite-dimensional matrix, meaning that the exact form of the expansion coefficients cannot be obtained once the expansion is truncated.

and Stewart – often referred to as *14-moment approximation* since one finds equations for 14 independent hydrodynamic quantities – can be recovered by such a truncation, however with a different definition of the transport coefficients and relaxation times. This set of fluid-dynamic equations is named after its authors Denicol-Niemi-Molnar-Rischke (DNMR). DNMR equations up to linear order in the dissipative currents and the method of irreducible moments will be used in the core of this work to describe equations of motion and transport coefficients for heavy-quark diffusion in the medium. More details on the method applied to the case of interest will be given in Chapter 5.

2.2   Analytic solutions to fluid-dynamic equations

To understand some general features of hydrodynamic equations, it is useful to consider simplified cases in which the calculations can be carried out analytically. Furthermore, in the context of numerical simulations, analytical solutions can be used as a baseline for code validation. We report here two famous examples of solutions for inviscid hydrodynamic equations, namely Bjorken and Gubser flow, which have been extensively employed in the heavy-ion literature.

Bjorken flow. The Bjorken approximation [60] describes a system that is invariant under longitudinal Lorentz boosts and azimuthally symmetric. These assumptions effectively reduce the fluid flow to a one-dimensional expansion along the beam axis (z) with no transverse flow in the x and y direction,

$$u^\mu = (u^t, 0, 0, u^z) \,. \tag{2.22}$$

This represents a valid description for the early expansion of the QGP at the center of the fireball before the time becomes of the order of the radius of the colliding nuclei. A suitable system of coordinates is given by

$$\tau = \sqrt{t^2 - z^2} \,, \qquad \eta = \frac{1}{2} \log\left(\frac{t+z}{t-z}\right) \,, \tag{2.23}$$

where τ is the *longitudinal proper time* and η the *spatial rapidity* describing the forward light-cone emanating from the collision point at $z = 0$. If the initial conditions on the energy density ϵ and spatial velocity $\vec{v}$ at $\tau = \tau_0$ are of the form

$$\epsilon(\tau_0, \eta) = \epsilon_0 \,, \qquad v^i(\tau_0, \eta) = (0, 0, z/t) \,, \tag{2.24}$$

such that they do not depend on rapidity, all thermodynamic quantities at future times will depend only on the proper time τ. By imposing the conservation of the energy-momentum tensor in Eq. (2.3) one gets,

$$\frac{d\epsilon}{d\tau} = \frac{\epsilon + p}{\tau} \,. \tag{2.25}$$

By exploiting the ideal gas EoS, $\epsilon = 3P \propto T^4$, one finds

$$\epsilon(\tau) = \epsilon_0 \left(\frac{\tau_0}{\tau}\right)^{4/3}, \qquad T(\tau) = T_0 \left(\frac{\tau_0}{\tau}\right)^{1/3}, \tag{2.26}$$

where $T_0 = T(\tau_0)$. One can define the expansion rate of the fluid θ as

$$\theta = \nabla_\mu u^\mu, \tag{2.27}$$

which in the case of Bjorken flow simply yields $\theta = \tau^{-1}$.

Gubser flow. Gubser flow [61] represents a generalization of Bjorken flow allowing for an expansion in the transverse direction. It is invariant under longitudinal Lorentz boosts along the beam axis, and is symmetric under $SO(3)$ transformations in a de Sitter space obtained from a Weyl rescaling of the metric tensor,

$$g_{\mu\nu} \longrightarrow \hat{g}_{\mu\nu} \equiv \Omega^{-2} g_{\mu\nu}. \tag{2.28}$$

The most suitable choice of coordinates is given by the union of Eq. (2.23) with

$$x_\perp = \sqrt{x^2 + y^2}, \qquad \phi = \arctan\frac{y}{x}, \tag{2.29}$$

where $x_\perp$ parametrizes the radius of the system and ϕ the azimuthal angle. Studying the flow in de Sitter space and mapping it back to Minkowski space leads to the following behavior for the energy density[6],

$$\epsilon = \frac{\hat{\epsilon}_0}{\tau^{4/3}} \frac{(2q)^{8/3}}{[1 + 2q^2(\tau^2 + x_\perp^2) + q^4(\tau^2 - x_\perp^2)^2]^{4/3}}, \tag{2.30}$$

where q has the dimensions of an inverse length and is related to the size of the system, while $\hat{\epsilon}_0$ is an integration constant. The choice of q and ϵ_0 can be made to fix the initial temperature and size of the system in the transverse plane at $x_\perp = 0$ and $\tau = \tau_0$. Using the ideal EoS, the temperature reads,

$$T = \frac{\hat{T}_0}{\tau^{1/3}} \frac{(2q)^{2/3}}{[1 + 2q^2(\tau^2 + x_\perp^2) + q^4(\tau^2 - x_\perp^2)^2]^{1/3}}. \tag{2.31}$$

---

[6]Further details on the calculations can be found in Appendix A.1.

Chapter 3

Transport theory

This Chapter is mostly inspired from [62, 63].

3.1 Introduction to heavy-flavor transport

The diffusion of heavy quarks (charm and beauty) in the hot and dense QCD medium has long been recognized as a promising concept and phenomenological tool to probe the features of the QGP. The idea behind this is that the heavy-quark mass, M_Q, is parametrically large compared to the typical energy scales that characterize the QCD medium. This entails a series of theoretical and phenomenological advantages, specifically,

1. $M_Q \gg \Lambda_{\mathrm{QCD}}$, where Λ_{QCD} is the energy scale identifying the border of the perturbative-QCD regime. This inequality implies that the initial heavy-quark production is dictated by pQCD hard-scattering processes. The calculations regarding the initial state are therefore under reasonable control.

2. $M_Q \gg T$, where T is the temperature the plasma. This means that the thermal production of heavy quarks in the expanding QGP produced at LHC energies is negligible. The thermal production is in fact Boltzmann-suppressed, $\sim \exp(-M_Q/T)$. Therefore, the heavy-quark momentum distribution is modified only through the interaction with the medium. This modification can be analyzed – e.g. by looking at the R_{AA} of heavy-flavor hadrons – to gain information on the underlying QGP.

3. $M_Q \gg gT$, where $g^2 = 4\pi\alpha_s$ is the strong coupling factor ($g \sim 2$). This sets the typical momentum exchange in the heavy quark-medium interaction. As long as this relation holds, many soft-scattering processes are needed to significantly change the heavy-quark momentum distribution. Therefore, at low transverse momenta, a Brownian description

of heavy-quark diffusion is justified[1].

Over the last decade, heavy-flavor observables, i.e., transverse-momentum spectra and elliptic flow of hadrons containing charm or bottom quarks (or their decay products), have been measured with increasing precision [64–75], establishing themselves as optimal probes of QCD properties. This has triggered intense theoretical activity aimed at understanding the experimental results. In general, the modeling of heavy-quark diffusion in most transport approaches (see e.g. Ref. [62] for a recent review) consists of a multi-step process, involving

- **Heavy-quark production.** An initial condition for the heavy-quark momentum distribution must be provided. The heavy-quark production is a pQCD process requiring energies that are available only within the hard scatterings happening at the very beginning of the collision. The initial transverse momentum distribution can be calculated via QCD event generators [76, 77] validated on pp data or analytical calculations at fixed perturbative order (FONLL [78, 79])[2]. Alternatively, one can rely on the momentum distribution of charm hadrons measured in pp collisions (see e.g. [70, 82]).

- **Bulk evolution.** A numerical code to treat heavy-quark diffusion in the medium requires the support of a hydrodynamic code simulating the evolution of the QGP, validated on soft-hadron observables (see e.g. [34–36]). In particular, information on the fluid four-velocity and temperature is needed at each point in spacetime to update the heavy-quark momentum distribution.

- **Heavy-quark transport coefficients.** The heavy-quark momentum and spatial diffusion coefficients are quantities that can in principle be computed in QCD. Semi-analytical calculations are able to provide such information under certain approximations, such as under the assumption of weak [83] or strong coupling [84]. LQCD calculations, however, have shown dramatic progress in the past years in the computation of heavy-quark transport coefficients. Results for momentum and spatial diffusion coefficients for physical values of light- and heavy-quark masses have recently been computed in a temperature range of $195 < T < 352$ MeV [85]. Alternatively, transport coefficients for the heavy quark can indirectly be inferred by systematically comparing the results of the transport equations with the experimental observables, namely momentum and angular distributions.

---

[1]At the energies reached in high-energy nuclear collisions at RHIC and at the LHC, where the temperature of the fireball produced in central collisions can reach ∼400-600 MeV, this relation is not always satisfied for charm quarks. A model based on charm as a "heavy" particle requires, therefore, a certain care.

[2]In this case, one needs additionally to take into account the modification of the parton distribution function (PDF) of the nucleons when they are found inside a nucleus. Due to an effect known as *shadowing*, nuclear PDFs are suppressed at low parton momentum fractions due to multiple scatterings of the projectile with quarks and gluons inside the nucleus [80, 81]. The modification of the hard production from nPDFs is one of the largest sources of uncertainty in the state-of-the-art transport models.

- **Heavy-quark dynamics.** The heavy-quark dynamics in the QGP can be addressed with relativistic transport approaches. They require input from the simulation of the bulk evolution of the medium and transport coefficients. A more detailed description of such approaches is presented in Sec. 3.2.

- **Hadronization.** At $T \sim T_{\text{pc}}$, the transition from quark to hadronic degrees of freedom takes place. The modeling of the transition from color charges to color-neutral objects is one of the most challenging tasks in high-energy nuclear physics. Besides already not being fully understood in pp collisions, the modification of the process in heavy-ion collisions due to the presence of the medium is not yet under control. This represents a source of systematic uncertainty in the extraction of the transport coefficients from phenomenological studies, since the measured observables are not the parent-heavy quarks but their hadronic daughters.

3.2 Transport theory

As anticipated in Sec. 3.1, a key point in the study of heavy flavors in heavy-ion collisions is the modeling of the heavy-quark in-medium dynamics. In a non-relativistic setup, the motion of the heavy quark can be described by the standard diffusion equation,

$$\partial_t n(t, \vec{x}) = D_s \nabla^2 n(t, \vec{x}) \,, \tag{3.1}$$

where n is the heavy-quark density, depending on spacetime, and $D_s > 0$ is the *spatial diffusion coefficient*. Eq. (3.1) can be directly solved in Fourier space, leading to the solution

$$\tilde{n}(t, \vec{k}) = \tilde{n}(0, \vec{k}) e^{-D_s |k|^2 t} \,. \tag{3.2}$$

Assuming as initial condition that all heavy quarks are placed in the origin,

$$n(0, \vec{x}) = N_0 \delta(\vec{x}) \longrightarrow \tilde{n}(t, \vec{k}) = N_0 \,, \tag{3.3}$$

it follows that

$$n(t, \vec{x}) = N_0 \int \frac{d^3 k}{(2\pi)^3} e^{ik \cdot x} e^{-D_s |k|^2 t} = N_0 \left(\frac{1}{4\pi D_s t} \right)^{3/2} e^{-\frac{x^2}{4 D_s t}} \,. \tag{3.4}$$

The density in the non-relativistic case evolves therefore as a Gaussian spreading in time. The broadening of the spatial distribution is quantified by the spatial diffusion coefficient via $\langle x(t)^2 \rangle = 2 D_s t$. It can be easily verified that this equation is in conflict with the relativistic causality principle. At a fixed time t, the density is not vanishing for $|x| > ct$, where $c = 1$ is the speed of light in natural units.

A relativistic generalization of the diffusion equation is therefore necessary. However, it is

not straightforward [63]. In particular, one can follow two main strategies,

- **Relativistic diffusion equation.** Also known as the *telegrapher's equation*, the relativistic diffusion equation takes the form

$$\tau_n \partial_t^2 n + \partial_t n = D_s \nabla^2 n \,, \tag{3.5}$$

  where the dependence of n on spacetime coordinates was omitted. This second-order partial differential equation (PDE) can be recast in a set of first-order PDE by using the continuity equation,

$$\partial_t n + \vec{\nabla} \cdot \vec{j} = 0 \,, \tag{3.6}$$

$$\tau_n \partial_t \vec{j} + \vec{j} = D_s \vec{\nabla} n \,. \tag{3.7}$$

  This formulation does not allow for acausal propagation, and it is equivalent to the diffusion equation presented in Chapter 2 when $\vec{\nabla} n \sim \vec{\nabla} \alpha$.

- **Relativistic Boltzmann/Fokker-Planck equation.** It is a generalization of the diffusion equation which requires following not only the position of the particle but also its momentum. From a practical point of view, these equations provide a useful tool for modeling the dynamics of relativistic particles in a random environment.

The majority of the approaches in the heavy-quark literature employ the second strategy. We will therefore elaborate more thoroughly on its main ingredients.

3.2.1 Relativistic Boltzmann equation

The relativistic Boltzmann equation describes the evolution of a thermodynamic system far from equilibrium. It does not follow the position $\vec{x}_i$ and momentum $\vec{p}_i$ of each relativistic particle, but considers the evolution over time of the phase-space density $f(\vec{x}, \vec{p})$, that is, the probability that a generic particle occupies a volume $d^3\vec{x}$ centered in $\vec{x}$ in coordinate space and a volume $d^3\vec{p}$ centered in $\vec{p}$ in momentum space.

Let $f_Q(t, \vec{x}, \vec{p})$ be the phase space distribution for the heavy quark Q. The Boltzmann equation describing the evolution over time of $f_Q(t, \vec{x}, \vec{p})$ reads[3],

$$\frac{d}{dt} f_Q(t, \vec{x}, \vec{p}) = C[f_Q] \,, \tag{3.8}$$

where $C[f_Q]$ is the *collision integral* which accounts for momentum exchanges due to scattering processes. The total derivative with respect to time acting on the phase space distribution can

---

[3]For simplicity, the Boltzmann equation is here treated in a non-covariant form. The derivation of Eq. (3.8) from its covariant equivalent can be found e.g. in Ref. [86].

be rewritten in the following way,

$$\frac{d}{dt} = \frac{\partial}{\partial t} + \vec{v}\frac{\partial}{\partial \vec{x}} + \vec{F}\frac{\partial}{\partial \vec{p}}.$$

(3.9)

The last term is relevant when the particles are subjected to external forces, such as in the presence of an external electromagnetic field. To discuss general features of transport calculations, however, we can neglect the $\vec{x}$-dependence and the mean force fields. Under this approximation, Eq. (3.8) becomes

$$\partial_t f_Q(t, \vec{p}) = C[f_Q].$$

(3.10)

In the case of interest, the collision integral must account for the elastic scattering processes between the heavy quark Q and the light partons i of the medium through which the heavy quarks move. It can be written as,

$$C[f_Q] = \int d\vec{p'}d\vec{p_1}d\vec{p_1'}\{\bar{w}(\vec{p'}, \vec{p_1'}|\vec{p}, \vec{p_1})f_Q(\vec{p'})f_i(\vec{p_1'}) - \bar{w}(\vec{p}, \vec{p_1}|\vec{p'}, \vec{p_1'})f_Q(\vec{p})f_i(\vec{p_1})\},$$

(3.11)

where $\bar{w}$ represents the scattering rate, accounting – depending on the argument – for gain and loss processes, respectively. $\vec{p_1}$ and $\vec{p_1'}$ refer to the initial and final momentum of the light parton of the medium (or vice versa), while $\vec{p}$ and $\vec{p'}$ are the initial and final momentum of the heavy quark (or vice versa). The equation is here written in its classical limit, i.e. quantum corrections due to Bose enhancement for bosons or Pauli blocking for fermions are not included. By assuming that the scattering processes are symmetric under time-reversal transformations, the collision integral can be simplified as

$$C[f_Q] = \int d\vec{p'}d\vec{p_1}d\vec{p_1'}\bar{w}(\vec{p'}, \vec{p_1'}|\vec{p}, \vec{p_1})(f_Q(\vec{p'})f_i(\vec{p_1'}) - f_Q(\vec{p})f_i(\vec{p_1})).$$

(3.12)

To find stationary solutions of Eq. (3.10), the collision integral must vanish. Hence, one has to impose

$$f_Q(\vec{p'})f_i(\vec{p_1'}) = f_Q(\vec{p})f_i(\vec{p_1}),$$

(3.13)

For heavy quarks placed in a thermalized system of light particles, this entails

$$f_Q(\vec{p}) = \exp\left(-\frac{E_p}{T}\right), \quad f_i(\vec{p_1}) = \exp\left(-\frac{E_{p_1}}{T}\right).$$

(3.14)

The Boltzmann equation always makes the heavy quarks relax to a thermal distribution at the same temperature T of the medium in which they live. This is the result we are going to use as a baseline to derive the approximations of the Boltzmann equation in Sec. 3.2.2.

3.2.2 The Fokker-Planck equation

The Fokker-Planck equation is the approximation of the Boltzmann equation in the limit of multiple soft scatterings between the heavy quark and the light partons. Let us consider the

expression for the collision integral in Eq. (3.12). One can easily rewrite it by considering $\vec{k} = \vec{p'} - \vec{p}$ as the momentum gained by the outgoing heavy quark. The expression for the collision integral then becomes

$$C[f_Q] = \int d\vec{k}\, w(\vec{p} + \vec{k}|\vec{p})(f_Q(\vec{p} + \vec{k}) - f_Q(\vec{p})), \qquad (3.15)$$

where the dependence on the distribution of light partons is absorbed in w, which accounts for the transition rate of the process:

$$p, q \rightarrow p + k, q - k\,,$$

in which the heavy quark with momentum $\vec{p}$ interacts with a light quark, anti-quark or gluon with momentum $\vec{q}$ of the medium, gaining the momentum k. In the limit of small momentum exchange $|\vec{k}|$, one obtains

$$w(\vec{p} + \vec{k}|\vec{p})f_Q(\vec{p} + \vec{k}) \sim w(\vec{p}|\vec{p})f_Q(\vec{p}) + k_i \frac{\partial}{\partial p_i}(wf_Q) + \frac{1}{2}k_i k_j \frac{\partial^2}{\partial p_i \partial p_j}(wf_Q)\,. \qquad (3.16)$$

By plugging this approximation into Eq. (3.15) we obtain the expression for the Fokker-Planck equation,

$$\frac{\partial f_Q(t, \vec{p})}{\partial t} = \frac{\partial}{\partial p^i}\left\{A^i(\vec{p})f_Q(t, \vec{p}) + \frac{\partial}{\partial p^j}[B^{ij}(\vec{p})f_Q(t, \vec{p})]\right\}, \qquad (3.17)$$

where A^i and B^{ij} are defined as,

$$A^i(\vec{p}) = \int d\vec{k}\, k^i w(\vec{p} + \vec{k}|\vec{p})\,, \qquad (3.18)$$

$$B^{ij}(\vec{p}) = \frac{1}{2}\int d\vec{k}\, k^i k^j w(\vec{p} + \vec{k}|\vec{p})\,. \qquad (3.19)$$

By exploiting their tensor structure in a isotropic medium, one can rewrite A^i and B^{ij} as

$$A^i(\vec{p}) = A(p)p^i\,, \qquad (3.20)$$

$$B^{ij}(\vec{p}) = (\delta^{ij} - \hat{p}^i\hat{p}^j)B_0(p) + \hat{p}^i\hat{p}^j B_1(p)\,, \qquad (3.21)$$

where $A(p)$ represents a *friction* coefficient and B_0 and B_1 play the role of *momentum diffusion* coefficients. The physical meaning of these quantities will be clarified later on in this section. However, we have shown how the problem of the calculation of a complicated collision integral is now reduced to the evaluation of three transport coefficients, namely A, B_0 and B_1, which can be derived directly from the scattering amplitude of the particles.

To find the steady solutions of the Fokker-Planck equation, one can exploit the equilibrium solutions obtained for the Boltzmann equation in Section 3.2.1 and plug them into Eq. (5.8). This is going to lead to the relation that must be satisfied by the transport coefficients to make the heavy quarks relax to a thermal distribution. In order to make the right-hand side of Eq.

(5.8) vanish we impose,

$$A^i(\vec{p})f_Q^{eq}(t,\vec{p}) = -\frac{\partial}{\partial p^j}[B^{ij}(\vec{p})f_Q^{eq}(t,\vec{p})]\,. \tag{3.22}$$

By plugging in the Boltzmann solution shown in Eq. (3.14) and exploiting the tensor structure of the transport terms one gets,

$$A(p)p^i = \frac{B_1(p)}{TE_p}p^i - \frac{\partial}{\partial p^j}\{\delta^{ij}B_0(p) + \hat{p}^i\hat{p}^j(B_1(p) - B_0(p))\}\,, \tag{3.23}$$

leading to Einstein fluctuation-dissipation relation,

$$A(p) = \frac{B_1(p)}{TE_p} - \left\{\frac{1}{p}\frac{\partial B_1(p)}{\partial p} + \frac{d-1}{p^2}[B_1(p) - B_0(p)]\right\}\,, \tag{3.24}$$

where d is the number of spatial dimensions. It is useful to see how the Einstein relation enters the game in the case of a non-relativistic particle. In this case, the momentum dependence of the transport coefficients can be neglected and the latter can be written as

$$\gamma = A(p)\,, \tag{3.25}$$

$$D = B_0(p) = B_1(p)\,. \tag{3.26}$$

The Fokker-Planck equation is therefore reduced to

$$\frac{\partial f_Q(t,\vec{p})}{\partial t} = \gamma\frac{\partial}{\partial p^i}[p^i f_Q(t,\vec{p})] + D\delta^{ij}\frac{\partial^2}{\partial p^i p^j}[f_Q(t,\vec{p})]\,. \tag{3.27}$$

Starting from the initial condition,

$$f_Q(t=0,\vec{p}) = \delta(\vec{p} - \vec{p_0})\,, \tag{3.28}$$

one finds

$$f_Q(t,\vec{p}) \propto \exp\left(-\frac{\gamma}{2D}\frac{[\vec{p} - \vec{p_0}\exp{(-\gamma t)}]^2}{1 - \exp{(-2\gamma t)}}\right)\,. \tag{3.29}$$

Asymptotically, for $t \to \infty$, the solution *forgets* about the initial condition and relaxes to,

$$f_Q(\vec{p}) \propto \exp\left(-\frac{\gamma M}{D}\frac{\vec{p}^2}{2M}\right)\,, \tag{3.30}$$

which is a thermal distribution, with M being the mass of the heavy quark. If one compares Eqs. (3.30) and (3.14), by using the non-relativistic relation between energy and momentum, one gets

$$D = \gamma MT, \tag{3.31}$$

which is the non-relativistic Einstein fluctuation-dissipation relation, as anticipated. At this point, it becomes easier to understand why we referred to the transport coefficients as friction and diffusion coefficients. In fact, if we calculate the first moment of the equilibrium distribution

for the Fokker-Planck equation we find,

$$\langle \vec{p}(t) \rangle = \vec{p}_0 \, e^{-\gamma t} \,, \tag{3.32}$$

that is, γ leads the average momentum of the heavy quark to vanish as time passes, playing the role of a friction term; notice that γ has the dimensions of an inverse time. If we calculate the second moment of the distribution we find,

$$\langle \vec{p}^2(t) \rangle - \langle \vec{p}(t) \rangle^2 = \frac{3D}{\gamma}(1 - e^{-2\gamma t}) \overset{t \to 0}{\sim} 6Dt \,. \tag{3.33}$$

This represents the momentum broadening of the distribution due to the diffusion coefficient.

3.3   Remarks

Several transport approaches (see e.g. [62, 87] for recent reviews) have accomplished a qualitative or semi-quantitative agreement with part of the existing data, but no single approach is yet able to quantitatively describe all available heavy-flavor measurements from RHIC and the LHC, from low to high transverse momenta. An example is displayed in Fig. 3.1, taken from Ref. [65]. Here the average nuclear modification R_{AA} (left panel) and elliptic flow v_2 (right panel) of prompt D^0, D^+, and D^{*+} mesons in the 0–10% centrality class are compared with predictions of models implementing the charm-quark transport in a hydrodynamically expanding medium. The comparison with experimental measurements helps in finding model parameters that provide a good description of data. However, it is not sufficient to identify the underlying fundamental physics mechanisms that take place in a real heavy-ion collision.

The complexity of the problem involves knowledge of transport coefficients not only as a function of p_{T}, but also as a function of temperature. In addition, the accuracy of the information extracted from heavy-flavor observables relies on realistic modeling of the QGP expansion dynamics, as well as initial conditions for the heavy-quark momentum distributions and hadronization mechanisms. The presence of modifications due to cold-nuclear-matter effects in the incoming nuclei before the collision (*shadowing*), constitutes an additional source of uncertainty. The variety of transport models in the literature encodes different approaches to each of these ingredients. This fact makes it difficult to pin down information on the underlying physics. Further input from first-principle QCD calculations is therefore required.
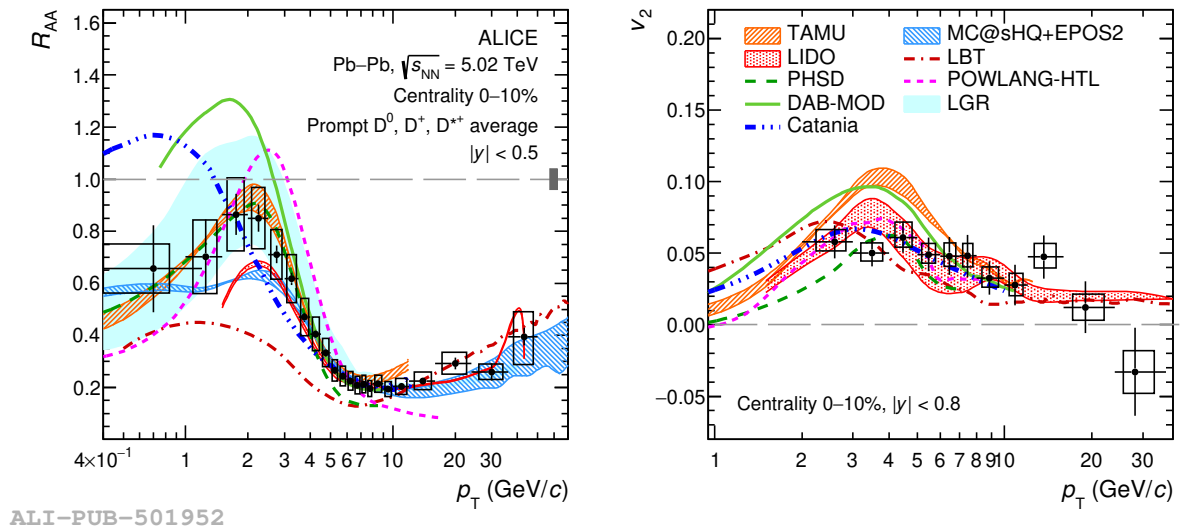
Figure 3.1: Average R_{AA} (left) and elliptic flow v_2 (right) of prompt D^0, D^+, and D^{*+} mesons in the 0–10% centrality class compared with predictions of models implementing the charm-quark transport in a hydrodynamically expanding medium. Fig. taken from Ref. [65].

Chapter 4

Hydrodynamization of heavy quarks

In this Chapter, an overview of the experimental and theoretical evidence regarding the possible thermalization of charm quarks in the medium is given. Furthermore, we will discuss the possible degree of thermalization of beauty quarks in the QCD medium.

4.1 Motivation

The question of heavy-quark thermalization in the medium has been challenging the scientific community for more than two decades [83, 88–92]. The modification of the heavy-quark momentum and spatial distribution is a signature of its interaction with the QGP constituents. Despite not being able to give a definitive answer, the first charm elliptic flow measurements in Au-Au collisions at RHIC [93] made it possible to understand that radiative scatterings could not be the only relevant process in the heavy-quark dynamics in the QGP. In particular, the role of elastic scatterings at low transverse momentum was highlighted in this context and required further investigation.

Heavy quarks are produced via hard (i.e. with high momentum transfer) scattering processes at the very beginning of the heavy-ion collision. Their initial momentum distribution is thus expected to be far from local kinetic equilibrium [78]. The dynamics of heavy quarks at high transverse momenta is dominated by radiative energy loss in the QGP. In the low transverse momentum region, on the other hand, heavy quarks offer a window to study equilibration processes. Especially for charm quarks, where the separation between the mass and temperature scale is not so obvious at LHC and RHIC top energies, the question of thermalization is particularly interesting.

As a rough estimate, the typical time required for a heavy quark to relax to thermal equilibrium is given by $\tau_{\text{heavy}} = M/T \tau_{\text{light}}$, where τ_{light} is the relaxation time associated with the light degrees of freedom (light quarks and gluons), $\tau_{\text{light}} \sim \eta/(\epsilon + P) \sim 1$ fm/c [7, 90]. Considering a plasma at a temperature of 250 MeV as in Ref. [90], a charm quark of mass $M \sim 1.5$ GeV would

take ~ 6 fm/c to reach thermal equilibrium. For beauty quarks, which have a mass of ~ 4.8 GeV, the relaxation time would be more than three times larger than the one of charm quarks. The lifetime of the QGP can be estimated, in the simplified case of Bjorken flow, as

$$\tau_{\text{lifetime}} = \tau_0 \left(\frac{T_0}{T_{\text{fo}}} \right)^3 , \tag{4.1}$$

where T_0 is the initial temperature of the medium, T_{fo} is the freeze-out temperature and τ_0 is the thermalization time of the QGP. By setting $\tau_0 = \tau_{\text{light}}$, $T_0 = 250$ MeV and $T_{\text{fo}} = 156.5$ MeV [94], one gets $\tau_{\text{lifetime}} \sim 4$ fm/c. Of course, this is just a raw picture, since in a realistic case the mass of the heavy quark should be substituted with its relativistic energy and the temperature of the surrounding medium depends on time and position. However, from these calculations, it seemed unlikely that charm quarks would thermalize within the lifetime of the QGP, and impossible that this could happen for beauty quarks. For this reason, as discussed in Chapter 3, many transport models were developed in the literature. In each of these models, the heavy quark is treated separately from the medium evolution, with a dedicated Boltzmann/Fokker-Planck-type simulation. The kinetic equilibration, in this case, comes in as an asymptotic solution at late times, possibly after the freeze-out occurs.

Besides being influenced by the bulk properties of the QCD medium (shear and bulk viscosity, hydrodynamic evolution, Equation of State), heavy quarks are mostly sensitive to the momentum diffusion coefficients (κ for elastic interactions, $\hat{q}$ for radiative energy loss) and spatial diffusion coefficient [90],

$$D_s = \lim_{p \to 0} \frac{T}{M A(p)} , \tag{4.2}$$

where $A(p)$ is the drag coefficient entering the Fokker-Planck equation defined in Chapter 3, which quantify their interaction with the surrounding thermal bath of light partons. These transport coefficients, together with their corresponding relaxation times, are fundamental properties of the QGP that can in principle be calculated from QCD. However, the state-of-the-art computations are performed far from realistic conditions. For example, the lattice community has always adopted the infinite-mass limit for the heavy quarks, and relied on the *quenched approximation*, that is, effectively considering an infinite mass for sea quarks. Only recently [85, 95], first results including physical masses for the light quarks and a mass dependence for the heavy-quark diffusion coefficient – therefore allowing for a distinction between charm and beauty quarks – have been produced. Furthermore, up to now there is no complete theoretical control over the dynamics of the system in the full temperature range covered by the heavy-ion collision down to $T \sim T_{\text{pc}}$.

Heavy quarks in the literature are usually treated as purely *hard* (i.e. associated with a high-energy scale) probes due to their large mass, even at low momentum. However, it is useful to consider that heavy quarks display a *soft* aspect as well. Specifically, the dynamics of charm

and beauty quarks at low momentum might not need the *ad hoc* description of an external probe randomly moving in a thermalized medium. The approach of heavy quarks towards thermalization is indeed part of their soft aspect, and it is mainly driven by D_s. Being sensitive to the transport coefficients, low-momentum heavy quarks can be used as a tool to constrain the transport properties of the QGP. This can be done by performing systematic comparisons with the experimental measurements of heavy-hadron momentum distributions and flow coefficients.

The interest in this matter lies in understanding the remarkable experimental results for harmonic flow coefficients of charmed hadrons and in particular of J/ψ [75, 96], which indicate the participation of charm quarks in the collective motion of the surrounding QGP medium. So far, no solid and agreed-upon answer to the thermalization question has been found within the context of transport models, calling for exciting new developments. In addition, the temperatures reached in Pb–Pb collisions at the LHC and Au-Au collisions at RHIC can be twice as large as 250 MeV [97], picturing a possible scenario where a certain level of thermalization takes place. Furthermore, recent experimental measurements and theoretical calculations point in the direction of early thermalization of charm quark in the plasma [75, 94–96, 98].

4.2 Thermalization versus hydrodynamization

To understand whether we can talk about the thermalization of heavy quarks in the QGP, we should first define what we mean by thermal equilibrium. In simple terms, thermal equilibrium is the state in which a system of particles with enough time to interact with each other would eventually relax. Let us now characterize this state more specifically, both from the macroscopic and the microscopic point of view.

Global and local thermal equilibrium. From the point of view of the second law of thermodynamics, *global* thermal equilibrium is achieved when the production rate of the entropy current s^μ is maximized and stationary, i.e. its differential satisfies $d(\nabla_\mu s^\mu) = 0$. The fulfillment of this condition generally depends on the spacetime metric [99]. However, in Minkowski spacetime, it is easily verified by having a uniform and constant fluid velocity, temperature (or energy density), and particle number (or chemical potential).

The condition of *local* thermal equilibrium postulated in fluid dynamics is that one can define the fluid velocity $u^\mu(x)$, temperature $T(x)$, and chemical potential $\mu(x)$ as general functions of space and time. The energy-momentum tensor and conserved current are assumed to have locally the same form as in global equilibrium. Imposing this condition gives rise to ideal hydrodynamic equations as presented in Section 2.

Kinetic and chemical equilibrium. Another distinction is the one between (local) kinetic equilibrium and (local) chemical equilibrium. These conditions require a more microscopic definition in terms of the momentum distribution of the particles in the system. In the case of

classical particles, kinetic equilibrium is achieved when the momentum distribution of the particles can be described by a Maxwell-Boltzmann distribution parametrized by a unique (local) temperature $T(x)$,

$$f(p, x) \propto \exp[-E(p)/T(x)] \,, \tag{4.3}$$

where p and x are the momentum and coordinate four vectors and E is the energy of the particle on shell. In the case of particles obeying quantum statistics, this is modified to be a Fermi-Dirac or Bose-Einstein distribution.

Chemical equilibrium means, on the other hand, that the momentum distribution can be parametrized by a unique (local) chemical potential $\mu(x)$,

$$f(p, x) \propto \exp[\mu(x)/T(x)] \,. \tag{4.4}$$

This exponential is often referred to as *fugacity* in Statistical Mechanics. In general, this chemical potential is given by a sum over all the conserved charges,

$$\mu = \sum_{i \in \{\text{charges}\}} q_i \mu_i = q_{\text{B}} \mu_{\text{B}} + q_{\text{S}} \mu_{\text{S}} + \ldots \,, \tag{4.5}$$

where μ_i is the chemical potential associated with the i-th conserved charge and q_i accounts for the amount of charge content. Here we highlighted, as an example, the baryon and strangeness contributions. In the following, we will focus on a single conserved charge, namely the heavy-quark pair number.

The case of heavy quarks. The expression for the heavy-quark pair chemical potential is given by

$$\mu = q_{Q\overline{Q}} \mu_{Q\overline{Q}} \,. \tag{4.6}$$

Charm quarks are initially produced out of chemical equilibrium. They are associated with the conservation of the number of charm-anticharm pairs – and therefore with the chemical potential given by Eq. (4.6). The constituents of the medium (light quarks, gluons) do not carry charm charge, and their corresponding charm-pair chemical potential is zero. An estimate of the chemical equilibration time for heavy quarks was studied in Ref. [100] and was found to be $\tau^{\text{chem}} \sim 65$ fm/c for charm quarks in a fireball with an initial temperature of 500 MeV. Compared with a typical expansion time of a fireball of order $\theta^{-1} \equiv (\nabla_\mu u^\mu)^{-1} \sim \tau \sim 0.5$ fm/c at the beginning of the collision, this implies that charm quarks stay out of chemical equilibrium for the whole lifetime of the expanding system. This means, in turn, that the annihilation rate of a heavy-quark pair $\Gamma^{\text{chem}}_{\text{heavy}} \equiv 1/\tau^{\text{chem}}_{\text{heavy}}$ is negligible both at RHIC and LHC energies. The heavy quark final abundance therefore remains unchanged throughout the whole fireball evolution and can be described by the initial hard production.

The initial hard production causes heavy quarks to be initially produced out of kinetic equi-

librium as well. If the deviations from local kinetic equilibrium are not too large, one can expand the distribution function of the heavy quark in terms of an equilibrium part and a first-order deviation,

$$f(x, p) \sim \exp[-E(p)/T(x) + \mu(x)/T(x)](1 + \delta f(x, p)). \tag{4.7}$$

The form of the equilibrium part follows from the grandcanonical formalism, since both the total energy of the system and the number of heavy quarks are conserved. Again, quantum corrections are here neglected and the equilibrium distribution function is assumed to be of the Boltzmann kind.

Studying the approach to equilibrium coincides with studying how the δf component evolves and (possibly) vanishes in time, e.g. using the Boltzmann equation presented in the previous Chapter. In this Thesis, however, we will present an alternative approach to study how the charm quarks relax to thermal equilibrium, based on fluid dynamics.

Hydrodynamization. Linear deviations from local thermal equilibrium in fluid dynamics can be expressed in terms of first-order gradients of the fluid velocity. These gradients are associated with dissipative quantities, namely the shear stress, bulk viscous pressure, and possible additional dissipative currents (e.g. charge diffusion), which contribute to the entropy production rate. In the second-order hydrodynamic formalism, the dissipative quantities are dynamical variables that obey an equation of motion. In particular, their relaxation towards their Navier-Stokes value happens on a time scale dictated by the correspondent relaxation time $\tau_{\rm R}$. This scale, which arises directly from the underlying microscopic theory [101], can be referred to as a *hydrodynamization* scale since it is the time scale in which the non-hydrodynamic modes are expected to exponentially decay. Non-hydrodynamic (or transient) modes are the excitations of the system whose dispersion relation $\omega(k)$ does not vanish in the short wavelength limit $(k \to 0)$. They can be observed by looking at the equations of motion in momentum space (see e.g. Ref [102]). They exponentially decay with $\tau_{\rm R}$, while the long-lived hydrodynamic modes survive. The system becomes describable by a set of few thermodynamic variables (T, u^{μ}, μ) and their gradients. However, the hydrodynamic system can be out of equilibrium, until the gradients do not vanish. In terms of distribution functions, the hydrodynamization process will lead δf to evolve to an asymptotic value which is not necessarily zero, as it would be in local kinetic equilibrium. The ratio of $\delta f/f_{\rm eq}$, as a sort of generalized inverse Reynolds number, gives an estimate of how far the system is out of equilibrium.

The validity of hydrodynamics is well established for the bulk of the QGP system, even if out-of-equilibrium corrections coming from the shear stress and the bulk viscous pressure survive the entire lifetime of the fireball. In this work, we will prove that the fluid-dynamic description can be extended to heavier degrees of freedom such as charm quarks. Studying the hydrodynamization of charm quarks provides us with a tool to determine how far they are from local kinetic equilibrium at all stages of the expanding system. At the same time, the fluid dynamic description of the
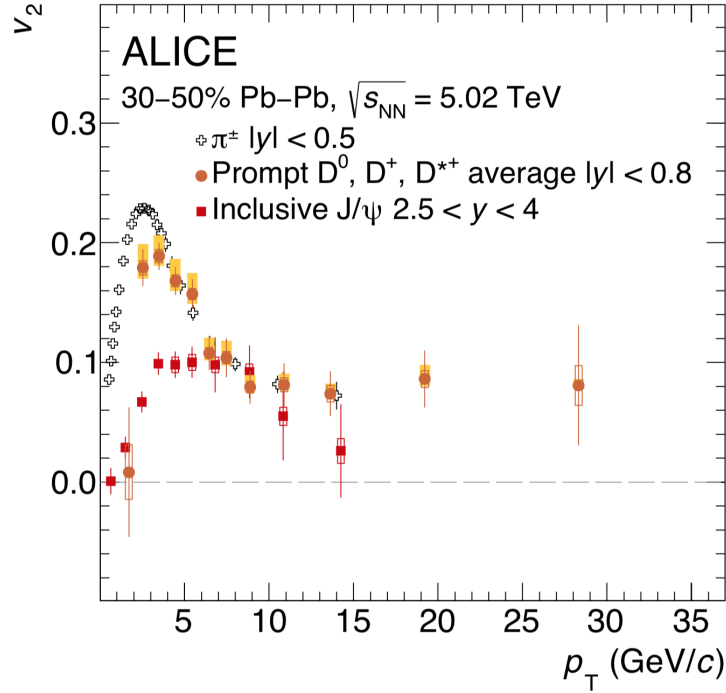
Figure 4.1: Recent experimental results [75, 96] show that open heavy-flavor and charmonium states – D mesons, J/ψ– have significantly positive elliptic flow, similarly to the one measured for light charged particles.

charm dynamics provides direct access to the spatial diffusion coefficient of the QGP, which is a fundamental quantity in QCD.

4.3   Evidence for charm-quark thermalization

Experimental evidence.   Recent experimental measurements of flow harmonics in Pb–Pb collisions at $\sqrt{s_{\mathrm{NN}}}$ = 5.02 TeV at the LHC [75, 96], carried out with unprecedented precision, show that open heavy-flavor and charmonium states – D mesons, J/ψ– have significantly positive elliptic flow. In Fig. 4.1, the v_2 of the average of D^0, D^+ and D^{*+} and the one of J/ψ as a function of transverse momentum p_T in the 30-50% centrality class is shown in comparison with the v_2 of charged pions. Remarkably, the measured elliptic flow for D mesons does not differ too much in magnitude from the one of light hadrons. Also, one should consider that a characteristic mass ordering at low p_T is induced by the radial flow. Radial flow leads to a depletion in the momentum spectrum by pushing the hadrons towards larger momenta, resulting in a reduction of v_2. Due to the dependence of momentum on the particle mass, this effect is more pronounced for heavier particles [2]. These observations raise questions about the possible heavy-quark (local) kinetic thermalization in the QGP. In a parton-like picture, the flow of open-charm states might be explained by the presence in the bound state of a light quark which was, before hadronization, part of the collectively-expanding QGP. On the other hand, the flow of J/ψ represents a striking
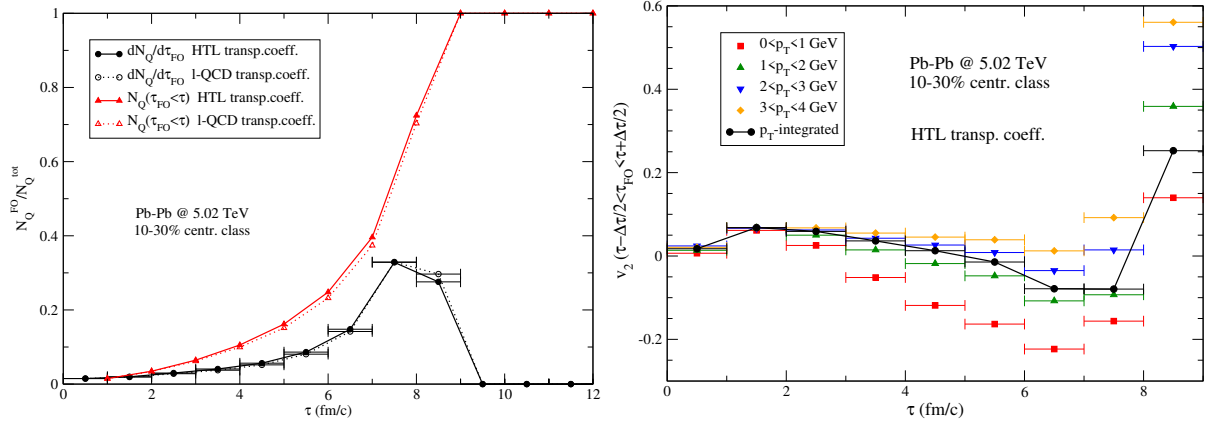
Figure 4.2: Left panel: fraction of charm quarks which decouple from the medium as a function of time for different values of the diffusion coefficient. Right panel: charm quark integrated v_2 in time for different p_T ranges. Figure from Ref. [98]

result: it must be attributed completely to the collective behavior of charm quarks due to their strong interaction with the QGP constituents.

The contribution of heavy quarks to v_2. In Ref. [98], the contribution of heavy quarks to flow harmonics in Pb–Pb collisions at $\sqrt{s_{NN}} = 5.02$ TeV as a function of the evolution time of the system has been studied. Transport coefficients computed in the Hard Thermal Loop (HTL) approximation [103] as well as results from Lattice-QCD [104] are employed. In the left panel of Fig. 4.2, the ratio between the number of charm quarks coupled to a frozen-out cell and the total number of charm quarks is shown as a function of proper time for different values of the transport coefficients (red curves). The black curves show instead the increment in the number of decoupled charm quarks with respect to the total number. Once all heavy quarks have decoupled from the medium, that is, when the correspondent fluid cell freezes out, the red curve reaches 1 and the black curve reaches 0. One can see that a large fraction of heavy quarks spends a long time in the medium before decoupling. In particular, only a small fraction of about 10% of heavy quarks spends in the medium a time shorter than 4 fm/c. The long-lived interaction with the surrounding QGP therefore must influence the final angular distribution of heavy quarks momenta. In the right panel of Fig. 4.2, the elliptic flow v_2 of charm quarks is computed as a function of proper time in different p_T-intervals (color online). The p_T-integrated v_2 of charm quarks is reported in black. From this plot, one can study how the elliptic flow signal is influenced by the time spent by the heavy quarks in the QGP. The observed positive elliptic flow for charm hadrons [75, 96] in different p_T intervals can be explained only if charm quarks spent a long time in the medium, around ~ 8 fm/c. This highlights the importance of the long-lived medium-heavy quark interplay and momentum exchange, which is behind the observed large elliptic flow signal measured at the LHC.

Charmed hadrons produced by a thermal source: the SHMc. In the context of the SHM, an extension was proposed in Ref. [94] to describe the integrated yields of charmed
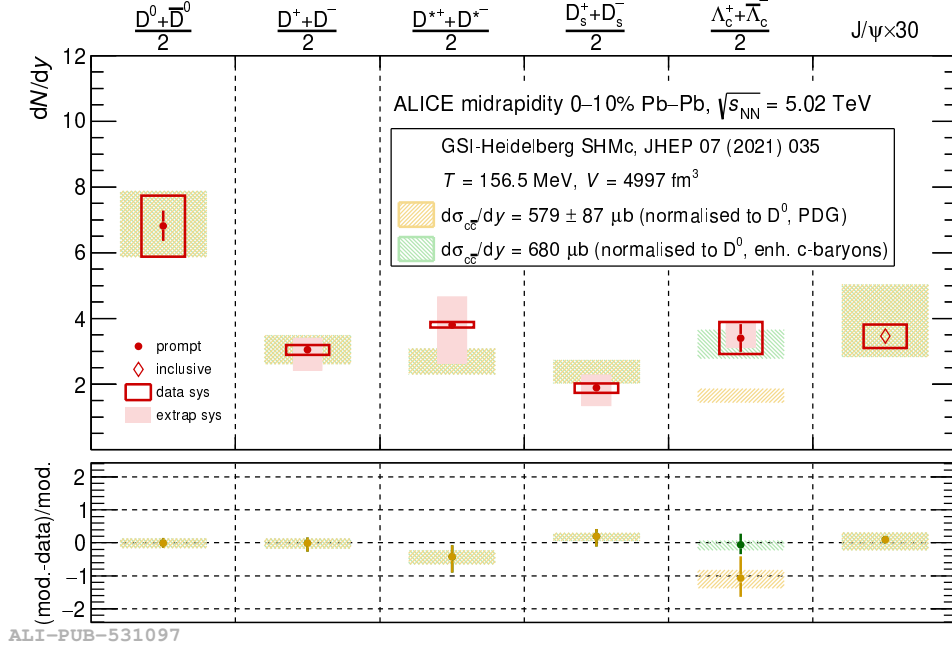
Figure 4.3: SHMc [94] predictions for charmed-hadrons integrated yields in comparison with the ALICE measurements [64–67]. The yellow bands include measured resonance states only. The green bands include estimations for not-yet measured resonance state contributions, which would enhance the final production of charmed baryons. Figure from Ref. [2].

hadrons. If the charm quark is fully thermalized within the QGP when the freeze-out occurs, the abundance of charm hadrons could be described by a thermal distribution at the same temperature of the system. This temperature – $T_{\text{fo}} = 156.5 \pm 1.5$ MeV for central Pb–Pb collisions at $\sqrt{s_{\text{NN}}} = 2.76$ TeV – together with an estimate of the volume of the system, was extracted from a fit to light hadrons integrated yields in Ref. [105]. The only additional parameter needed to reproduce the experimental measurements for charm hadrons is the aforementioned fugacity factor g_c, which results in $g_c = 29.6 \pm 5.2$ [94]. This factor enters the charm balance equation and scales with the charm-charge content of the hadron of interest (g_c for states containing one charm/anticharm quark, g_c^2 for states with two charm quarks and so on). Assuming full thermalization of charm quarks, the integrated yields of charm hadrons are then determined by the total charm production cross section. The abundance of the different species depends on their thermal weight ($\sim e^{-M/T_{\text{fo}}}$) and charm content. When including resonance decay contributions, the model manages to successfully describe the experimental data for both open- and hidden-charm meson states as shown in Fig. 4.3. Some tension is observed in the description of Λ_c^+ baryons. This deviation might be caused by the absence in the PDG of additional higher resonance states that have not been measured yet [106–108]. The inclusion of estimates of such states, leads to a better description of the data (see the green band in the Figure). Other explanations based on a coalescence mechanism [109, 110] were also proposed and managed to successfully describe the data without the need to include additional resonance states. Future experimental measurements

will help in clarifying this discrepancy.

The fact that charm-hadron integrated yields can be described assuming that they are produced from a thermal source at the same temperature as the light hadrons suggests that charm quarks are close to local kinetic equilibrium when the freeze-out occurs. At the same time, the large value of the fugacity factor ($g_c \gg 1$) is in agreement with the fact that charm quarks are still out of chemical equilibrium and no charm-pair annihilation process has taken place. This is therefore a strong indication of charm-quark kinetic thermalization in the QGP at LHC energies.

Heavy-quark spatial diffusion coefficient. The heavy-quark spatial diffusion coefficient is directly proportional to the kinetic equilibration time of heavy quarks in the QGP medium in the zero-momentum limit. Therefore, the calculation of D_s gives an insight into the level of thermalization of heavy quarks. In Fig. 4.4 we show results for the heavy-quark spatial diffusion coefficient (lower axis) and correspondent kinetic equilibration time for charm quarks (upper axis) from various calculations evaluated at the pseudo-critical temperature $T_{\mathrm{pc}} \sim 155$ MeV and from data. The kinetic equilibration time is here defined as the inverse of the Fokker-Planck drag coefficient $A(p)$ at $p = 0$,

$$\tau_{\mathrm{kin}} = \frac{1}{A(p=0)} = \frac{M}{T}D_s = \frac{M}{2\pi T^2}(2\pi D_s T) \qquad (4.8)$$

The calculation of D_s can be performed via phenomenological studies or, under some approximations, on the lattice.

In the plot, STAR [69] and ALICE [65] are shown as examples of data-driven approaches to the estimate of D_s. In the case of STAR, it was observed that transport models with $2 \lesssim 2\pi D_s T_c \lesssim 12$ could reproduce the results for the R_{AA} and v_2 of D^0 meson. However, this finding still suffered from a large uncertainty in determining the expected value for the kinetic relaxation time of charm quarks due to the shortage of experimental measurements. More recently, the ALICE Collaboration [65] published a new result by performing simultaneous fits of various transport models to R_{AA} and flow coefficients of D mesons in Pb–Pb collisions at $\sqrt{s_{\mathrm{NN}}} = 5.02$ TeV. The spatial diffusion coefficient was to be $1.5 < 2\pi D_s T < 4.5$ at the pseudo-critical temperature $T_{\mathrm{pc}} = 155$ MeV. This results in turn in a thermalization time of 3-8 fm/c for charm quarks. Considering that the QGP produced in most central collisions lives for $\sim$10 fm/c, this would give charm quarks the time to thermalize within the plasma before the freeze-out occurs. This result is consistent with other Bayesian analysis approaches such as Ref. [111], where Pb–Pb results at $\sqrt{s_{\mathrm{NN}}} = 5.02$ TeV and 2.76 TeV were combined with Au-Au results at RHIC at 200 GeV. The data-driven approaches are therefore compatible within uncertainties, and they suggest that a kinetic equilibration of charm quarks might take place. Nevertheless, the precision of their results is still limited, forbidding to draw a definitive conclusion.

On the theoretical side, D_s can be computed by evaluating color-electric field correlators on the lattice [83], which provide the momentum broadening of an infinitely heavy quark (for
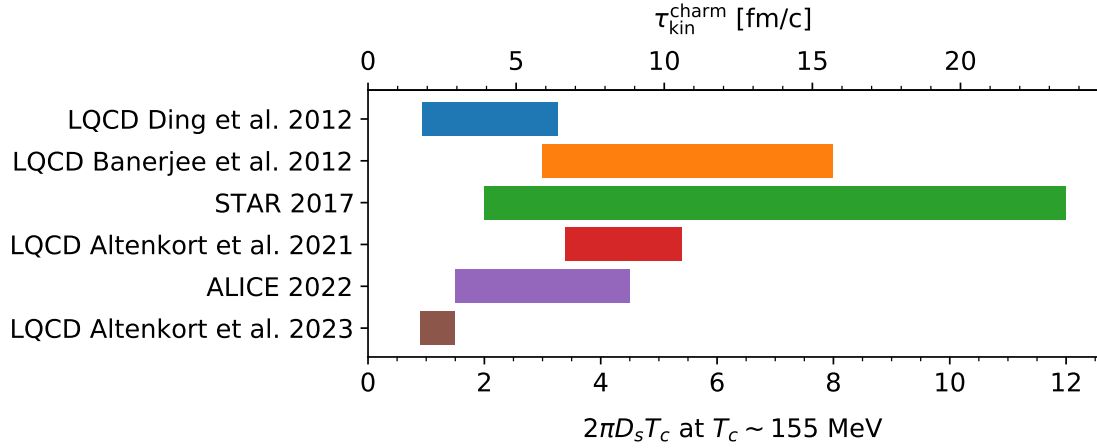
Figure 4.4: Results for the heavy-quark spatial diffusion coefficient (lower axis) and kinetic relaxation time of charm quarks computed as inverse drag coefficient A^{-1} (upper axis) from various calculations and experimental data [65, 69, 95, 104, 115, 116] evaluated in the vicinity of the pseudo-critical temperature $T_{\mathrm{pc}} \sim 155$ MeV.

more details see Ref. [62] and references therein). The above estimates for D_s are expected to be more reliable for objects with a larger mass, such as beauty quarks [112]. Nevertheless, as done in Ref. [113], one can attempt to apply these results to charm quarks as well. Furthermore, usually, these calculations are performed in the quenched approximation [114]. More recently, however, a new calculation on the Lattice with physical values for the light-quark masses was performed [95]. This provided a new and strong indication of charm thermalization in the QGP. The computation of the heavy-quark spatial-diffusion coefficient D_s with finite light-quark masses produced surprising results in comparison to previous calculations [115–117]. Very low values of D_s ($0.9 < 2\pi D_s T < 1.5$ at $T = 195$ MeV) correspond to a kinetic equilibration time of charm quarks of $\sim$1-1.5 fm/c. This means that, even if the heavy quarks are initially produced out of kinetic equilibrium, they will partake in the collective flow of the QGP early during the fireball evolution.

Recently, a study of the mass dependence of the heavy-quark spatial diffusion coefficient has been performed within the LQCD community [85]. The mass dependence enters as a correction to the momentum diffusion coefficient coming from magnetic-field correlators. The results from the LQCD calculation of $2\pi D_s T$ as a function of T/T_{pc} for charm, beauty and an infinitely massive quark are reported in Fig. 4.5 together with AdS/CFT [84], pQCD calculations [83] and phenomenological estimates from the ALICE collaboration [65] and transport models (QPM [112], Bayesian [111], T-Matrix [118]). The results for $2\pi D_s T$ for charm, beauty and infinitely massive quarks do not depend strongly on the heavy-quark mass in the investigated temperature range ($195 < T < 300$ MeV). At the same time, a clear discrepancy is observed between the LQCD results and the results extracted by transport models. In contrast, the LQCD results resemble the ones obtained in a strongly-coupled regime (AdS/CFT). This leaves room for exciting phenomenolog-
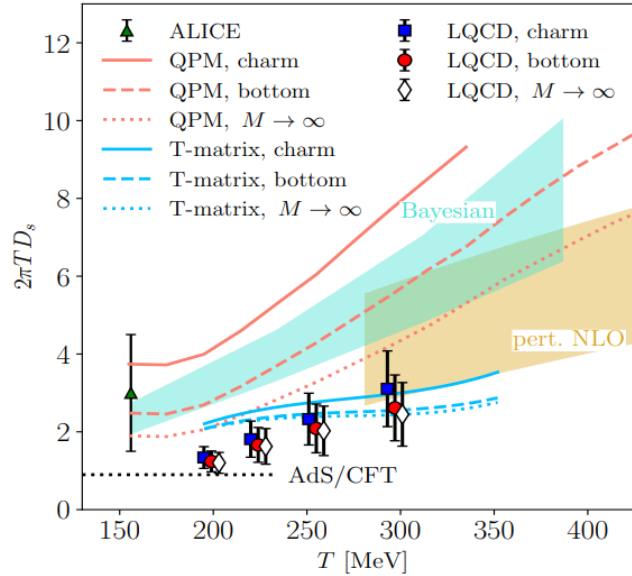
Figure 4.5: Results of LQCD calculation of $2\pi D_s T$ as a function of T/T_{pc} for charm, beauty and an infinitely massive quark together with AdS/CFT [84], pQCD [83] calculations and phenomenological estimates from the ALICE collaboration [65] and transport models (QPM [112], Bayesian [111], T-Matrix [118]).

ical developments since LQCD seems to predict a much faster hydrodynamization with respect to transport models and data-driven approaches.

4.4 Perspective on beauty quarks

Beauty quarks are, in a sense, a golden probe of the QGP. In fact, not only they are sensitive to the momentum and spatial diffusion coefficients of the QGP, but also, due to their large mass, their theoretical setup is much more under control with respect to charm quarks. On the one hand, they are much closer to the infinite-mass limit often adopted in theoretical calculations. On the other hand, the quasi-particle picture is expected to be more reliable and transport approaches are better justified [119]. Therefore, a better understanding of their dynamics is of huge relevance to pin down the properties of the QGP they interact with.

Having a larger mass with respect to charm, beauty quarks are less likely to achieve thermal equilibrium within the lifetime of the QGP. From a trivial mass-scale argument,

$$\tau_{\mathrm{kin}}^{\mathrm{beauty}} \sim \frac{M_b}{T}\tau_{\mathrm{kin}}^{\mathrm{light}} = \frac{M_b}{M_c}\tau_{\mathrm{kin}}^{\mathrm{charm}}, \tag{4.9}$$

they should take $\frac{M_b}{M_c} \sim 3$ times longer than charm quarks to thermalize. A quick rescaling of the upper x-axis in Fig. 4.4 immediately tells us that, according to most calculations, there is a chance for beauty quarks to thermalize only in the latest stages of the fireball – if at all.

A study from the authors of the SHM presented at Quark Matter 2022 [120] has shown
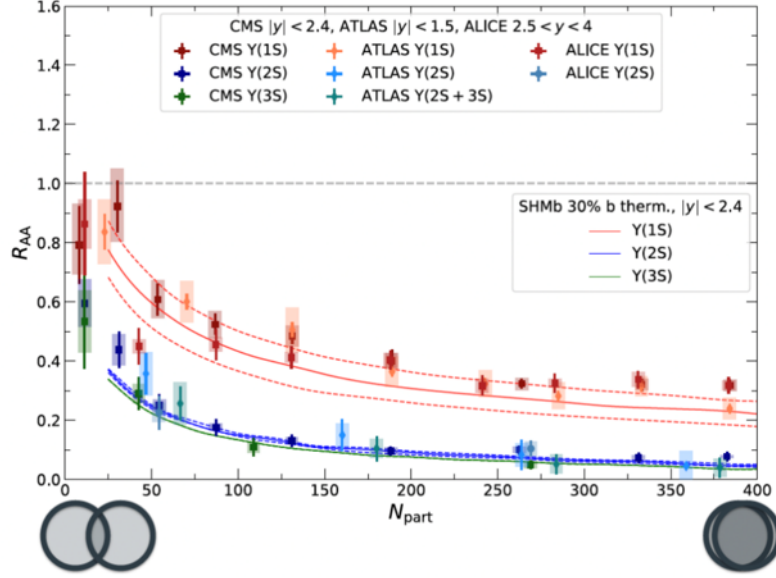
Figure 4.6: Nuclear modification factor R_{AA} of different bottomonium states measured by CMS [121], ATLAS [122] and ALICE [74] is shown as a function of the number of participant nucleons. The SHM calculations describe the experimental data if $\sim 30\%$ of beauty quarks are assumed to thermalize. Figure taken from [120].

how the assumption that only a fraction of the number of beauty quarks thermalizes allows to describe experimental measurements of integrated yields and R_{AA} of bottomonium states. In Fig. 4.6, the nuclear modification factor R_{AA} of different bottomonium states measured by CMS, ATLAS and ALICE [74, 121, 122] is shown as a function of the number of participant nucleons. The SHM calculations describe the experimental data if $\sim 30\%$ of beauty quarks are assumed to thermalize. In analogy with the case of charm quarks, this requires the introduction of a new parameter associated with a beauty fugacity g_b, of the order of 10^{10}. This opens the door to the possibility of a *partial thermalization* of beauty quarks in the medium produced at the LHC. At the same time, it raises the interesting question about the destiny of the non-thermalized beauty quarks.

The most recent LQCD computations [95] estimate that beauty quarks in the zero-momentum limit could thermalize within $\sim$3-4.5 fm/c. In addition, a recent study from the Catania group within a Boltzmann approach [112] pointed out that the naive mass scaling for the relaxation time might be violated when D_s is allowed to be mass-dependent. In fact, they obtained that $\tau_{\mathrm{kin}}^{\mathrm{beauty}} \sim 2\tau_{\mathrm{kin}}^{\mathrm{charm}}$, indicating a possible earlier thermalization for beauty quarks as well. Recently, first-principle calculations of mass-dependent D_s have been carried out on the lattice [85]. According to this study, no strong dependence of D_s on the heavy-quark mass is detected. Therefore, further studies are necessary to understand the observed discrepancy between the lattice calculations and the fit of transport models to experimental measurements available in the literature.

State-of-the-art measurements of the elliptic flow of bottomonium states from the CMS col-
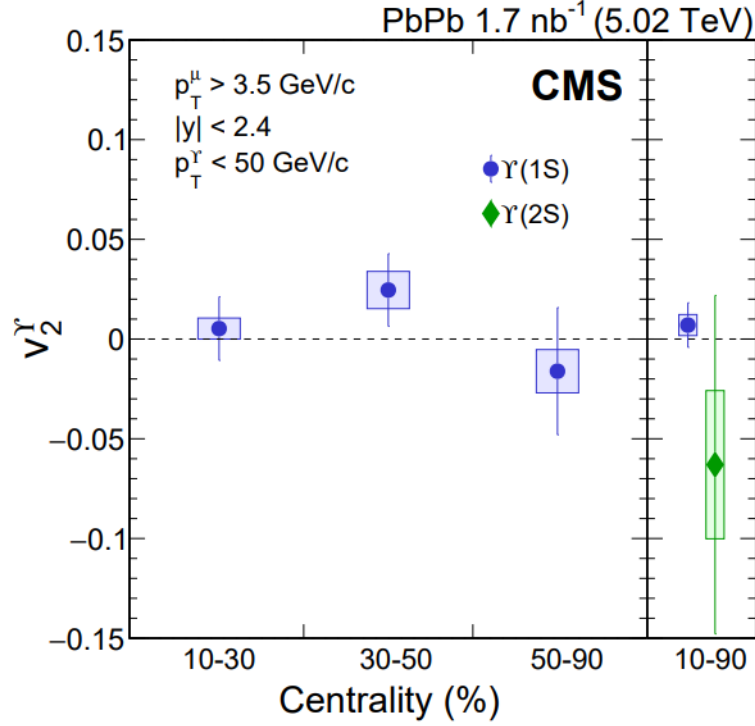
Figure 4.7: p_{T}-integrated v_2 values for $\Upsilon(1S)$ mesons measured in three centrality classes and for the $\Upsilon(2S)$ meson in the 10–90% centrality range for Pb–Pb at $\sqrt{s_{\mathrm{NN}}} = 5.02$ TeV. Figure from Ref. [123].

laboration [123] show that the v_2 signal in Pb–Pb collisions at $\sqrt{s_{\mathrm{NN}}} = 5.02$ TeV as a function of centrality is compatible with zero, meaning that possibly beauty quarks are mostly insensitive to the surrounding collective expansion (see Fig. 4.7). However, the precision of these measurements is not yet close to the one for charm or light hadrons. Also, the presence of not-yet-measured bottomonia states might still change the magnitude of the observed integrated yields for the lowest-energy states. Only more precise measurements of beauty hadrons at low transverse momenta will allow us to assess at which level beauty quarks relax to thermal equilibrium. It is in fact in this regime that beauty quarks have a higher chance to interact with the light partons and possibly reach kinetic equilibrium. In the near future, Run 3 at the LHC will provide beauty measurements with unprecedented precision, especially at low p_{T}. This will hopefully help clarify the question of beauty (partial) thermalization and the mass dependence of D_s.

Chapter 5

Heavy-quark transport in a fluid-dynamic approach

This Chapter is based on [124].

In this Chapter, we address the question of heavy-quark in-medium thermalization from the point of view of relativistic fluid dynamics. We consider a thermalized medium of light quarks and gluons and introduce an additional conserved current associated with the total number of heavy quark pairs. We build a mapping between the Fokker-Planck equation and second-order fluid dynamics to determine conductivities and relaxation times governing the spatial diffusion of heavy quarks. By investigating the relation between the two approaches, we provide insights concerning the level of local thermalization of charm and beauty quarks inside the expanding QGP. Our results indicate that a fluid-dynamic description of diffusion is feasible for charm quarks at least for the latest stages of the fireball evolution.

5.1   Introduction

In Chapter 4 experimental and theoretical evidence in favor of (partial) hydrodynamization of charm and beauty quarks in the QGP was presented. On these grounds, we outline here a way to treat the heavy quarks as part of the medium itself. Similarly to the most recent implementation of the Statistical Hadronization Model [94, 125–127], we work under the assumption that heavy quarks are close to local kinetic equilibrium in the QGP. However, we propose a fully dynamical treatment, studying how the heavy-quark spatial distribution evolves in time. This aspect has often been neglected in the literature but can provide deep insight into the level of thermalization of heavy quarks in the medium.

We assume that heavy quarks have enough time to interact with the light constituents of the thermalized plasma and to approach local kinetic equilibrium. This will be found to be a

reasonable assumption for charm in the stages in which the expansion of the medium is not too violent, that is, once the pressure gradients, at late times, have diminished. As was already mentioned, while one can realistically assume that charm quarks manage to get quite close to local kinetic equilibrium, a chemical thermalization would only happen over larger time scales, way beyond the typical timescale of a heavy-ion collision. The absence of chemical equilibration is a crucial ingredient in our approach and, as will be clarified in Sec. 5.2, guarantees that the heavy quark multiplicity is set by the initial production in hard scattering processes and remains almost unchanged during the medium evolution. The assumption of heavy-quark number conservation is a fundamental building block for the approach we are going to develop. Heavy-quark number conservation laws and the related continuity equations can be used to describe the diffusion dynamics in spacetime.

A universal fluid-dynamic description can be exploited to study the dynamics of both light and heavy degrees of freedom in the low transverse-momentum region. This is achieved without introducing new phenomenological parameters but exclusively using fundamental quantities such as viscosities for the light sector and the spatial diffusion coefficient plus relaxation rate for the heavy quarks. This approach requires the introduction of new dissipative quantities to initialize, namely the heavy-quark diffusion current, which describes the out-of-kinetic-equilibrium component of the heavy-quark current. Nevertheless, such a theoretical description is still much more economical than a numerical solution of the Boltzmann equation. At the same time, the implementation of an *ad hoc* transport code to be interfaced with the standard fluid-dynamic simulation of the QGP becomes unnecessary.

Eventually, heavy quarks could even affect the dynamics of the QGP itself and this could be naturally encoded into a system of coupled hydrodynamic equations. In other words, one could simultaneously study the dynamics of heavy quarks and their "back reaction" on the medium they are moving through. However, as a starting point, it is reasonable to assume that the heavy quarks do not influence significantly the energy density, pressure, velocity, or shear stress of the medium, since they are present in the QGP in a very small amount (e.g. ~ 15 $c\bar{c}$ pairs are produced in central collisions at $\sqrt{s_{\mathrm{NN}}} = 5.02$ TeV at mid-rapidity at the LHC). These quantities are mostly determined by the thermodynamics of the light quark and gluon degrees of freedom. The heavy quarks can be added "on top" of the fluid and their fluid dynamics is described by additional conserved currents. In the following, we pursue such an "on top" description.

5.2   Fluid-dynamic approach to heavy-quark diffusion

The present Section aims to introduce the heavy-quark conserved current that propagates causally in the QGP and the associated transport coefficient and relaxation time. It is crucial to construct the hydrodynamic approach such that causality is preserved even in the presence of dissipative ef-

fects associated with the finite mean-free path of the plasma particles. We employ a second-order hydrodynamic formalism in which the dissipative quantities (the heavy-quark diffusion current in this case) are promoted to dynamical variables that evolve according to certain equations of motion. These equations are governed by conductivities and relaxation times. The relaxation times have to be large enough to prevent the non-causal behavior; at the same time, they have to be smaller than the inverse expansion rate θ of the fireball (coinciding with the longitudinal proper time τ for a pure longitudinal Bjorken expansion) for the hydrodynamic approach to hold. The relaxation time (or hydrodynamization scale) tells us that we are dealing with out-of-equilibrium transient hydrodynamics for a time scale of the order of the relaxation time itself.

In our specific case, we want to include the conservation of a heavy quark-antiquark ($Q\overline{Q}$) current. Two relevant heavy-quark currents are

$$N_+^\mu \equiv \frac{N_Q^\mu + N_{\overline{Q}}^\mu}{2} \quad \text{and} \quad N_-^\mu \equiv N_Q^\mu - N_{\overline{Q}}^\mu, \tag{5.1}$$

associated to the conservation of the average $(+)$ and net $(-)$ heavy-quark number, respectively. In ultrarelativistic heavy-ion collisions, the net heavy-quark number vanishes and their average number coincides with the number of $Q\overline{Q}$ pairs initially produced in the hard scattering processes and conserved throughout the fireball evolution. The number of $Q\overline{Q}$ pairs is expected to be *accidentally* conserved during the evolution of the QGP. The mass of the heavy quarks is too large for them to be thermally produced [128]. At the same time, their annihilation rate is too small to lead to a measurable loss of $Q\overline{Q}$ pairs during the short lifetime of the plasma [100]. Hence their final multiplicity is fixed by the initial production in hard partonic processes described by pQCD. On the other hand, the net heavy-quark number is expected to be *exactly* conserved in QCD due to the symmetry of the strong interaction. In fact, the loss of a single quark/antiquark is forbidden by flavor conservation. The net heavy-quark current is not conserved by electroweak interactions instead. However, electroweak processes can be considered negligible within the lifetime of the QGP since they require much longer timescales.

Since the numbers of heavy quarks and antiquarks are separately conserved within the fireball lifetime, following the work in Ref. [45], we write the corresponding conserved currents including dissipative corrections as

$$\begin{aligned} N_{(r)}^\mu &= n_{(r)} u^\mu + \nu_{(r)}^\mu \,, \\ \nabla_\mu N_{(r)}^\mu &= 0 \,. \end{aligned} \tag{5.2}$$

Here $r = Q$ or $\overline{Q}$. The currents $N_{(r)}^\mu$ are decomposed along u^μ, the fluid four-velocity, and $\nu_{(r)}^\mu$, the heavy-(anti)quark diffusion currents, constructed to be orthogonal to u^μ, i.e. $u_\mu \nu_{(r)}^\mu = 0$. Notice that this last condition entails that in the Local Rest Frame (LRF) of the fluid – in which $u^\mu = (1, 0, 0, 0)$ – the time component of the diffusion currents $\nu_{(r)}^0$ vanishes. In this frame the time component of the current $N_{(r)}^\mu$ defines then the heavy-(anti)quark density $n_{(r)}$ even in the

presence of dissipative corrections.

At local kinetic equilibrium, we consider for quarks and antiquarks a classical[1] Boltzmann distribution,

$$f_{0k}^{(r)} = \exp\left(\frac{-E_k + \mu_r}{T}\right) = \exp\left(\frac{-E_k + q_r\mu_Q^{\text{net}} + \mu_Q^{\text{ave}}/2}{T}\right), \tag{5.3}$$

where $E_k = u_\mu k^\mu$ and corresponds to the heavy-quark energy k^0 in the LRF of the fluid, and μ_r is the heavy-quark/antiquark chemical potential. On the right-hand-side of Eq. (5.3), we decomposed μ_r in

$$\mu_Q = \mu_Q^{\text{ave}}/2 + \mu_Q^{\text{net}}, \qquad \mu_{\overline{Q}} = \mu_Q^{\text{ave}}/2 - \mu_Q^{\text{net}}. \tag{5.4}$$

The μ_Q^{net} is the chemical potential associated with the net N_-^μ conserved current and q_r is a charge factor – positive for quarks and negative for antiquarks. Additionally, one should consider that heavy quarks are produced out of chemical equilibrium in the QGP and their number is conserved during the subsequent evolution of the fireball. A chemical potential μ_Q^{ave}, the same for quarks and antiquarks, associated with their average number must be included to account for such a deviation from full thermodynamic equilibrium. This decomposition is consistent with the thermodynamic identities

$$n_{(r)} = \frac{\partial P}{\partial \mu_r}, \quad n_- = \frac{\partial P}{\partial \mu_Q^{\text{net}}}, \quad n_+ = \frac{\partial P}{\partial \mu_Q^{\text{ave}}}, \tag{5.5}$$

where P denotes here the heavy-quark pressure. It is often convenient to introduce the heavy-quark fugacity $\gamma_Q \equiv e^{\mu_Q^{\text{ave}}/2T}$[2] which can be factored out from the heavy (anti)quark distributions,

$$f_{0k}^{(r)} = \gamma_Q \exp\left(\frac{-E_k + q_r\mu_Q^{\text{net}}}{T}\right). \tag{5.6}$$

In the following, we simply focus on the conservation of the average heavy-quark number, since in most cases one is not interested in distinguishing hadrons arising from a Q or $\overline{Q}$ parent parton [3]. Furthermore, for simplicity, we assume that $N_-^\mu = 0$, i.e. $\mu_Q^{\text{net}} = 0$, since the initial hard processes lead to the production of the same number of quarks and antiquarks and we neglect any local unbalance developing during the hydrodynamic evolution. We define then $\sum_r n_{(r)}/2 \equiv n_+$ and $\sum_r \nu_{(r)}^\mu/2 \equiv \nu_+^\mu$. In this case, the dynamic evolution of the relevant diffusion current will be driven by a single chemical potential $\mu_Q = \mu_{\overline{Q}} = \mu_Q^{\text{ave}}/2$.

---

[1]Later in this Chapter we will analyze the contribution of quantum modifications to the heavy-quark distribution function.

[2]In Sec. 5.6 we provide an estimate of γ_Q in the case of a fluid undergoing Bjorken flow.

[3]An exception could be the difference Δv_1 in the directed flow of D^0 and $\overline{D}^0$ mesons proposed as a tool to extract information on the primordial magnetic field in the plasma [129]

We look for an equation of motion for the particle diffusion current in the form

$$\tau_n \Delta^\mu_\rho u^\sigma \partial_\sigma \nu^\rho_+ + \nu^\mu_+ = \kappa_n \Delta^{\mu\nu} \nabla_\nu \left(\frac{\mu_Q}{T} \right) , \tag{5.7}$$

This is a relaxation-type equation in which terms of higher order in the gradients are neglected. Two transport coefficients are present in Eq. (5.7), namely the relaxation time τ_n and the particle-diffusion coefficient κ_n. The presence of a relaxation time, as anticipated, is necessary in order to ensure the causality of the equation. For $\tau \gg \tau_n$, ν^μ_+ relaxes to its Navier-Stokes limit, $\nu^\mu_+ = \kappa_n \Delta^{\mu\nu} \nabla_\nu (\mu_Q / T)$.

5.3 Heavy-quark relaxation time and transport coefficients

The purpose of this Section is twofold. First, we study the relation between the transport coefficients defined in the hydrodynamic approach and the ones defined in transport theory (Fokker-Planck equation). Secondly, we show our numerical results for the hydrodynamic transport coefficients.

5.3.1 Matching Fokker-Planck with hydrodynamics

The definitions of the heavy-quark relaxation time τ_n and diffusion coefficient κ_n are deeply related to the collision integral entering the Boltzmann equation. One can start from the Fokker-Planck equation for the heavy (anti)quark distribution function $f_k^{(r)}$, written for the case of a homogeneous fluid at rest,

$$k^\mu \partial_\mu f_k^{(r)} = k^0 \frac{\partial}{\partial k^i} \left\{ A^i f_k^{(r)} + \frac{\partial}{\partial k^j} \left[B^{ij} f_k^{(r)} \right] \right\} , \tag{5.8}$$

where the indices $i, j = 1, 2, 3$ run over the spatial components of the correspondent four-momentum vector, and integrate subsequent moments of it, taking at the end the proper linear combination to get an equation for the diffusion current ν^μ_+. The mapping between the heavy-quark distribution function[4] and the fluid-dynamic quantities is encoded in the set of equations

---

[4] These relations quantify only the relative contribution of the heavy quark to the density, energy, pressure and dissipative currents of the total system. To compute the same quantities for the total system one should consider the sum over all the particle species, namely light quarks and gluons.

from kinetic theory (see e.g. [45]),

$$n_{(r)} = \langle E_k \rangle \,, \tag{5.9}$$

$$\nu^\mu_{(r)} = \langle k^{\langle \mu \rangle} \rangle \,, \tag{5.10}$$

$$\epsilon_{(r)} = \langle E_k^2 \rangle \,, \tag{5.11}$$

$$\pi^{\mu\nu}_{(r)} = \langle k^{\langle \mu} k^{\nu \rangle} \rangle \,, \tag{5.12}$$

$$P_{(r)} + \Pi_{(r)} = -\frac{1}{3} \langle \Delta^{\mu\nu} k_\mu k_\nu \rangle \,, \tag{5.13}$$

where we defined the average as

$$\langle ... \rangle = \int dK (...) f_k^{(r)} \,. \tag{5.14}$$

We decompose the distribution function $f_k^{(r)}$ in an equilibrium part plus a deviation,

$$f_k^{(r)} = f_{0k}^{(r)} + \delta f_k^{(r)} \,, \tag{5.15}$$

where in the equilibrium part we allow the chemical potential to depend on the spacetime point x, allowing for the development of a local excess of heavy quarks. The two pressure scalars are then separated into an equilibrium part and its deviation from equilibrium,

$$P_{(r)} = -\frac{1}{3} \langle \Delta^{\mu\nu} k_\mu k_\nu \rangle_0 \,, \quad \Pi_{(r)} = -\frac{1}{3} \langle \Delta^{\mu\nu} k_\mu k_\nu \rangle_{,,} \tag{5.16}$$

where we introduced the average over the equilibrium distribution function $f_{0k}^{(r)}$,

$$\langle ... \rangle_0 = \int dK (...) f_{0k}^{(r)} \,, \tag{5.17}$$

and the average over the deviation from equilibrium:

$$\langle ... \rangle_\delta = \langle ... \rangle - \langle ... \rangle_0 \,. \tag{5.18}$$

The zeroth moment of the Fokker-Planck equation simply gives the conservation or continuity equation, which, in the fluid rest frame, reduces to

$$\partial_t n_+ + \partial_i \nu^i_+ = 0 \,. \tag{5.19}$$

The first moment gives

$$\partial_t \int dK k^0 k^l f_k^{(r)} + \partial_i \int dK k^l k^i f_k^{(r)}$$

$$= \int dK k^l \left(k^0 \frac{\partial}{\partial k^i} \left\{ A^i f_k^{(r)} + \frac{\partial}{\partial k^j} \left[B^{ij} f_k^{(r)} \right] \right\} \right) \,. \tag{5.20}$$

In the following, we employ a simplified version of the approach developed by Denicol *et al.* in Ref. [45], i.e. the method of irreducible moments already mentioned in Chapter 2. We

first present the general features of the method. Later on, we truncate the moment expansion at rank-2 tensors, indicating that the only relevant dissipative quantities are the heavy-quark bulk pressure, diffusion current, and shear-stress tensor, often referred to as the 14-moment approximation.

Method of irreducible moments for heavy quarks. The moments of the out-of-equilibrium component of the heavy-quark/antiquark distribution function are expressed by

$$\rho_{(r)}^{\langle\mu_1..\mu_l\rangle} \equiv \Delta_{\nu_1..\nu_l}^{\mu_1..\mu_l} \int dK k^{\langle\nu_1}..k^{\nu_l\rangle} \delta f_k^{(r)} , \tag{5.21}$$

and are employed as a complete orthogonal basis onto which $\delta f_k^{(r)}$ is expanded,

$$\delta f_k^{(r)} = f_{0k}^{(r)} \left(\sum_{l=0}^{\infty} a_l^{(r)} \rho_{(r)}^{\mu_1..\mu_l} k_{\langle\mu_1}..k_{\mu_l\rangle} \right) , \tag{5.22}$$

where $a_l^{(r)}$ are the coefficients of the linear expansion. The projectors $\Delta_{\nu_1..\nu_l}^{\mu_1..\mu_l}$ to the fully symmetric, transverse and traceless part of a tensor are defined as in [45, 130]. Given a tensor $A^{\nu_1..\nu_l}$, by applying the projector $\Delta_{\nu_1..\nu_l}^{\mu_1..\mu_l}$ one obtains

$$A^{\langle\mu_1..\mu_l\rangle} \equiv \Delta_{\nu_1..\nu_l}^{\mu_1..\mu_l} A^{\nu_1..\nu_l} . \tag{5.23}$$

In order to obtain fluid-dynamic equations of motion, it is enough to consider the moments $\rho_{(r)}^{\langle\mu_1..\mu_l\rangle}$ up to rank two[5]. Stopping the expansion at second order, one only needs the usual transverse projector Δ_ν^μ and the four-index projector

$$\Delta_{\nu_1\nu_2}^{\mu_1\mu_2} \equiv \frac{1}{2}(\Delta_{\nu_1}^{\mu_1}\Delta_{\nu_2}^{\mu_2} + \Delta_{\nu_2}^{\mu_1}\Delta_{\nu_1}^{\mu_2}) - \frac{1}{3}\Delta^{\mu_1\mu_2}\Delta_{\nu_1\nu_2} . \tag{5.24}$$

Employing Eq. (5.21) to define the first three moments and exploiting the definitions in Eqs. (5.9), (5.10), (5.11), (5.12) and (5.13), one obtains

$$\begin{aligned} \rho_{(r)} &= -\frac{3}{M^2}\Pi_{(r)} , \\ \rho_{(r)}^\mu &= \nu_{(r)}^\mu , \\ \rho_{(r)}^{\mu\nu} &= \pi_{(r)}^{\mu\nu} , \end{aligned} \tag{5.25}$$

with $\Pi_{(r)}$, $\nu_{(r)}^\mu$ and $\pi_{(r)}^{\mu\nu}$ being respectively the bulk pressure, the diffusion current and the shear-stress tensor associated with the heavy (anti)quarks of mass M. In getting these results one has

---

[5]These moments can be, in fact, mapped onto the set of dissipative quantities employed in standard second-order relativistic fluid dynamics, namely shear stress, bulk viscous pressure, and diffusion current. Furthermore, their equations of motion derived within this approach can be systematically truncated at fixed order in Knudsen and inverse Reynolds numbers such that their evolution also depends only on up-to-rank-2 tensors.

exploited the Landau matching conditions, which ensure that

$$\int dK(k\cdot u)\delta f_k^{(r)} = 0 \quad \text{and} \quad \int dK(k\cdot u)^2\delta f_k^{(r)} = 0\,. \tag{5.26}$$

They are a way of fixing the temperature and chemical potential of the system, even when the latter is off-equilibrium, starting from the knowledge of the particle and energy density, obtained from the first two moments of the particle distribution.

Truncation scheme. By neglecting moments $\rho_{(r)}^{\mu_1\cdots\mu_l}$ of rank higher than 2, the dissipative correction to the heavy-quark distribution reads then

$$\delta f_k^{(r)} = f_{0k}^{(r)}\left(-a_0^{(r)}\frac{3}{M^2}\Pi_{(r)} + a_1^{(r)}\nu_{(r)}^{\mu}\,k_{\langle\mu\rangle} + a_2^{(r)}\pi_{(r)}^{\mu\sigma}\,k_{\langle\mu}k_{\sigma\rangle}\right). \tag{5.27}$$

In the expression above one can determine the coefficients $a_l^{(r)}$ by exploiting the definition of the bulk pressure, diffusion current, and shear stress in terms of the first three moments of $\delta f_k^{(r)}$ respectively (see Appendix B.1) obtaining

$$a_0^{(r)} = \frac{1}{I_{00}^{(r)}}\,, \quad a_1^{(r)} = -\frac{1}{P_{(r)}}\,, \quad a_2^{(r)} = \frac{1}{2I_{42}^{(r)}}\,, \tag{5.28}$$

where $P_{(r)}$ is the heavy-quark contribution to the pressure and the thermodynamic integrals $I_{nq}^{(r)}$, for the case of a medium at rest, are defined according to Ref. [45] as

$$I_{nq}^{(r)} = \frac{1}{(2q+1)!!}\int dK(k^0)^{n-2q}k^{2q}f_{0k}^{(r)}\,, \tag{5.29}$$

where n and q are integers. Notice that the bulk pressure $\Pi_{(r)}$ and shear stress $\pi_{(r)}^{\mu\nu}$ associated with the heavy (anti)quarks are expected to be much smaller than the ones appearing in the stress-energy tensor of the fluid dominated by gluons and light quarks. Furthermore, they will enter the equation for the heavy-quark diffusion current only through their derivatives (see Appendix B.2), providing corrections at least of second order in the gradients. Thus, we will neglect them in our treatment. We can then approximate

$$\delta f_k^{(r)} \approx -\frac{1}{P_{(r)}}f_{0k}^{(r)}\nu_{(r)}^{\mu}\,k_{\langle\mu\rangle}\,. \tag{5.30}$$

At first order in the gradients (i.e. neglecting bulk and shear corrections – see Appendix B.2 for more details on the calculations) we find a relaxation-type equation for the diffusion current of the form of Eq. (5.7), where the transport coefficients read

$$\tau_n = \frac{I_{31}^{(r)}}{(1/3)\int dK k^0 A(k)\,k^2 f_{0k}^{(r)}}\,, \tag{5.31}$$

$$\kappa_n = \frac{P_{(r)}T}{(1/3)\int dK k^0 A(k) k^2 f_0^{(r)}}\,n_{(r)}\,. \tag{5.32}$$

Eqs. (5.31) and (5.32) contain the information of the Fokker-Planck drag coefficient $A(k)$, which is in turn related to the momentum-diffusion coefficients $B_0(k)$ and $B_1(k)$ through the Einstein fluctuation-dissipation relation. Let us study how these relations simplify when neglecting the momentum dependence of the momentum-diffusion coefficients, assuming $D \equiv B_0 = B_1$, which is shown to be a reliable approximation up to heavy-quark momentum $k \sim 5$ GeV for beauty quarks [131]. By imposing the Einstein relation under this approximation, $A(k) = D/E_k T$, one obtains

$$\tau_n = \frac{T I_{31}}{DP} = \frac{D_s I_{31}}{T P_0} = \frac{(2\pi D_s T)}{96\pi T} \left(\frac{M}{T}\right)^3 \frac{2K_1(M/T) - 3K_3(M/T) + K_5(M/T)}{K_2(M/T)}, \qquad (5.33)$$

$$\kappa_n = \frac{T^2}{D} n_{(r)} = D_s n_{(r)}, \qquad (5.34)$$

where in Eq. (5.31) we have rewritten I_{31} in terms of Bessel functions of the second kind K_i[6]. The index r was omitted in Eq. (5.31) since the ratio I_{31}/P_0 is equal for quarks and antiquarks. Notice that in the non-relativistic limit we have

$$k^0 \sim M \,,$$

$$I_{31} \sim MP \,, \qquad (5.35)$$

and thus $\tau_n = A^{-1}$. This represents an important consistency check, since τ_n approaches, in the $M \gg T$ limit, the well-known result for the relaxation time arising from the solution of the non-relativistic Fokker-Planck equation.

We find that the relation $D_s = T^2/D$ between the spatial (D_s) and momentum (D) diffusion coefficients, usually found in studying the non-relativistic Brownian motion, arises naturally and holds also in this case in which the heavy particle undergoes a relativistic dynamics, with $E_k = \sqrt{k^2 + M^2}$. This is a non-trivial result, valid as long as the momentum dependence of D can be neglected.

5.3.2 Heavy-quark relaxation time

In Eqs. (5.33) and (5.34), we emphasized the linear dependence of the heavy-quark relaxation time on the spatial diffusion coefficient D_s. As an input for it, we use either LQCD calculations or experimentally extracted values.

In Fig. 5.1 the relaxation time τ_n multiplied by the temperature is shown as a function of the ratio M/T. Here and in the next plots the range of values assumed by τ_n is highlighted by the colored bands. Different colored bands correspond to different D_s estimates coming from LQCD simulations [114] and from fits to ALICE experimental data [65] (see Fig. 4.4). The heavy-quark relaxation time increases linearly with the M/T ratio when the latter is large enough. At

---

[6]This will be useful in the numerical implementation of these equations in Chapter 6.

a given temperature, the relaxation time is then larger for heavier quarks, as expected. This entails that the non-hydrodynamic phase lasts longer for beauty quarks than for charm quarks. The relaxation time τ_n is observed to be positive even at zero mass. This observation, although referring to a limiting case outside the domain of validity of our approximations, agrees with the second-order hydrodynamic description and guarantees causal propagation.
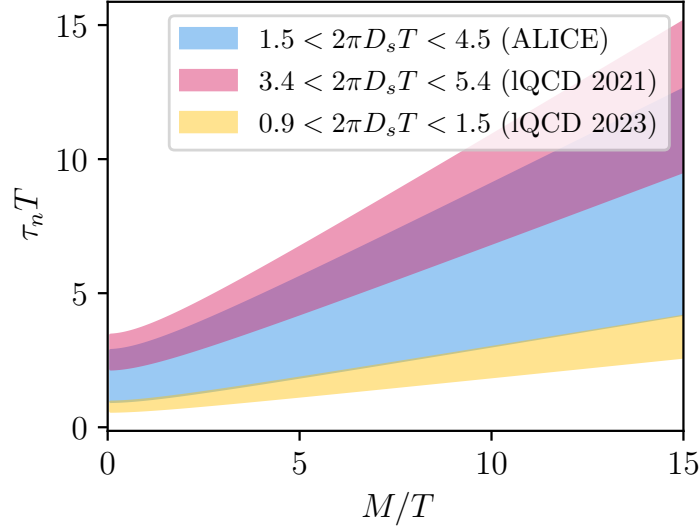

Figure 5.1: Heavy-quark relaxation time τ_n multiplied by temperature T as a function of M/T. The pink and yellow bands are computed using D_s estimates coming from LQCD simulations [85, 114]. The blue band is computed using estimates for D_s coming from fits to ALICE experimental data [65]. Fig. updated from Ref. [124].

In Fig. 5.2 we compare – in dimensionless units rescaled by the temperature – our estimate for the relaxation time τ_n with the inverse of the Fokker-Planck drag coefficient A arising from the non-relativistic Einstein fluctuation-dissipation relation $A^{-1} = (M/T)D_s$. Notice that one can recast the non-relativistic Einstein relation in a dimensionless form suited to highlight its linear (M/T) scaling,

$$A^{-1}T = \frac{1}{2\pi}\left(\frac{M}{T}\right)(2\pi D_s T),\tag{5.36}$$

manifest in Fig. 5.2. Both τ_n and A^{-1} are computed according to a spatial diffusion coefficient given by $2\pi D_s T_c = 3.7$, which falls in both the LQCD and ALICE ranges. If one assumes that this last estimate holds also at higher temperatures[7], the results plotted in Fig. 5.2 do not depend on the specific value of T. We observe that for large values of M/T the two curves coincide, demonstrating that our calculation for the heavy-quark relaxation time τ_n leads to the correct

---

[7]This assumption is motivated if one recalls, for example, the comparison between the LQCD and ALICE estimates for the spatial diffusion coefficient presented in Chapter 4. There, it was found that the values spanned by the linear growth of $D_s T$ with T predicted by LQCD are covered by the experimental uncertainties of the ALICE measurement, in the range of temperatures of interest. In Sec. 5.4, however, we will drop this assumption and consider a linear dependence of $D_s T$ with the temperature to mimic the trend observed in LQCD calculations.
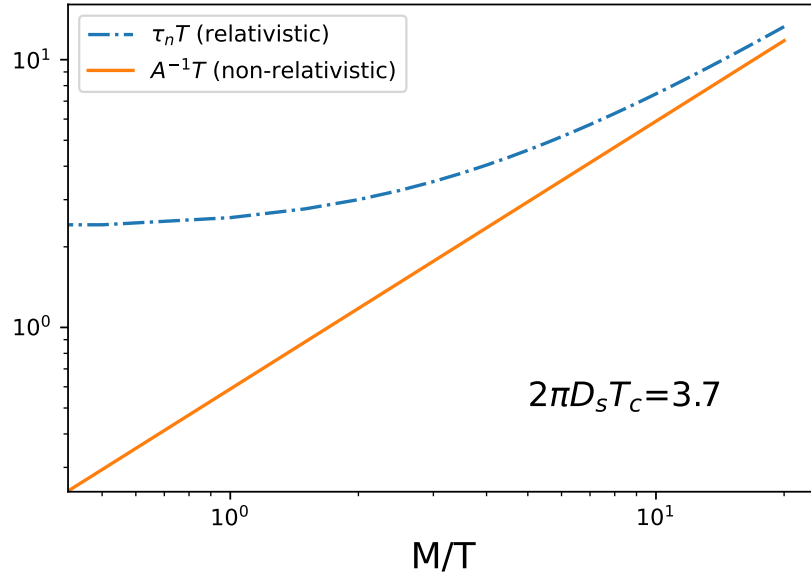
Figure 5.2: The heavy-quark relaxation time as a function of M/T is compared to the inverse of the Fokker-Planck drag coefficient A. Dimensionless units rescaled by the temperature are employed. The two curves coincide in the non-relativistic limit, i.e. for large values of M/T. Fig. from Ref. [124].

non-relativistic limit. One is therefore allowed to get, at the same time, a more realistic estimate for the the relaxation time in a kinematic range in which the non-relativistic approximation is not justified. This is the case, for example, for a charm quark of $M = 1.5$ GeV in a plasma at a temperature of 500 MeV. At $M/T \sim 3$, the difference between A^{-1} and τ_n is $\sim 20\%$, indicating that under realistic experimental conditions a relativistic treatment, as the one provided by our approach, is required.

5.4   Validity of the hydrodynamic description of heavy quarks

In this Section, we test the validity of the fluid-dynamic description of heavy quarks in the case of a QGP undergoing Bjorken flow. Although Bjorken flow is not able to describe the full evolution of the plasma but rather only the first instants after the collision, it still allows us to get a semi-realistic estimate of how fast the diffusion process happens for heavy quarks.

In order to estimate whether it is conceivable for the heavy quarks to be described by fluid dynamics within an expanding medium before the freeze-out occurs, the relaxation time τ_n of charm and beauty quarks is compared with the typical expansion time $\tau_{\exp}$ of the fluid, defined as the inverse of its expansion rate. One would be able to treat heavy-quark transport with hydrodynamics only if $\tau_n \ll \tau_{\exp}$. This condition, similar to a relation between Knudsen numbers, implies that the heavy quarks are interacting strongly enough with the other constituents of the

medium to fall under a hydrodynamic description even within an expanding system. We assume here the fluid expansion to be described by the Bjorken flow model [60], in which a purely longitudinal expansion along the beam axis is considered. From Chapter 2, we recall that in the Bjorken framework, all the thermodynamic quantities depend only on $\tau \equiv \sqrt{t^2 - z^2}$, that is, the longitudinal proper time measured by a clock in the local rest frame of the fluid. In the case of an ideal expansion, due to entropy conservation, the temperature follows the power law

$$T(\tau) = T_0 \left(\frac{\tau_0}{\tau} \right)^{\frac{1}{3}}, \tag{5.37}$$

with $T_0 = T(\tau_0)$ being the temperature of the system at τ_0 (formation time of the QGP). The expansion rate of the fluid in the case of this simple flow is given by $\theta = \nabla_\mu u^\mu = 1/\tau$, so the typical expansion time-scale is $\tau_{\text{exp}} \equiv 1/\theta = \tau$, coinciding with the longitudinal proper time. Before displaying our numerical results we can attempt some parametric estimates for the heavy-quark relaxation time arising from the Einstein Fluctuation-Dissipation relation in Eq. (5.36) under the assumption that the product $D_s T$ remains constant. One has

$$\tau_Q^{\text{EFD}} \equiv A^{-1} \sim 1/T^2 \sim \frac{1}{(T_0^3 \tau_0)^{2/3}} \tau^{2/3}. \tag{5.38}$$

Hence, for large enough time, one has

$$\tau_Q^{\text{EFD}} \sim \tau^{2/3} < \tau_{\text{exp}} = \tau. \tag{5.39}$$

If this occurs before hadronization, at least for a fraction of the fireball lifetime the heavy-quark evolution can be described by hydrodynamic equations, as the other conserved quantities.

We now consider the numerical results of our approach. In Figs. 5.3 and 5.4 the comparison between τ_{exp} and τ_n as functions of the longitudinal proper time are reported, respectively for charm and beauty quarks. This is done assuming an initial temperature of 0.45 GeV, initialization time $\tau_0 = 0.5$ fm/c, and employing different values of the transport coefficient D_s at $T \sim T_c$. The mass dependence of D_s, explored in a recent work from the HotQCD Collaboration [85] and shown in Fig. 4.5, is here neglected.

For charm quarks, we can see that τ_n goes below τ_{exp} quite fast when using transport coefficients arising from fits to experimental data or the latest LQCD results[8] [95], indicating that the conditions for a fluid-dynamic description are fulfilled for a sizeable fraction of the deconfined fireball lifetime. Earlier LQCD estimates [114] of the transport coefficients suggest a later hydrodynamization time scale. In this case, a hydrodynamic description for charm quarks might still be applicable but only for late times in the fireball evolution and in proximity of the freeze-out surface. This calculation, however, was carried out in the quenched approximation, therefore

---

[8]Recent results for D_s distinguishing between charm and beauty quark mass have also been produced [85]. The presented calculations are not expected to be significantly changed by that and fall within the colored bands reported in Figs. 5.3 and 5.4.

neglecting the impact of the dynamics of sea quarks on the spatial diffusion coefficient.

Regarding beauty quarks, D_s estimates from ALICE and from earlier LQCD calculations predict the hydrodynamization time scale to be of the order of the typical lifetime of the QGP or larger. On the other hand, it is worth noticing that the LQCD results in the non-quenched approximation suggest a possible hydrodynamization at late times for beauty quarks as well. This would certainly have an impact on the elliptic flow of beauty quarks in the QGP, which so far has been only measured with large uncertainties [123] and is compatible with zero.
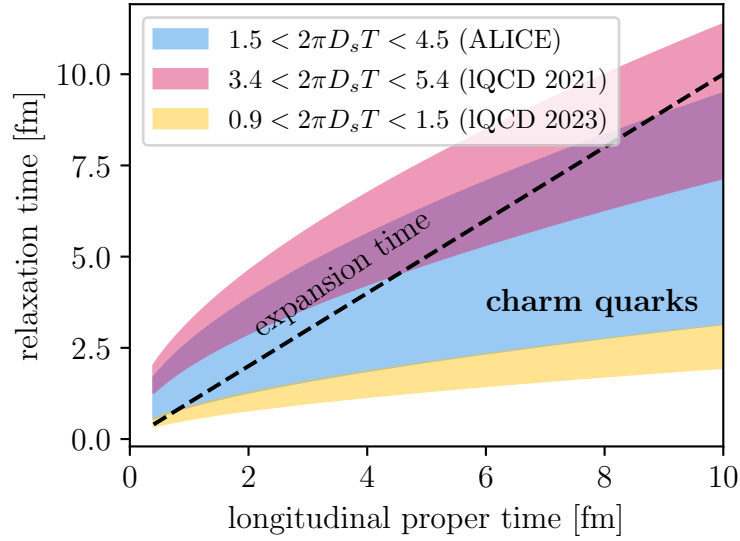

Figure 5.3: The relaxation time τ_n of charm quarks as a function of the longitudinal proper time is compared to the typical expansion timescale τ_{exp} of the fluid undergoing a Bjorken flow. Fig. updated from Ref. [124].

The exact value of τ_n clearly depends on the initial temperature and formation time of the QGP, as suggested by the estimate in Eq. (5.38). These are not independent parameters but are linked by entropy conservation to the final rapidity density of produced particles. One has

$$T_0^3 \tau_0 \sim s_0 \tau_0 \sim \left. \frac{dS_0}{d\eta_s} \right|_{\eta_s=0} \sim \left. \frac{dN}{dy} \right|_{y=0} , \qquad (5.40)$$

where S_0 (s_0) is the initial entropy (density), $\eta_s \equiv (1/2) \ln \frac{(t-z)}{(t-z)}$ the spacetime rapidity and $y \equiv (1/2) \ln \frac{(E+p^z)}{(E-p^z)}$ the rapidity of the final detected particles. Hence, according to Eq. (5.38), the higher the rapidity density of produced particles, the faster the relaxation of heavy quarks toward equilibrium.

We conclude that the applicability of hydrodynamics to the study of charm quark diffusion in the fireball produced in heavy-ion collisions is not forbidden. Regarding beauty quarks, the answer remains uncertain, indicating, if at all, only a late hydrodynamization in the plasma.
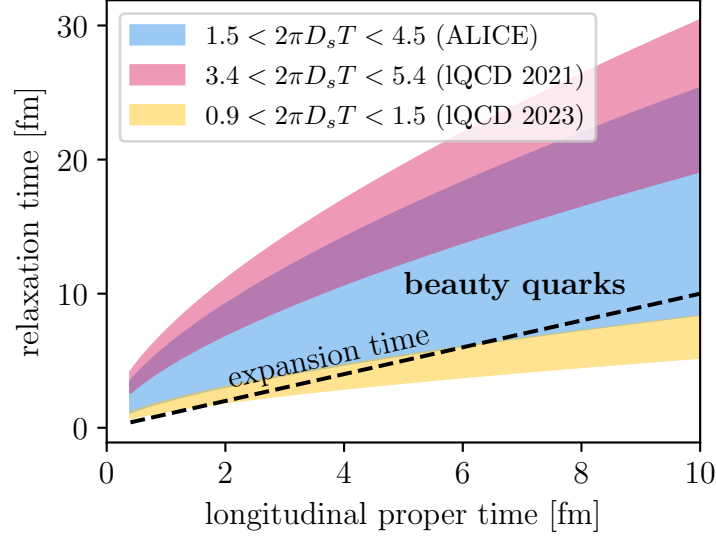
Figure 5.4: The relaxation time τ_n of beauty quarks as a function of the longitudinal proper time is compared to the typical expansion timescale τ_{exp} of the fluid undergoing a Bjorken flow. Fig. updated from Ref. [124].

5.5 Quantum corrections to the Fokker-Planck equation

So far we have used the Boltzmann and Fokker-Planck equations in their classical limit, namely neglecting quantum corrections associated with the fermionic statistics of heavy quarks (Pauli blocking). Therefore, the distribution function at equilibrium for heavy quarks was expected to be a classical Boltzmann exponential as in Eq. (5.3). A more accurate estimate for the transport coefficients can be provided by implementing quantum corrections in the Boltzmann equation and the subsequent Fokker-Planck equation. However, including them can lead to complications concerning the determination of the distribution function of heavy quarks at thermal equilibrium. In fact, finding a stationary solution for the Fokker-Planck equation becomes nontrivial in this case [132]. Nevertheless, if one considers the case of a single momentum-independent diffusion coefficient – namely $B_0 = B_1 \equiv D$ – the corresponding Fokker-Planck equation reads

$$C[f_k^{(r)}] = k^0 \frac{\partial}{\partial k^i} \left\{ A(k) k^i f_k^{(r)} \tilde{f}^{(r)} + D \delta^{ij} \frac{\partial}{\partial k^j} f_k^{(r)}] \right\} , \qquad (5.41)$$

where $\tilde{f}_k^{(r)} = 1 - f_k^{(r)}$ accounts for Pauli blocking. This equation admits an analytical stationary solution in terms of a Fermi-Dirac distribution,

$$f_{0k}^{(r)} = \left[\gamma_Q^{-1} \exp\left(\frac{E_k - q_r \mu_Q^{\mathrm{net}}}{T}\right) + 1 \right]^{-1} . \qquad (5.42)$$

The procedure to derive an equation of motion for the diffusion current and the correspondent relaxation time and transport coefficient is the same as outlined in Sec. 5.3.1. The quantum

modifications arise from having terms of order $(f_{0k}^{(r)})^2$, which cannot be recast in terms of the thermodynamic averages expressed by the $I_{nq}^{(r)}$ integrals. The relaxation time and diffusion coefficient in this case read

$$\tau_n^{\text{quantum}} \sim \frac{I_{31}}{P} \frac{T}{D} \left(1 + 2\frac{1}{3P_{(r)}} \int dK k^2 (f_{0k}^{(r)})^2 \right)$$

$$= \tau_n + \text{correction},$$

(5.43)

$$\kappa_n^{\text{quantum}} \sim \frac{T^2}{D} n_{(r)} \left(1 + 2\frac{1}{3P_{(r)}} \int dK k^2 (f_{0k}^{(r)})^2 \right)$$

$$= \kappa_n + \text{correction}.$$

(5.44)

Since the correction to the classical value depends on the square of the distribution function, which is exponentially suppressed with M/T, we expect a deviation from the classical value only for very small value of M/T.

Figure 5.5: Relaxation time times the temperature as a function of M/T. The different bands correspond respectively to the classical and quantum computation of the relaxation time.

Looking at the numerical results for the above coefficients one can see that this is actually the case. We start considering the situation of full chemical equilibrium for the heavy quarks, in which $\gamma_Q = 1$ and $\mu_Q^{\text{net}} = 0$. In Fig. 5.5 deviations from the classical behavior in the relaxation time are visible only at very small values of M/T. Therefore, they are irrelevant for the realistic conditions realized in the experiment. Similar considerations apply to Fig. 5.6, where only at small M/T values the diffusion coefficient times the temperature differs from its classical constant behavior.

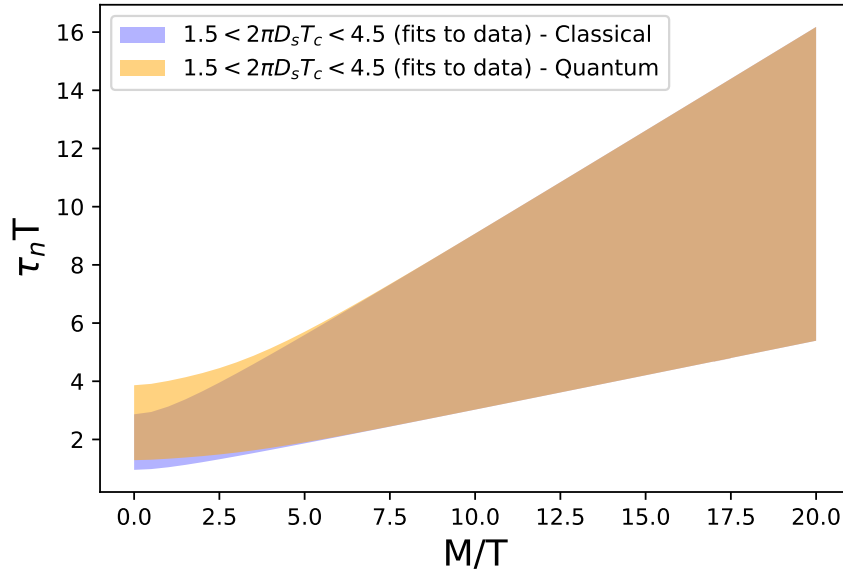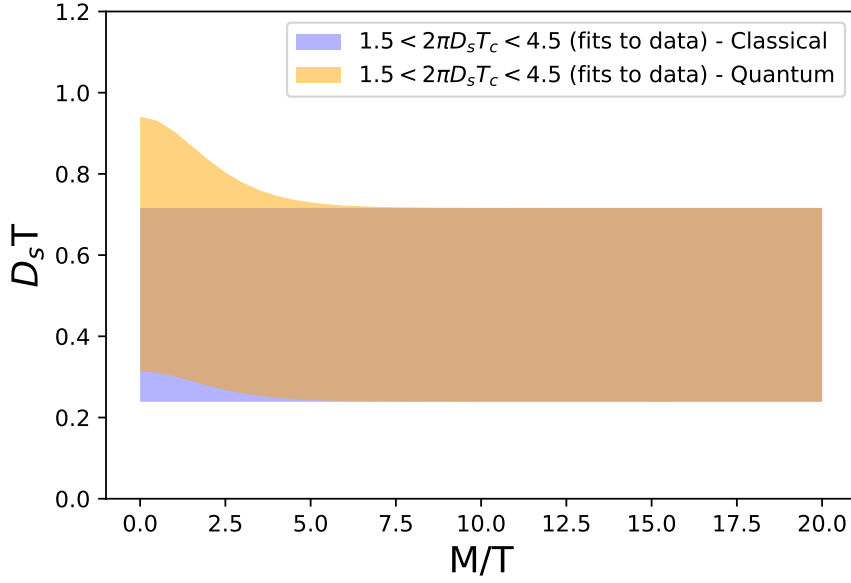Figure 5.6: Diffusion coefficient times the temperature as a function of M/T. The different bands correspond respectively to the classical and quantum computation of the diffusion coefficient.

One may worry that for charm quarks at the very beginning of the fireball evolution, when $T \sim 0.5$ GeV, the condition $M/T \gg 1$ is only marginally satisfied. However in this case what matters is that in the early stages charm quarks – produced in the initial hard scattering processes – are strongly underpopulated with respect to what would be their equilibrium abundance. This occurrence, discussed in detail in Sec. 5.6, is quantified by the fugacity factor $\gamma_Q \ll 1$ which should be included in Eqs. (5.43) and (5.44). The relevance of quantum statistics depends on the ratio between the thermal de-Broglie wavelength $\lambda_{\text{th}} \equiv (2\pi/MT)^{1/2}$ of the particle and the average interparticle distance $\bar{d} \sim n^{-1/3}$. The classical limit corresponds to $\lambda_{\text{th}}/\bar{d} \ll 1$. At the beginning of the fireball evolution, the charm quarks are highly underpopulated with respect to their thermal distribution, and the density n is suppressed by the fugacity factor. Therefore, a classical treatment is better justified also in the early stages at the collision. The subsequent fireball evolution can only improve the accuracy of the approximation. Considering for simplicity the case of a Bjorken expansion one has

$$\lambda_{\text{th}} \sim T^{-1/2} \sim \tau^{1/6} \quad \text{and} \quad \bar{d} \sim n^{-1/3} \sim \tau^{1/3} \,,$$

so that $\lambda_{\text{th}}/\bar{d} \sim \tau^{-1/6}$. When performing actual numerical simulation of heavy-quark diffusion, quantum effects will therefore be neglected.

5.6 Heavy-quark chemical potential in the case of Bjorken flow

In this Section, we discuss how to fix the heavy-quark chemical potential referring to the conservation of the average heavy-quark number $N_{Q\overline{Q}} \equiv (N_Q + N_{\overline{Q}})/2$. The mid-rapidity density at τ_0 arising from the initial hard production is given by

$$n_{\mathrm{hard}}^{Q\overline{Q}}(\tau_0, r, y = 0) = \frac{1}{\tau_0} \frac{d^3 N^{Q\overline{Q}}}{r\,dr\,d\phi\,dy}\bigg|_{y=0} , \qquad (5.45)$$

In the above expression, the $Q\overline{Q}$ rapidity distribution in nucleus-nucleus collisions is set by the pQCD $Q\overline{Q}$ cross-section, rescaled by the total number of binary nucleon-nucleon collisions,

$$\frac{dN^{Q\overline{Q}}}{dy} = \langle N_{\mathrm{coll}} \rangle \frac{1}{\sigma^{\mathrm{in}}} \frac{d\sigma^{Q\overline{Q}}}{dy} , \qquad (5.46)$$

where σ^{in} is the inelastic proton-proton cross-section and $\sigma^{Q\overline{Q}}$ is the hard production cross-section, possibly containing cold-nuclear-matter effects (nPDF's). We indicate with $\langle N_{\mathrm{coll}} \rangle$ the average number of binary nucleon-nucleon collisions per event at mid-rapidity. When plugging Eq. (5.46) into Eq. (5.45), one gets

$$n_{\mathrm{hard}}^{Q\overline{Q}}(\tau_0, r, y = 0) = \frac{1}{\tau_0} n_{\mathrm{coll}}(r) \frac{1}{\sigma^{\mathrm{in}}} \frac{d\sigma^{Q\overline{Q}}}{dy} , \qquad (5.47)$$

where $n_{\mathrm{coll}}(r)$ represents the average density per event of binary nucleon-nucleon collisions at mid-rapidity. We assume that when averaging over a large number of events happening with a random orientation in the transverse plane (as it occurs in a real heavy-ion collision experiment), the angular dependence is integrated out and the density n_{coll} depends only on the radius. In case one considers homogeneous conditions in the transverse plane, nevertheless representative of a central Pb-Pb collision, one can estimate

$$n_{\mathrm{hard}}^{Q\overline{Q}}(\tau_0, y = 0) = \frac{1}{\tau_0} \frac{\langle N_{\mathrm{coll}} \rangle}{\pi R_{\mathrm{Pb}}^2} \frac{1}{\sigma^{\mathrm{in}}} \frac{d\sigma^{Q\overline{Q}}}{dy} , \qquad (5.48)$$

where R_{Pb} is the average radius of a lead nucleus.

To fix at each point the initial $Q\overline{Q}$ chemical potential μ_Q (the same for quarks and antiquarks, which are produced in equal amount), this density has to be set equal to the equilibrium thermal multiplicity

$$n_{\mathrm{therm}}^{Q\overline{Q}}(x) = (2s + 1)N_c \left(\frac{MT(x)}{2\pi}\right)^{\frac{3}{2}} e^{-M/T(x)} e^{\mu_Q(x)/T(x)} . \qquad (5.49)$$

$T(x)$ is extracted from the initial local energy density of the medium through its Equation of

State. For the sake of simplicity let us introduce the fugacity $\gamma_Q \equiv e^{\mu_Q/T}$. One has then:

$$n_{\text{therm}}^{Q\overline{Q}}(x) = (2s+1)N_c\,\gamma_Q(x)\left(\frac{MT(x)}{2\pi}\right)^{\frac{3}{2}}e^{-M/T(x)}\,. \tag{5.50}$$

Let us perform some estimates for pp the initial density of charm-quark pairs with mass $M = 1.5$ GeV taking the central prediction by FONLL [79] for collisions at 5.02 TeV. One gets, at $y = 0$, $d\sigma^{Q\overline{Q}}/dy = 0.463$ mb, with $\sigma^{\text{in}} = 70$ mb. For the 0-10% most central Pb-Pb collisions at $\sqrt{s_{\text{NN}}} = 5.02$ TeV one has $n_{\text{coll}}(r = 0) = 31.57\,\text{fm}^{-2}$ and $\langle N_{\text{coll}}\rangle = 1653$. Assuming a thermalization time $\tau_0 = 0.5$ fm/c one gets at the center of the fireball

$$n_{\text{hard}}^{Q\overline{Q}}(\tau_0, r = 0, y = 0) \approx 0.42\,\text{fm}^{-3}\,. \tag{5.51}$$

The average density in the transverse plane can be estimated as slightly lower. Starting form Eq. (5.48) and setting $R_{\text{Pb}} = 6.62$ fm one gets

$$n_{\text{hard}}^{Q\overline{Q}}(\tau_0, y = 0) \approx 0.16\,\text{fm}^{-3}\,. \tag{5.52}$$

This has to be compared with the thermal abundance in the case of full chemical equilibrium of the heavy quarks, i.e. $\gamma_Q = 1$. Assuming an initial temperature of the fireball of $T_0 = 0.45$ GeV one would obtain

$$n_{\text{chem.eq.}}^{Q\overline{Q}}(\tau_0, y = 0) \approx 0.98\,\text{fm}^{-3}\,. \tag{5.53}$$

Initially, the heavy quarks are then underpopulated with respect to their chemical-equilibrium abundance. The initial heavy-quark fugacity can be estimated as

$$\gamma_Q(\tau_0) = n_{\text{hard}}^{Q\overline{Q}}(\tau_0)/n_{\text{chem.eq.}}^{Q\overline{Q}}(\tau_0) \approx 0.16\,. \tag{5.54}$$

We now try to estimate the evolution of the heavy-quark density and fugacity while the fireball undergoes an ideal Bjorken expansion. In this case, particle conservation entails:

$$n^{Q\overline{Q}}(\tau)\tau = n_0^{Q\overline{Q}}\tau_0\,, \tag{5.55}$$

where $n_0^{Q\overline{Q}} = n_{\text{hard}}^{Q\overline{Q}}(\tau_0)$. The Landau matching condition applied to the heavy-quark density allows one to extract the heavy-quark fugacity $\gamma_Q(\tau)$:

$$(2s+1)N_c\,\gamma_Q(\tau)\left(\frac{MT(\tau)}{2\pi}\right)^{\frac{3}{2}}e^{-M/T(\tau)}\frac{\tau}{\tau_0} = n_0^{Q\overline{Q}} \tag{5.56}$$

In the above, neglecting dissipative effects and deviations from a Stefan-Boltzmann EoS, we estimate the temperature evolution from entropy conservation:

$$s(\tau)\tau = s_0\tau_0 \quad \longrightarrow \quad T^3(\tau)\tau = T_0^3\tau_0 \tag{5.57}$$

Let us estimate the value of the heavy-quark fugacity at chemical-freeze-out at $T_{\text{FO}} = 0.15$ GeV, occurring at $\tau_{\text{FO}} = (T_0/T_{\text{FO}})^3\tau_0 = 27\tau_0 = 13.5$ fm/c. One gets $\gamma_Q(\tau_{\text{FO}}) \approx 24.6$, not far from the one obtained with SHM fits [127] ($\gamma_c \sim 30$).

The evolution of the fugacity of charm quarks as a function of temperature, extracted from Eq. (5.56), is displayed in Fig. 5.7. It is worth stressing that, going from high temperatures (early collision times) to low temperatures (late collision times), and employing realistic values for the initial conditions on γ_c, one observes a dramatic increase in the values of the fugacity, from $\gamma_c \sim 0$ to $\gamma_c \gg 1$. Recalling the definition of fugacity as $\gamma_Q = \exp(\mu_Q/T)$, this implies that the chemical potential of the charm quark spans from negative values to values of the order of the temperature T of the QGP. This reflects the fact that although the heavy quarks are initially underpopulated with respect to their chemical-equilibrium abundance, this is no longer the case at the end of the fireball evolution.
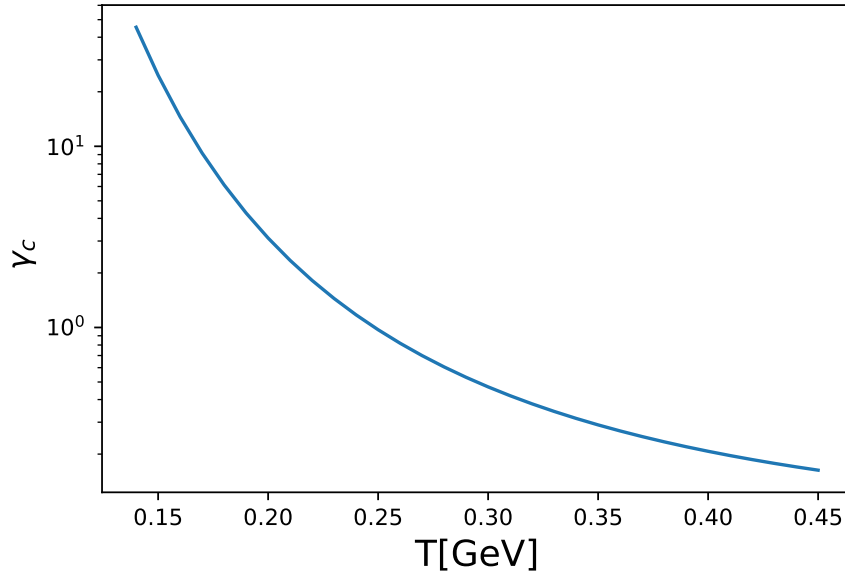

Figure 5.7: Charm quark fugacity as a function of temperature in logarithmic scale with $T_0 = 0.45$ GeV.

Chapter 6

Fluid-dynamic description of charm quarks

This chapter is mostly taken from [133].

In the previous Chapter, the question of charm thermalization was addressed by studying the hydrodynamization time of charm quarks in the context of an expanding medium. It was shown that the time required for charm quark to hydrodynamize, and therefore to be included in the fluid-dynamic description of the QGP, is shorter than the typical expansion time scale of the medium. This result serves as motivation to develop a fluid-dynamic description of charm quarks, which is the subject of the current Chapter. We expect such a description to be relevant for the low transverse momentum (p_T) region, as it is for the light-flavor particles. At high momentum, the path-length-dependent energy loss mechanisms, are more important in defining the shape of the p_T spectra.

The method developed in this Chapter is only applied to charm quarks. However, it can be straightforwardly extended to study the dynamics of beauty-quark diffusion, assuming that such a hydrodynamic description is applicable. The only changes concern, of course, the heavy-quark mass, the number of heavy quarks – which is fixed by the initial conditions – and the list of hadronic states and resonances to be included.

6.1 Fluid-dynamic equations

The fluid-dynamic equations to solve are mainly given by the system of equations

$$\nabla_\mu T^{\mu\nu} = 0 \,, \tag{6.1}$$

$$\nabla_\mu N^\mu = 0 \,, \tag{6.2}$$

which expresses the conservation of the energy-momentum tensor $T^{\mu\nu}$ and of an additional conserved current N^{μ}. The latter is associated with conserving the number of charm-anticharm pairs [124]. The Landau frame is chosen such that $T^{\mu\nu}$ and N^{μ} can be decomposed as

$$T^{\mu\nu} = (\epsilon + P)u^{\mu}u^{\nu} + \Delta^{\mu\nu}(P + \Pi) + \pi^{\mu\nu}, \tag{6.3}$$

$$N^{\mu} = nu^{\mu} + \nu^{\mu}, \tag{6.4}$$

where ϵ, P, u^{μ}, Π and $\pi^{\mu\nu}$ are the energy density, thermodynamic pressure, fluid four-velocity, bulk viscous pressure, and shear-stress tensor of the fluid, respectively. The charm-quark fields are the heavy-quark density n and the diffusion current ν^{μ}. The local temperature T and the chemical potential to temperature ratio α are determined by the Landau matching conditions,

$$\epsilon(T) \equiv \epsilon_{\text{equilibrium}}(T) \tag{6.5}$$

$$n(T, \alpha) \equiv n_{\text{equilibrium}}(T, \alpha). \tag{6.6}$$

We assume that the energy density is approximately independent of the heavy-quark contribution, such that any energy density dependence on α is negligible[1]. The thermal equilibrium heavy-quark density is taken to be one of the hadron-resonance gas, including all measured charm states (HRGc),

$$n(T, \alpha) = \frac{T}{2\pi^2} \sum_{i \in \text{HRGc}} q_i M_i^2 e^{q_i \alpha} K_2(M_i/T), \tag{6.7}$$

where M_i is the mass of each charm hadron, and q_i is its charm charge. The HRGc is expected to give the correct limit for the thermodynamics of the charm density at temperatures close to the phase transition. This relation is assumed to also hold at high temperatures. In the temperature regime reached by the fireball in most central collisions, the HRGc yields larger values (of about a factor 5) than the density of the free charm quarks. Nevertheless, due to the absence of first principle calculations for the Equation of State of charm quarks at physical QGP temperatures, we assume this relation to hold also at high temperatures. In the future, a more realistic Equation of State will be developed.

The equations of motion for each of the dissipative currents in a second-order hydrodynamic formalism are solved,

$$\tau_{\Pi} u^{\mu} \partial_{\mu}\Pi + \Pi + \zeta\nabla_{\mu}u^{\mu} = 0, \tag{6.8}$$

$$P^{\mu\rho}_{\nu\sigma}\left[\tau_{\pi}(u^{\lambda}\nabla_{\lambda}\pi^{\sigma}_{\rho} - 2\pi^{\sigma\lambda}\omega_{\rho\lambda} + \tfrac{4}{3}\nabla_{\lambda}u^{\lambda}\pi^{\sigma}_{\rho}) + 2\eta\nabla_{\rho}u^{\sigma} + \pi^{\sigma}_{\rho}\right] = 0, \tag{6.9}$$

$$\tau_n \Delta^{\alpha}_{\beta}u^{\mu}\nabla_{\mu}\nu^{\beta} + \nu^{\alpha} + \kappa_n\Delta^{\alpha\beta}\partial_{\beta}\alpha = 0, \tag{6.10}$$

---

[1]This assumption could be relaxed in view of studying the back reaction that the motion of the charm quarks has on the QGP medium. However, at the moment no calculation of the LQCD EoS including the the dependence on the heavy-quark pair chemical potential is available in the literature.

where one defines the projector $P^{\mu\nu}_{\rho\sigma} = \frac{1}{2}[\Delta^\mu_\rho \Delta^\nu_\sigma + \Delta^\mu_\rho \Delta^\nu_\sigma - \frac{2}{3}\Delta^\mu_\rho \Delta^\nu_\sigma]$ and the vorticity tensor $\omega^{\mu\nu} = (\nabla^\mu u^\nu - \nabla^\nu u^\mu)/2$. Here we introduced the transport coefficients for the bulk viscosity ζ, shear viscosity η, and the heavy-quark diffusion coefficient κ_n, with the corresponding relaxation times τ_Π, τ_π and τ_n. The values of the viscosities are taken from Ref. [134], while the expression for the diffusion coefficient was derived in Ref. [124] and presented in Chapter 5. We remark that κ_n and τ_n are proportional to the heavy-quark spatial diffusion coefficient D_s.

The equations are solved in Bjorken coordinates assuming boost and azimuthal rotation invariance, restricting effectively to 1+1 dimensions. We organize the fluid fields for the QGP into a Nambu spinor $\Phi = (T, u^\mu, \pi^{\mu\nu}, \Pi)$, which satisfies the hyperbolic equation of motion. We assume that none of these fields or transport coefficients depend on the heavy-quark variables. Eqs. (6.1), (6.8) and (6.9), can be used to determine the time derivatives of the fluid fields explicitly. Let us now consider another Nambu spinor including also the heavy-quark fields $\Xi = (T, u^\mu, \pi^{\mu\nu}, \Pi, \alpha, \nu^\mu)$. The new system of hyperbolic equations satisfied by Ξ can be numerically solved by setting the fluid fields contained in Φ on shell. This is equivalent to neglecting the back reaction of the heavy-quark field on the fluid background evolution.

6.1.1 Details on fluid-dynamic equations

The equations are solved effectively in 1+1 dimensions with Bjorken coordinates (r, τ) supplemented by azimuthal angle ϕ and rapidity η. The metric tensor is defined as $g_{\mu\nu} = \text{diag}(-1, 1, r^2, \tau^2)$. The independent components of the fluid fields in the azimuthally symmetric and boost-invariant case are, for the energy-momentum tensor $T^{\mu\nu}$

$$T, u^r, \pi^\eta_\eta, \pi^\phi_\phi, \Pi, \tag{6.11}$$

where $u^2 = -1$ and $\pi^{\mu\nu}$ is a symmetric, traceless tensor transverse to the four-velocity. The independent charm fields are

$$\alpha, \nu^r, \tag{6.12}$$

where the diffusion current is orthogonal to the fluid velocity $u \cdot \nu = 0$, and α is the conjugate variable of the density n, i.e., $\alpha = \mu/T$. A generic Nambu spinor, whose components are the background fluid fields $\Phi_{\text{bg}} = (T, u^\mu, \pi^\eta_\eta, \pi^\phi_\phi, \Pi)$, is considered. The general hyperbolic equations for the background fluid field can be written as

$$A_{\text{bg}}(r, \tau, \Phi_{\text{bg}})\partial_\tau \Phi_{\text{bg}} + B_{\text{bg}}(r, \tau, \Phi_{\text{bg}})\partial_r \Phi_{\text{bg}} = S_{\text{bg}}(r, \tau, \Phi_{\text{bg}}), \tag{6.13}$$

where A_{bg} and B_{bg} are 5×5 matrices and S_{bg} is a source term vector depending non-linearly on the fluid fields Φ_{bg}. This equation is used to derive the expressions for the time derivatives of the fields in Φ_{bg},

$$\partial_\tau \Phi_{\text{bg}} = -A^{-1}_{\text{bg}} B_{\text{bg}} \partial_r \Phi_{\text{bg}} + A^{-1}_{\text{bg}} S_{\text{bg}}. \tag{6.14}$$

We can now define another Nambu spinor $\Phi_{\mathrm{HQ}} = (\alpha, \nu^r)$. The equation of motion for Φ_{HQ} is given by

$$A_{\mathrm{HQ}}\partial_\tau \Phi_{\mathrm{HQ}} + B_{\mathrm{HQ}}\partial_r \Phi_{\mathrm{HQ}} + C_{\mathrm{HQ}}\partial_\tau \Phi_{\mathrm{bg}} + D_{\mathrm{HQ}}\partial_r \Phi_{\mathrm{bg}} = S_{\mathrm{HQ}}, \qquad (6.15)$$

where the 2×2 matrices A_{HQ}, B_{HQ}, C_{HQ}, D_{HQ} and the two-component vector S_{HQ} are generic non-linear functions of the fluid fields Φ_{bg} and the heavy quarks variables Φ_{HQ}. We substitute the equation of motion Eq. (6.14) in Eq. (6.15), leading to

$$A_{\mathrm{HQ}}\partial_\tau \Phi_{\mathrm{HQ}} + B_{\mathrm{HQ}}\partial_r \Phi_{\mathrm{HQ}} + (D_{\mathrm{HQ}} - C_{\mathrm{HQ}}A_{\mathrm{bg}}^{-1}B_{\mathrm{bg}})\partial_r \Phi_{\mathrm{bg}} = S_{\mathrm{HQ}} - C_{\mathrm{HQ}}A_{\mathrm{bg}}^{-1}S_{\mathrm{bg}}. \qquad (6.16)$$

In this formulation, the evolution of the background Φ_{bg} is not influenced by the dynamics of the diffusion current and density in Φ_{HQ}. The equations of motion read

$$\begin{pmatrix} A_{\mathrm{bg}} & 0 \\ 0 & A_{\mathrm{HQ}} \end{pmatrix} \partial_\tau \begin{pmatrix} \Phi_{\mathrm{bg}} \\ \Phi_{\mathrm{HQ}} \end{pmatrix} + \begin{pmatrix} B_{\mathrm{bg}} & 0 \\ B_{\mathrm{mix}} & B_{\mathrm{HQ}} \end{pmatrix} \partial_r \begin{pmatrix} \Phi_{\mathrm{bg}} \\ \Phi_{\mathrm{HQ}} \end{pmatrix} = \begin{pmatrix} S_{\mathrm{bg}} \\ \widetilde{S}_{\mathrm{HQ}} \end{pmatrix} \qquad (6.17)$$

where the mixing matrix is given by $B_{\mathrm{mix}} = D_{\mathrm{HQ}} - C_{\mathrm{HQ}}A_{\mathrm{bg}}^{-1}B_{\mathrm{bg}}$ and $\widetilde{S}_{\mathrm{HQ}} = S_{\mathrm{HQ}} - C_{\mathrm{HQ}}A_{\mathrm{bg}}^{-1}S_{\mathrm{bg}}$. Using that the equations are hyperbolic, and therefore the matrix of the time derivative,

$$\begin{pmatrix} A_{\mathrm{bg}} & 0 \\ 0 & A_{\mathrm{HQ}} \end{pmatrix},$$

is invertible, the equations of motion can be written explicitly as

$$\partial_\tau \begin{pmatrix} \Phi_{\mathrm{bg}} \\ \Phi_{\mathrm{HQ}} \end{pmatrix} + \begin{pmatrix} A_{\mathrm{bg}}^{-1}B_{\mathrm{bg}} & 0 \\ A_{\mathrm{HQ}}^{-1}B_{\mathrm{mix}} & A_{\mathrm{HQ}}^{-1}B_{\mathrm{HQ}} \end{pmatrix} \partial_r \begin{pmatrix} \Phi_{\mathrm{bg}} \\ \Phi_{\mathrm{HQ}} \end{pmatrix} = \begin{pmatrix} A_{\mathrm{bg}}^{-1}S_{\mathrm{bg}} \\ A_{\mathrm{HQ}}^{-1}\widetilde{S}_{\mathrm{HQ}} \end{pmatrix}. \qquad (6.18)$$

6.1.2   Numerical scheme

The equations of motion for relativistic fluid dynamics with the conservation of a heavy-charm pair current are hyperbolic equations of motion due to the inclusion of the evolution equation of the dissipative currents $\pi^{\mu\nu}, \Pi$ and ν^μ. Schematically, the equations can be written as quasi-linear partial differential equations (PDEs). We will restrict ourselves to discussing the equations in one spatial dimension for simplicity. However, the extension to a higher number of dimensions is trivial. We consider a collection of independent variables called ϕ, whose equations of motion are

$$\partial_t \phi + A(\phi)\partial_x \phi + S(\phi) = 0, \qquad (6.19)$$

where $A(\phi)$ is a matrix in field space that depends non-linearly on the fields themselves, and $S(\phi)$ is a vector containing the source term in the equation. Usually, the numerical solutions of the fluid dynamic equations are discussed in a conservative form since the ideal limit of the

equations is the divergence of a current – typically the energy-momentum and particle density current. Let

$$\nabla_\mu \mathcal{J}^\mu = 0$$

be the conservation equation, where $\mathcal{J}^\mu$ represents generically the conserved current. However, including the dynamics of the dissipative current like diffusion and shear/bulk viscous stress spoils this property for Israel-Stewart-Müller theory [56]. For this type of theory, the equations are non-conservative by construction, and it is impossible to cast them in a conservative form. In the relativistic viscous fluid dynamic literature, the equations are solved with a splitting algorithm: First, solve using a finite volume conservative scheme, then correct the intermediate solution using a central approximation of the dissipative equations, as in the so-called SHASTA algorithm [135], or some variations of it like KT [136]. This type of algorithm performs well if the dissipative currents are minor corrections to the ideal step and do not modify the ideal evolution substantially. However, this is not always the case, especially when the system is far from the ideal approximation, meaning the non-equilibrium effects are important. In this work, we implement a different strategy. Instead of using the ideal-viscous splitting, we solve the equations together as a quasi-linear system of PDEs. The naive discretization of equations like Eq. (6.19) can be obtained by replacing the first derivative with its central approximation. Denoting x_i the central position of a cell of size Δx, the the central derivative approximation is

$$\partial_x \phi|_{x_i} \simeq \frac{1}{2\Delta x}(\phi_{i+1} - \phi_{i-1}), \tag{6.20}$$

where $\phi_i = \phi(x_i)$. The semi-discretized version of the equations is

$$\partial_t \phi_i + A(\phi_i)\partial_x \phi|_{x_i} + S(\phi_i) = 0. \tag{6.21}$$

This naive discretization, however, is unstable since there is no dissipation mechanism in the discretization to reduce the high-frequency mode of the discretized solution. The physical motivation for this instability can be understood considering the nature of the PDE. The system of hyperbolic equations is a collection of propagating waves that interact non-linearly and with a non-constant velocity. The waves are usually (except in simple cases) a complicated combination of the primary variables ϕ, defined as the left eigenvector of the matrix $A(\phi)$. The eigenvalue is characteristic of the hyperbolic PDE and represents how fast the wave propagates. Each of the waves propagates at a different speed and direction. In a one-dimensional case, there will be right- and left-moving waves. To have a stable discretization, the numerical derivative should respect – up to some degree of accuracy – the direction of propagation of the different waves. If a wave is right-moving, the correct derivative discretization should involve only points in the past of the wave – i.e. on its left – and vice versa. This mechanism is called *upwinding* [137]. Therefore, the central approximation of the first derivative goes against this principle since it

does not distinguish the direction of propagation of the waves.

A natural solution is to separate right-moving and left-moving waves and discretize them accordingly. By calling λ_i the eigenvalues, one can separate them into positive and negative ones (λ_i^+ and λ_i^-, respectively)[2],

$$A^+ = U \begin{bmatrix} \lambda_1^+ & & \\ & \ddots & \\ & & 0 \end{bmatrix} U^{-1}, \quad A^- = U \begin{bmatrix} 0 & & \\ & \ddots & \\ & & \lambda_1^- \end{bmatrix} U^{-1}. \tag{6.22}$$

Each matrix has only information about the left and right propagating waves, respectively. With this construction, it is then easy (in principle) to construct an upwinding discretization as,

$$\partial_t \phi_i + A^+(\phi_i) \partial_x \phi|_{x_i}^- + A^-(\phi_i) \partial_x \phi|_{x_i}^+ + S(\phi_i) = 0, \tag{6.23}$$

where the derivatives are taken from the left or the right, respectively,

$$\phi|_{x_i}^- = \frac{1}{\Delta x}(\phi_i - \phi_{i-1}), \quad \phi|_{x_i}^+ = \frac{1}{\Delta x}(\phi_{i+1} - \phi_i). \tag{6.24}$$

The proposed discretization is sometimes called the flux-splitting technique and was already introduced in [137–139]. The drawback of this scheme is that it relies on the complete knowledge of the spectrum of the characteristic matrix. Only in a few cases is this achievable due to the complexity of the non-linearities of the characteristic matrix A.

The discretization reported in Eq. (6.23) can be expressed in terms of the absolute value of the matrix A,

$$|A| = A^+ - A^-, \tag{6.25}$$

such that

$$A^+ = \frac{1}{2}(A + |A|), \quad A^- = \frac{1}{2}(A - |A|). \tag{6.26}$$

Therefore, Eq. (6.23) becomes

$$\partial_t \phi_i + \frac{1}{2}A(\partial_x \phi|_{x_i}^- + \partial_x \phi|_{x_i}^+) + \frac{1}{2}|A|(\partial_x \phi|_{x_i}^- - \partial_x \phi|_{x_i}^+) + S(\phi_i) = 0. \tag{6.27}$$

The derivative operators now become

$$\frac{1}{2}(\partial_x \phi|_{x_i}^- + \partial_x \phi|_{x_i}^+) = \frac{1}{2\Delta x}(\phi_{i+1} - \phi_{i-1}) = \partial_x \phi|_{x_i}, \tag{6.28}$$

$$\partial_x \phi|_{x_i}^- - \partial_x \phi|_{x_i}^+ = \frac{1}{\Delta x}(\phi_{i+1} + \phi_{i-1} - 2\phi_i) = \Delta x \partial_x^2 \phi|_{x_i}, \tag{6.29}$$

---

[2]For hyperbolic systems of partial differential equations, it is always possible to left-diagonalize the characteristic matrix and the corresponding eigenvalues are real.

leading to a discretized equation of the form

$$\partial_t \phi_i + A \partial_x \phi|_{x_i} - \frac{1}{2}|A|\Delta x \partial_x^2 \phi|_{x_i} + S(\phi_i) = 0\,. \tag{6.30}$$

The extra contribution introduced to upwind the derivative acts like a viscous terms into the equation, with an amplitude proportional to the lattice spacing Δx.

A standard approximation for the absolute value of the matrix is $|A| = \lambda I$ where $\lambda = \max(|\lambda_i|)$, which is the fastest characteristic speed in the system. Under this assumption, the scheme can be considered a non-conservative version of the Lax-Friedrichs scheme. However, this requires knowledge of the characteristic structure, which is possible only for exceptional cases.

An appealing alternative is to approximate $|A|$ with a suitable expansion, as discussed in [139, 140]. Among the possible expansion choices that one can make, the simplest is a polynomial approximation around $\max(|\lambda_i|) = 1$,

$$|A| \simeq \frac{1}{2}(I + A^2) + \mathcal{O}(A^4)\,, \tag{6.31}$$

assuming that all the $|\lambda_i| < 1$, such that the fastest wave speeds are modified correctly. Different and more performing possibilities are Chebyshev polynomials and rational functions. However, in this work, we restrict ourselves to the simplest choice and will study these possibilities in the future.

For the evolution, we use the explicit Runge-Kutta with adaptive time-step as described in [141, 142] and with the Proportional-Integral-Derivative (PID) controller as described in [143–145]. For the integration on the freeze-out surface we used [146–149].

6.1.3 Validation against Gubser flow

Comparing it against a known analytic (or semi-analytic) solution is useful to verify and validate the numerical scheme. For Israel-Stewart-type theories, such a solution with azimuthal rotation symmetry, longitudinal boost invariance, and an additional conformal symmetry has been found by Gubser [61]. For symmetry reasons, the evolution of the diffusion current in this setup is trivial. So we will leave it out of the discussion in the rest of this section. The set of equations for the evolution of temperature, fluid velocity, shear stress, and number density in the presence of a conformal symmetry reads,

$$\frac{u^\lambda \nabla_\lambda T}{T} + \frac{\nabla_\mu u^\mu}{3} + \frac{\pi^{\mu\nu}\sigma_{\mu\nu}}{3sT} = 0\,, \tag{6.32}$$

$$u^\lambda \nabla_\lambda u^\mu + \frac{\Delta^\mu_\lambda \nabla^\lambda T}{T} + \frac{\Delta^\mu_\lambda \nabla_\alpha \pi^{\alpha\lambda}}{sT} = 0\,, \tag{6.33}$$

$$\frac{\tau_\pi}{sT}\left(\Delta^\mu_\alpha \Delta^\nu_\beta u^\lambda \nabla_\lambda \pi^{\alpha\beta} + \frac{4}{3}\nabla_\lambda u^\lambda \pi^{\mu\nu}\right) + \frac{\pi^{\mu\nu}}{sT} = -\frac{2\eta}{sT}\sigma^{\mu\nu}\,, \tag{6.34}$$

$$u^\lambda \nabla_\lambda n = -n\theta - \nabla_\mu \nu^\mu\,, \tag{6.35}$$

where $\theta = 2\tanh\rho$ is the scalar expansion rate for Gubser flow. In de Sitter space, by applying the Gubser flow profile $\hat{u}^\mu = (1, 0, 0, 0)$, the equations read,

$$\frac{1}{\hat{T}}\partial_\rho\hat{T} + \frac{2}{3}\tanh\rho = \frac{1}{3}\bar{\pi}^\eta_\eta\tanh\rho\,, \tag{6.36}$$

$$\frac{c}{\hat{T}}\frac{\eta}{\hat{s}}\left[\partial_\rho\bar{\pi}^\eta_\eta + \frac{4}{3}(\bar{\pi}^\eta_\eta)^2\tanh\rho\right] + \bar{\pi}^\eta_\eta = \frac{4}{3}\frac{\eta}{\hat{s}\hat{T}}\tanh\rho\,, \tag{6.37}$$

$$\partial_\rho\hat{n} + 2\tanh\rho\hat{n} = 0\,, \tag{6.38}$$

where ρ is the Gubser conformal time variable and $\bar{\pi}^{\mu\nu} = \pi^{\mu\nu}/(\hat{s}\hat{T})$. The transformation rules to obtain the fluid variables in Milne coordinates are given by

$$T(\tau, r) = \hat{T}(\rho(\tau, r))/\tau\,, \tag{6.39}$$

$$u_\mu(\tau, r) = \tau\frac{\partial\hat{x}^\nu}{\partial\hat{x}^\mu}\hat{u}_\nu(\rho(\tau, r))\,, \tag{6.40}$$

$$\pi_{\mu\nu}(\tau, r) = \frac{1}{\tau^2}\frac{\partial\hat{x}^\alpha}{\partial\hat{x}^\mu}\frac{\partial\hat{x}^\beta}{\partial\hat{x}^\mu}\hat{\pi}_{\alpha\beta}(\rho(\tau, r))\,, \tag{6.41}$$

$$n(\tau, r) = \frac{1}{\tau^3}\hat{n}(\rho(\tau, r))\,. \tag{6.42}$$

The conformal Equation of State at finite α can be written as

$$e = 3p\,, \quad s = h(\alpha)T^3\,, \quad n \equiv g(\alpha)\alpha T^3\,, \tag{6.43}$$

where one defines the dimensionless coefficients

$$f = 3p_0 + \frac{N_f}{6}\alpha^2 + \frac{Nf}{108\pi^2}\alpha^4\,, \tag{6.44}$$

$$h = 4p_0 + \frac{N_f}{9}\alpha^2\,, \tag{6.45}$$

$$g = \frac{N_f}{9}\alpha + \frac{N_f}{81\pi^2}\alpha^2\,. \tag{6.46}$$

Here we use $p_0 = (16 + 10.5N_f)\pi^2/90$ and the number of flavors $N_f = 2.5$. In this setup, the equations for the charge current are decoupled from the rest of the system. In Fig. 6.1 the comparison between the semi-analytical solution by Gubser and the one obtained numerically is presented. The initialization time is $\tau_0 = 1$ fm, the shear viscosity to entropy ratio is 0.2; the shear relaxation time is $\tau_S = 5\eta/(sT)$. The overall agreement is good for all fields in the full radial range.

In Fig. 6.2, the percent deviation of the numerical solution for the temperature field with respect to Gubser's solution is shown for different numbers of discretization points at $\tau = 2$ fm. As one can see, the finer the spatial grid is, the smaller the deviation. In particular, the deviation around 2 fm, corresponding to the maximum of the temperature profile, is progressively suppressed.
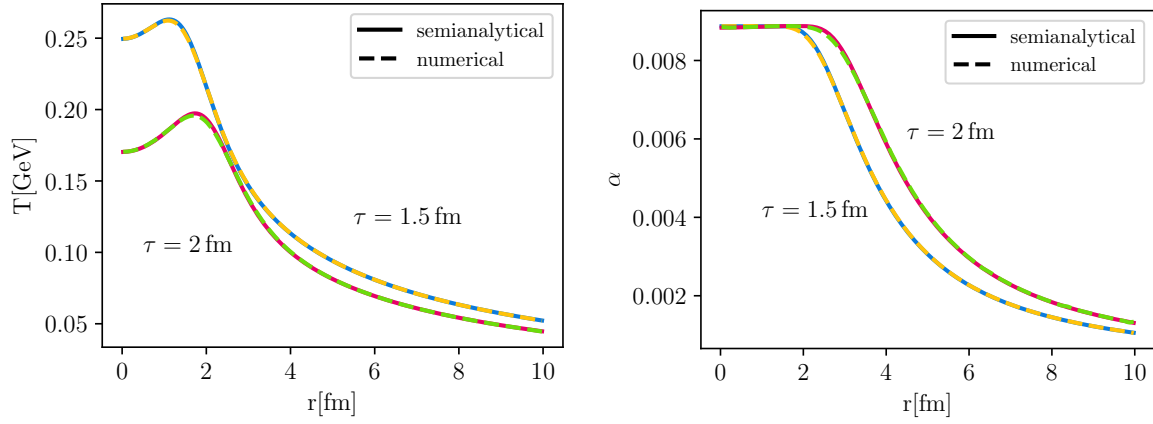
Figure 6.1: Temperature (left panel) and chemical potential to temperature ratio α (right panel) as a function of radius r at Bjorken times $\tau = 1.5$ fm/c and $\tau = 2$ fm/c. The solid lines correspond to the semianalytic Gubser solution, while the dashed lines are the numerical results with $N = 200$ discretization points. We have here chosen the maximal radius to be 10 fm.

Figure 6.2: Percent deviation of the absolute value of $\Delta T = T_{\text{numerical}}/T_{\text{semianalytical}} - 1$ of the temperature at $\tau = 2$ fm as a function of radius and the number of discretization point N. The numerical solution converges to the semi-analytical one as the number of points increases.

6.2   Initial conditions for the fluid fields

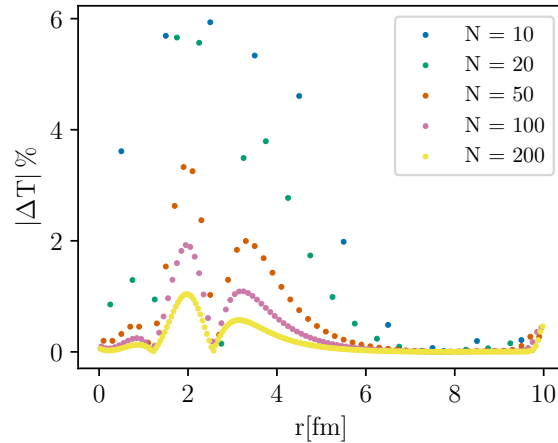The initial condition for the entropy density is computed with T_RENTo [31] simulating Pb-Pb collisions at $\sqrt{s_{NN}} = 5.02$ TeV. The T_RENTo parameters are set based in Refs. [150, 151]; the T_RENTo output is used as entropy density. The nucleon-nucleon cross section for Pb-Pb collisions at $\sqrt{s_{NN}} = 5.02$ TeV is taken from [152], i.e. $x = 67.6$ mb. The nucleons in the Pb ion are sampled from a spherically symmetric Woods-Saxon distribution with radius $R = 6.65$ fm and surface thickness $a = 0.54$ fm. Using this set of parameters, the transverse density $T_R(x, y)$ is generated for $1.5 \cdot 10^6$ minimum-bias collisions, among which the ones belonging to the 10% most central are selected. The normalization of the T_RENTo profile is computed by fixing the multiplicity of protons to the measured one [153]. The proton multiplicity in our calculation is obtained by employing a Cooper-Frye+FastReso approach at the end of the fluid-dynamic evolution as in Refs. [38, 42, 134]. In the future, when performing a Bayesian analysis to fit the experimental measurements, the normalization will be left as a free parameter of our model as in Ref. [38]. The initial conditions for the temperature field are then obtained through the thermodynamics EoS described in Ref. [154]. Radial fluid velocity, shear-stress tensor components, and bulk viscous pressure are initialized at zero.

6.3   Initial conditions for charm fields

The midrapidity density of charm quarks at the initialization time of the hydrodynamic evolution τ_0 comes from the initial hard production,

$$n_{\mathrm{hard}}^{Q\overline{Q}}(\tau_0, \vec{x}_\perp, y = 0) = \frac{1}{\tau_0} \left. \frac{d^3 N^{Q\overline{Q}}}{d\vec{x}_\perp dy} \right|_{y=0} . \tag{6.47}$$

In the above expression, the $Q\overline{Q}$ rapidity distribution in nucleus-nucleus collisions is set by the pQCD $Q\overline{Q}$ cross-section

$$\frac{dN^{Q\overline{Q}}}{dy} = \langle N_{\mathrm{coll}} \rangle \frac{1}{\sigma^{\mathrm{in}}} \frac{d\sigma^{Q\overline{Q}}}{dy} , \tag{6.48}$$

where σ^{in} is the inelastic proton-proton cross-section and $\sigma^{Q\overline{Q}}$ is the hard production cross-section. The average number of collisions N_{coll} is computed with a Glauber model and depends on the impact parameter of the collision, providing:

$$n_{\mathrm{hard}}^{Q\overline{Q}}(\tau_0, \vec{x}_\perp, y = 0) = \frac{1}{\tau_0} n_{\mathrm{coll}}(\vec{x}_\perp) \frac{1}{\sigma^{\mathrm{in}}} \frac{d\sigma^{Q\bar{Q}}}{dy} , \tag{6.49}$$

where n_{coll} is assumed to be distributed according to the fluid energy density $n_{\mathrm{coll}} \propto T^4$. As a future development, one could evaluate the radial distribution of binary collisions directly from T_RENTo, not to neglect space-momentum correlations that are important for flow observables. The integral of the density in the transverse plane provides the total number of heavy quarks

to be conserved throughout the QGP evolution. As discussed in [124], we remark that the current associated with the number of heavy quark-antiquark pairs is *accidentally* conserved. The heavy-quark mass is too large for them to be produced thermally throughout the QGP evolution; moreover, the annihilation rate of a $Q\overline{Q}$ pair is negligible within the lifetime of the plasma.

To fix at each point the initial value for α for the $Q\overline{Q}$ pair,

$$n(T, \alpha) = n_{\text{hard}}^{Q\overline{Q}} \tag{6.50}$$

Taking the central prediction by FONLL [79] for collisions at $\sqrt{s_{\text{NN}}} = 5.02$ TeV, one gets, at $y = 0$, $d\sigma^{Q\overline{Q}}/dy = 0.463$ mb, with $\sigma^{\text{in}} = 67.6$ mb [152]. At the beginning of the system evolution, the thermal distribution at zero chemical potential overshoots the density of charm quarks in the middle of the fireball. Therefore, α assumes negative values initially to match the hard production. This is not expected to happen at the fireball evolution's end, where the charm species' thermal abundance will be strongly suppressed. The total multiplicity of $Q\overline{Q}$ pairs per unit of rapidity is given by the integrated density profile, e.g. at $\tau = \tau_0$,

$$N^{Q\overline{Q}} = \tau_0 2\pi \int dr r n_{\text{hard}}^{Q\overline{Q}}. \tag{6.51}$$

In terms of fluid variables, due to the conservation of the charm current, the conserved charge is rewritten as,

$$N^{Q\overline{Q}} = \int d^3x \sqrt{|g|} N^0(\vec{x}) = 2\pi\tau \int r(nu^\tau + \nu^\tau) dr \tag{6.52}$$

where $|g|$ is the determinant of the metric. Besides the density, we can initialize the heavy-quark diffusion current. The assumed symmetries would allow a non-vanishing radial component, but we set it to zero in the absence of a more detailed initial state model.

6.4   Evolution of the fields

The initial conditions for the fields are set on a hypersurface at constant proper time $\tau_0 = 0.4$ fm. In Fig. 6.3 (upper panel), the time evolution of the charm density times the longitudinal proper time as a function of the radial coordinate is reported for different values of τ. This is shown for a non-diffusive ($D_s = 0$) and temperature-dependent D_s case obtained by linearly fitting results from LQCD calculations [95]. As expected, the density becomes more diluted when the temperature decreases. In the diffusive case, the density evolution is concurrent with developing the radial component of the diffusion current (Fig. 6.3, lower panel). Its values are always negative, thus negatively contributing to the conserved current N^μ. This results in a higher density n in the diffusive case, as shown in Fig. 6.3. Comparing it to the equilibrium composition of the heavy-quark density n, one finds that the condition of $|\nu^r| \ll n$ is not satisfied in the
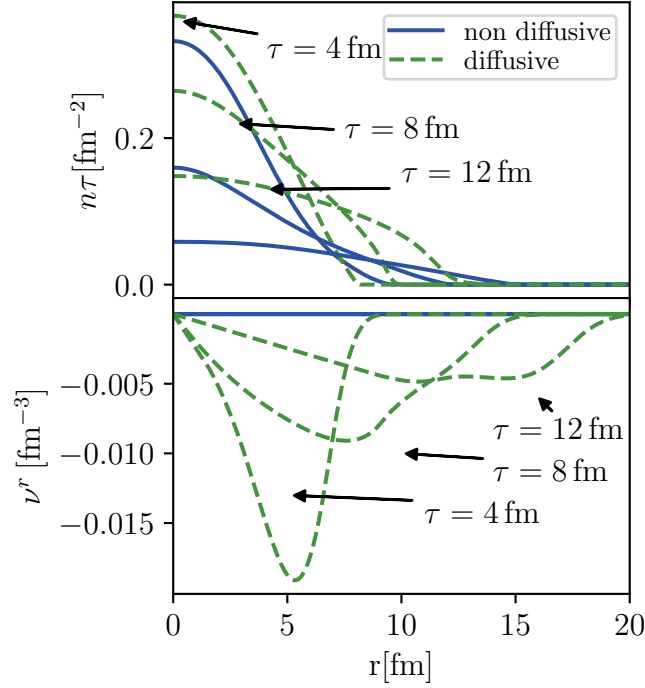
Figure 6.3: Charm density times the longitudinal proper time (upper panel) and diffusion current (lower panel) as a function of radius for different times. Solid lines correspond to an ideal hydrodynamic evolution, with $D_s = 0$. Dashed lines correspond to a diffusive hydrodynamic evolution, with $2\pi D_s T$ taken from LQCD [95].

entire radial region. This indicates that the out-of-equilibrium components of the heavy-quark distribution remain large throughout the evolution of the plasma. However, the magnitude of the diffusion current strongly depends on the spatial diffusion coefficient and its correspondent relaxation time. LQCD computations [95] favor a fast hydrodynamization of charm quarks and, thus, a reduction of the out-of-equilibrium correction. Around freeze-out we decompose the single-particle distribution functions, $f_i = f_{i,\text{eq}} + \delta f_i$, where the equilibrium part $f_{i,\text{eq}}$ is given by the ideal gas distribution and δf_i represents the out-of-equilibrium correction. In general, the δf_i correction receives a contribution from all the dissipative stresses Π, $\pi^{\mu\nu}$ and ν^μ, such that $\delta f_i = \delta f_{i,\text{bulk}} + \delta f_{i,\text{shear}} + \delta f_{i,\text{diffusion}}$. In our case, the open-charm hadrons distribution function includes both light and heavy components. To properly describe it, one should derive its expression in a multi-species fluid setup. As for now, we neglect out-of-equilibrium corrections to the fluid variables at the freeze-out surface. In the future, we will address the inclusion of non-linear terms in the evolution equation for the dissipation current and the derivation of a more consistent expression of the total distribution function.

6.5   Integrated yields

The charmed-hadron production is assumed to occur on a freeze-out hypersurface at a constant temperature. This chosen temperature is $T_{\mathrm{fo}} = 156.5$ MeV [105, 108]. The freeze-out hypersurface in the plane of Bjorken time τ and radius r is parametrized by a parameter $\gamma \in (0, 1)$. According to the Cooper-Frye prescription, a sudden decoupling is assumed at the freeze-out temperature, and the thermal momentum distribution of the particles is computed according to

$$\frac{dN_{h_c}}{p_T d\phi dp_T dy} = \frac{g_{h_c}}{(2\pi)^3} \int_{\Sigma_{\mathrm{fo}}} d\gamma d\phi dy \tau(\gamma) r(\gamma) \times \tag{6.53}$$
$$e^{q\alpha} \left[\frac{\partial r}{\partial \gamma} m_T K_1 \left(m_T \frac{u^r}{T} \right) I_0 \left(p_T \frac{u^r}{T} \right) - \frac{\partial \tau}{\partial \gamma} K_0 \left(m_T \frac{u^r}{T} \right) I_1 \left(p_T \frac{u^r}{T} \right) \right],$$

where g_{h_c} accounts for the degeneracy of the produced charmed hadron and q accounts for the charm content of the hadron. The total integrated yield dN_{h_c}/dy per unit rapidity for charmed and anti-charmed hadrons is measured by integrating Eq. (6.53). The feed-down from resonance decays is calculated using the FastReso package [42]. The list of resonances is taken from the PDG [155]. In Fig. 6.4, the comparison between the obtained integrated yields and experimental measurements [64–67] is shown for the 0-10% centrality interval. The yields and the p_T spectra correspond to the sum of particle and anti-particle divided by two, as reported by experiments. The p_T integration range is from 0 to 10 GeV/c. These results are computed for $D_s = 0$ since the integrated yield should not depend on the spatial diffusion coefficient. However, since out-of-equilibrium corrections to the single-particle distribution function at freeze-out are neglected, there can be a non-physical dependence of the yields on D_s. While the relative abundance of each charmed-hadron species depends mainly on the mass of the hadron, the absolute value of the integrated yields strongly depends on the EoS for the charm density as a function of T and α. The HRGc as EoS is the most suitable choice to estimate the thermal production of the hadrons and resonances included in the HRGc. The role played by the resonance decays is then to reshuffle the relative abundance of the hadrons while keeping the total number of charm quarks fixed. The agreement between the model and the measurements is quantified in the lower panel of Fig. 6.4. We observed that the mesons are compatible with the experimental uncertainties, computed as the sum in quadrature of the statistical and systematic uncertainties. A deviation of 2.4σ is observed for the Λ_c^+ baryons. This deviation might be caused by missing higher resonance states in the PDG [106–108]. Due to the resonances decay, the yield of the D^0 increases by a factor 4.3, while the one of the Λ_c^+ of a factor 5. Another factor 2.3 would be needed to reproduce the experimentally measured yield. Estimates for the yields of the Ξ_c^+ and Ω_c^0, whose experimental measurements are not yet available, are provided. Most likely, these values will underestimate the actual yields due to the lack of knowledge of higher resonance states. In other phenomenological models, the charmed-baryon enhancement is attributed to a
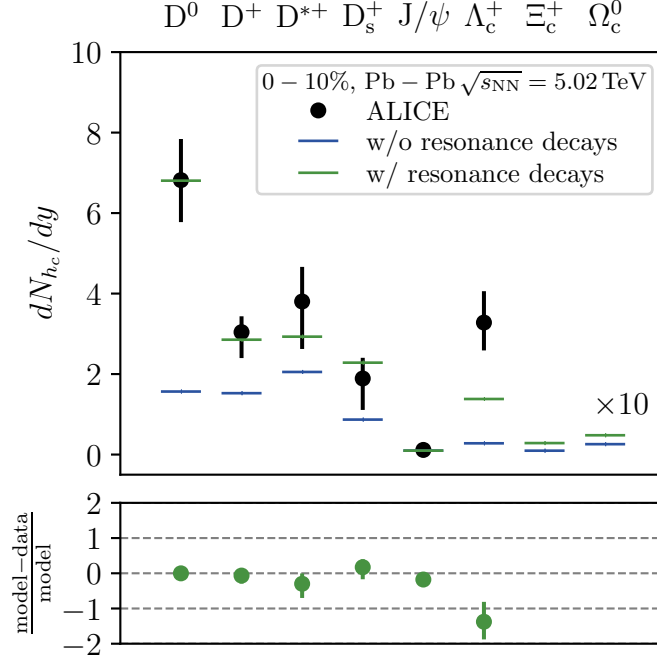
Figure 6.4: Charmed-hadron integrated yields with and without feed-down contributions from resonance decays and comparison with experimental data from the ALICE collaboration.

recombination process between the heavy quark and light thermal partons [109, 110, 156, 157].

6.6   Momentum distributions

In Fig. 6.5, the p_T-differential spectra for the same hadron species are reported and compared with the experimental measurements [64–67]. A ratio plot with the data to model comparison can be found in Appendix 6.6.1. The bands correspond to a spread of the input value of the spatial diffusion coefficient D_s going from a non-diffusive case ($D_s = 0$) to a temperature-dependent $2\pi D_s T$ [95]. The fluid-dynamic description seems to capture the physics of D mesons up to $p_T \sim 4$–5 GeV/c. This implies that, even if the charm does not move collectively with the rest of the fluid in the early stage of the evolution, it relaxes to the same radial flow of the QGP before the freeze-out occurs. As observed for the integrated yield, the Λ_c^+ calculation underestimates the experimental measurement. The J/ψ p_T distribution describes the experimental measurements for $p_\mathrm{T} < 3$ GeV/c, while it overpredicts the yield for higher p_T. This discrepancy for $p_\mathrm{T} > 3$ GeV/c might be attributed to the dominant contribution from primordial J/ψ, which is not accounted for in our model since it is not expected to reach thermal equilibrium [158–160], but is mainly sensitive to path-length-dependent effects, like survival probability and energy loss. It is also important to note that the experimental measurements consist of J/ψ directly produced in the collisions plus the contribution from beauty hadron decays. Including the out-
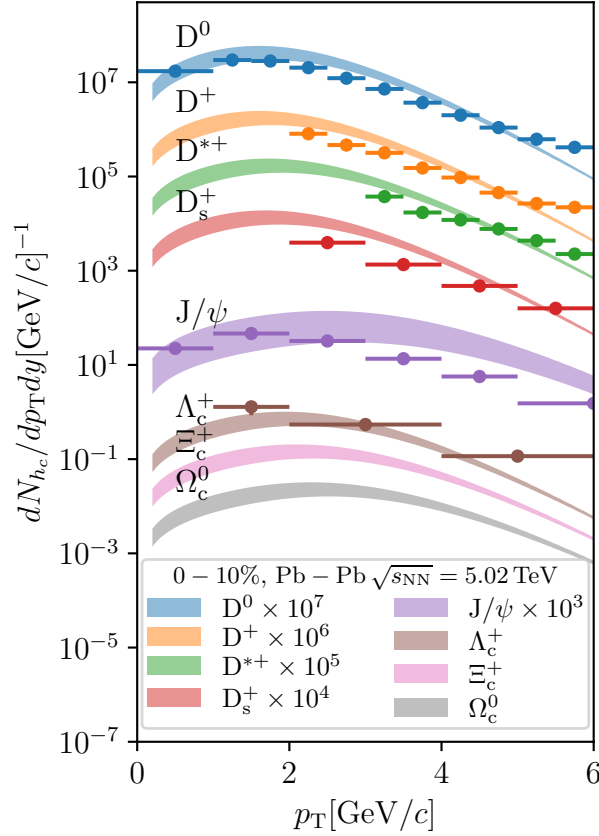
Figure 6.5: Results for the momentum distributions of D^0, D^+, D^{*+}, D_s^+, Λ_c^+, and J/ψ are shown in comparison with experimental measurements from the ALICE Collaboration [64–67]. Predictions for Ξ_c^0 and Ω_c^0 baryon states, which have not been measured yet, are also shown.

of-equilibrium corrections in the model at the freeze-out surface will influence the shape of the momentum distributions. They would modify the spectra at intermediate/high p_T. When adequately included, we do not expect such a strong dependence on D_s in the spectra but rather only a tilt in the momentum distribution. A further remark regards the dependence of the final momentum distribution on the initial conditions for the charm fields. In particular, a broader initial distribution for the charm density results in a larger average p_T at freeze-out. A more thorough study of the charm initial conditions will improve the description of the transverse momentum distribution of the charm hadrons, without of course impacting the results for the integrated yields.

6.6.1 Details on the results of charm-hadron momentum distributions

In Fig. 6.6 the results for the ratio between the experimental measurements of charm-hadron momentum distributions and the results from our fluid-dynamic model are shown. The bands correspond to a spread of the input value of the spatial diffusion coefficient D_s going from a non-
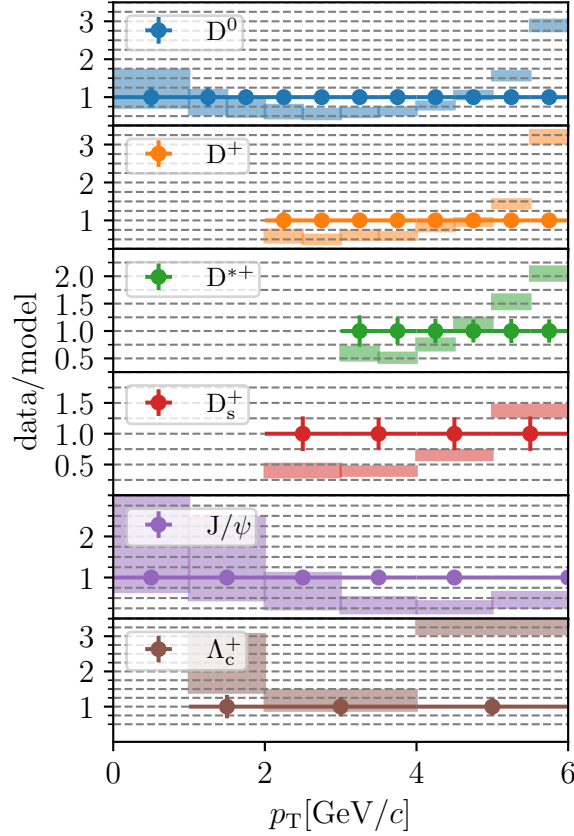
Figure 6.6: Data-to-model ratios for D^0, D^+, D^{*+}, D_s^+, Λ_c^+, and J/ψ momentum distributions. Experimental measurements are taken from [64–67].

diffusive case ($D_s = 0$) to a temperature-dependent $2\pi D_s T$ obtained by linearly fitting results from LQCD calculations [95]. The fluid-dynamic descriptions captures the behavior to D^0 and J/ψ up to $p_T \sim 2$ GeV. At intermediate transverse momentum, our calculation for the D mesons deviates of 25% from the experimental measurements for the $D_s = 0$ case. A larger deviation is hereby observed for J/ψ attributed to the dominant contribution from primordial J/ψ, which is not accounted for in our model since it is not expected to reach thermal equilibrium [158–160], but is mainly sensitive to path-length-dependent effects, like survival probability and energy loss. As observed for the integrated yield, the Λ_c^+ calculation underestimates the experimental measurement. This deviation might be caused by missing higher resonance states in the PDG [106–108]. At p_T larger than 5 GeV, the fluid-dynamic model seems no longer applicable since it's not able to capture the behavior of the particle spectra.

A further remark regards the dependence of the final momentum distribution on the initial conditions for the charm fields. In particular, a broader initial distribution for the charm density results in a larger average p_T at freeze-out. A more thorough study of the charm initial conditions will improve the description of the transverse momentum distribution of the charm hadrons, without of course impacting the results for the integrated yields.

Chapter 7

Conclusions and outlook

A volte uno si crede incompleto ed è
soltanto giovane.
– Sometimes you feel incomplete but
you are just young.

ITALO CALVINO, *Il visconte dimezzato*

7.1   Summary of achievements

In this work, we developed a new way of studying heavy-quark dynamics in the QGP based on
fluid dynamics. The steps leading to formulating such an approach can be summarized in the
following key points:

- **Experimental evidence of charm-quark equilibration.** The experimental measure-
  ments of v_2 of open- and hidden-charm hadrons at the LHC raised the question regarding
  the collective behavior of charm quarks in the QGP, which we decided to tackle with fluid
  dynamics (see Chapter 4).

- **Preliminary assessment of hydrodynamization.** A fundamental motivation to imple-
  ment the fluid-dynamic approach derived from the theoretical formulation of heavy-quark
  relaxation times as a function of the spatial diffusion coefficient. With the current knowl-
  edge of D_s, we have been able to assess the applicability of a hydrodynamic approach for
  charm quarks and, at later evolution times, also for beauty quarks in the QGP produced
  at LHC energies.

- **Support from first-principle QCD calculations.** The LQCD results on the heavy-
  quark spatial diffusion coefficient highlighted how the hydrodynamization of charm quarks
  in the medium could happen on short timescales compared with the lifetime of the QGP

produced in ultrarelativistic heavy-ion collisions. These results became available shortly after our first inquiries into this matter and served as a boost in the motivation and reliability of our approach.

- **Fluid-dynamic code.** We developed a fluid-dynamic code to solve the equation of motion of the heavy-quark density and diffusion current coupled with the evolution of QGP fluid fields. The 1+1 dimensional implementation allows us, at present, to compute integrated yields and transverse momentum distribution of charm hadrons per unit rapidity.

Finally, we would like to remark on the two main concepts that drive this research work:

- **Access to QCD properties.** Our approach is based on the idea of kinetic equilibration of heavy quarks within the expanding medium. It is therefore sensitive to transport properties that correspond to first-principle quantities in QCD, computed under the assumption of thermal equilibrium. In particular, our model will be able to provide constraints on the spatial diffusion coefficient D_s, which quantifies the interaction of the heavy quark with the QGP in the soft-momentum regime.

- **Universality of the fluid-dynamic approach.** In our approach, we extend the fluid-dynamic description, usually limited to the light flavors that compose the QGP medium, to heavy degrees of freedom. The idea of a universal effective description behind light and heavy flavors is fascinating by itself and therefore worth investigating. It asks the fundamental question of whether the behavior of such a complex system, that spans over three orders of magnitude in mass scales (from MeV to GeV), can be described by a few macroscopic thermodynamic quantities defined in local kinetic equilibrium.

7.2   Outlook

The approach we have developed in this work represents the first step in a new direction in the treatment of heavy quarks in heavy-ion collisions. Heavy quarks have always been considered pure hard probes of the QGP. Taking into account the soft aspect of their dynamics is a way of gaining new information on the underlying field theory in many-body systems. The success that our model has shown so far serves as a strong motivation to continue its development. Its present "incompleteness" stems from it being a young, new approach. To make it more competitive, able to stand out and capture the rich phenomenology of heavy-ion collisions, several improvements will be pursued. Our transparent and flexible implementation allows for straightforward extensions of the approach. In the following, some examples of such extensions, whose implementation is in progress or planned, are presented.

7.2.1 Out-of-equilibrium corrections

A first important direction of improvement is represented by a consistent treatment of out-of-equilibrium corrections to the heavy-quark distribution function.

As mentioned in Chapter 6, a finite contribution from the heavy-quark diffusion current ν^μ to the initial state has not been considered so far. No model at present provides a first-principle description for such a contribution. Nevertheless, one could study how the heavy-quark current behaves if the Navier-Stokes limit for ν^μ is imposed as an initial condition. As an alternative, one could study the effect of a free-streaming phase between $\tau = 0$ and $\tau = \tau_0$ on the heavy-quark current[1]. These would be two ways of effectively implementing an out-of-kinetic equilibrium description for the heavy-quark distribution from the very beginning of the collision evolution, making the comparison with standard transport models in the literature more direct.

Out-of-equilibrium corrections must also be consistently considered on the freeze-out hypersurface to compute charm-hadron momentum distributions and integrated yields. As stressed in Chapter 6, the inclusion of diffusion leads to a non-physical increase in the integrated yields if the correct counter-contribution from the diffusion current is neglected. There are two ways that one could exploit to obtain them:

- **Multi-fluid description.** One possibility is to rewrite the fluid-dynamic description assuming the presence of multiple species contributing to the diffusion current. Such an approach was explored in a series of theoretical papers in the framework of kinetic theory (see Refs. [161, 162]). This approach leads to an unambiguous description of the phase space distribution function of hadronic species at freeze-out that are composed of both light and heavy degrees of freedom (such as all open-charm states). It also includes naturally out-of-equilibrium contributions from the diffusion current, shear-stress tensor, and bulk viscous pressure. It requires, however, a redefinition of all transport coefficients and relaxation times.

- **Maximum entropy approach.** Recently, a maximum-entropy approach has been proposed in Ref. [163] to compute the time evolution of the single-particle distribution function with minimal assumptions. We plan to extend this approach to include the presence of a diffusive heavy-quark current and apply it on the freeze-out hypersurface to compute heavy-flavour particle spectra. The idea is to define a Boltzmann entropy functional,

$$S[f] = \int dP f(x, p)(\log f(x, p) - 1), \qquad (7.1)$$

and then minimizing it with respect to the distribution function f. The distribution function is required to satisfy a set of constraints via the method of Lagrange multipliers.

---

[1]A free-streaming description leads, when applied to the energy-momentum tensor, to finite values for the fluid 4-velocity and the dissipative fields, even if they are initially set to zero [32, 33].

The distribution function will eventually depend on the particle's 4-momentum and on the set of Lagrange multipliers, which in turn depend on spacetime. Specifically, we constrain the first moment of the distribution function to match at each point in spacetime the heavy-quark current N^μ,

$$N^\mu = \int dP p^\mu f(x,p)\,. \tag{7.2}$$

Since the heavy-quark current has in principle four independent components, four Lagrange multipliers are needed. They can be encoded for convenience in a 4-vector λ^μ. The minimization of the entropy functional in this case reads

$$\frac{d\tilde{S}[f]}{df} = \frac{dS[f]}{df} - \frac{d}{df}\left[\lambda_\mu\left(N^\mu - \int dP p^\mu f\right)\right] = 0\,, \tag{7.3}$$

where $\tilde{S}[f]$ indicates the constrained version of the entropy functional $S[f]$. The four Lagrange parameters are reduced to two when exploiting the symmetries of the system as in our work, such that the fluid equations are effectively solved in 1+1 dimensions. By solving Eq. (7.3), one finds for f,

$$f \propto \exp(-\lambda_\mu k^\mu)\,. \tag{7.4}$$

The Lagrange parameters can be determined by solving the equations encoded in Eq. (7.2). The LHS of Eq. (7.2) is provided by the fluid-dynamic code by solving the hydrodynamic equations of motion as outlined in Chapter 6.

7.2.2   Heavy-quark equation of state

In Chapter 6, we faced the necessity of implementing an EoS to describe the heavy-quark density as a function of temperature and heavy-quark chemical potential. This is a fundamental ingredient in order to have a closed system of equations in fluid dynamics. Such an EoS has never been computed by first principles in QCD. Therefore, our solution was to exploit the hadron-resonance gas description of all known charm states even at high temperatures, where it might not be justified. The main reason why such a quantity has never been computed by the LQCD community is that the sum of heavy quark-antiquark pairs is not a conserved current in QCD. However, such a need motivated the theory community to compute this quantity. Even if there are no results available yet, the interest in this calculation has been triggered both in the LQCD community and in the area of functional approaches to QCD transport properties. We are looking forward to seeing such results and assessing how they influence our description of charm hadrons.

7.2.3 Flow coefficients

To finally answer the question regarding charm thermalization in the medium, it will be necessary to go beyond charm hadron distributions and integrated yields. A key observable is represented by anisotropic flow coefficients of open- and hidden-charm states. We are currently working on their implementation in our code. This requires giving up the azimuthal symmetry of the system and effectively solving 2+1-dimensional equations. In our code, the implementation profits of the background-fluctuation splitting approach already developed for the fluid fields in the absence of additional conserved currents outlined in Ref. [36]. In the minimal case, entropy density fluctuations with respect to a radially symmetric background in the initial state (that imply, through the use of the EoS, fluctuations in the initial temperature), will also determine fluctuations in the heavy-quark density profile. In a more sophisticated approach, also azimuthal perturbations in the initial heavy-quark chemical potential can be considered to mimic fluctuations in the initial hard production.

7.2.4 Fluid dynamics for beauty quarks

In Chapter 4, we mentioned the relevance of beauty quarks as golden probes of the QGP. Their large mass allows in fact for robust control of theoretical calculations regarding their in-medium dynamics and their associated transport coefficients. Furthermore, in Chapter 5 we have shown how the applicability of the hydrodynamic picture for their diffusion in the QGP is more complicated than for charm quarks. However, by employing the most recent LQCD results, we observed that a fluid-dynamic approach might be applicable in the late stages of the fireball evolution.

To give a definitive answer to the question of (partial) thermalization of beauty quarks in the hot QCD medium, higher precision experimental measurements of beauty hadrons in the low transverse momentum kinematic region are needed. Such measurements would provide a key set of new and independent constraints on heavy-flavor transport and hadronization, in particular on the diffusion coefficient D_s and its temperature dependence. The ongoing experimental effort during Run 3 and Run 4 at the LHC is expected to deliver such measurements in the next years. In the future, the major upgrade of the ALICE detector (ALICE3 [164]) planned for Run 5, currently scheduled to start in 2035, would allow to perform measurements of both the production and anisotropy of beauty mesons and baryons down to $p_{\mathrm{T}} = 0$ with unprecedented precision.

The framework developed in this Thesis can be straightforwardly extended to address the dynamics of beauty quarks in the plasma. The needed modifications concern

- adding the equation for the current associated with the $b\bar{b}$ number conservation to the system of equations. To ensure causal behavior, analogously as for charm quarks, an equation of motion for the beauty-quark diffusion current must be included. Its evolution

is regulated by the beauty chemical potential-over-temperature ratio, the spatial diffusion coefficient D_s, and the relaxation time – calculated for the beauty-quark mass (see Chapter 5);

- employing perturbative calculations (FONLL) for the beauty-production cross section per unit rapidity to get initial conditions for the beauty density. Employing the FONLL result of $d\sigma^{b\bar{b}}/dy = 0.0296$ mb at midrapidity for $M_b = 4.8$ GeV [78], and $\langle N_{\text{coll}} \rangle = 1653$ for the 0-10% most central Pb–Pb collisions at $\sqrt{s_{\text{NN}}} = 5.02$ TeV [31], the total number of $b\bar{b}$ pairs per unit rapidity is expected to be

$$\frac{dN^{b\bar{b}}}{dy} = \langle N_{\text{coll}} \rangle \frac{1}{\sigma^{\text{in}}} \frac{d\sigma^{Q\overline{Q}}}{dy} \sim 0.7 \,. \tag{7.5}$$

- modifying the heavy-quark HRG EoS to include all measured beauty hadrons and resonance states (HRGb). The accuracy of this equation is of course influenced by the experimental knowledge of the masses and quantum numbers of such states, but most importantly is affected by the fact that there might be contributing states that have not yet been measured.

As presented so far, no notion of "partial" thermalization, such as the one exploited by the SHMb, has been introduced. In a full-thermalization scenario, the formation of beauty hadrons from the QGP would occur only at T_{pc}, according to the hadrons' statistical weights. In the case of partial thermalization, some of the initially produced $b\bar{b}$ pairs might diffuse so fast that they would escape the QGP medium and produce a pair of open-beauty hadrons via string fragmentation in the vacuum, without having the chance of hadronizing into a $b\bar{b}$ bound state. One would therefore observe an effective reweighing of the hadron states produced at freeze-out. In particular, as observed within the SHMb, the yields of bottomonia states seem to be reduced with respect to the thermal case. As a counter effect, one would expect the yields of open-beauty hadrons to be enhanced.

A way to effectively introduce the concept of partial thermalization in our approach could be to introduce a non-thermal weight $W < 1$ in the HRGb as a phenomenological parameter,

$$n(T, \alpha) = \frac{T}{2\pi^2} \sum_{i \in \text{open b}} q_i M_i^2 e^{q_i \alpha} K_2(M_i/T) + W \frac{T}{2\pi^2} \sum_{i \in \text{hidden b}} q_i M_i^2 e^{q_i \alpha} K_2(M_i/T) \,. \tag{7.6}$$

The total number of beauty quarks remains the same and it is fixed by the initial hard production. The fugacity, however, changes to accommodate for the reweighing. The parameter W can then be fixed by comparing our model results with experimental measurements and can give a measure of the percentage of thermalized beauty quarks in the medium. In contrast to the SHMb, our model allows us to see how the modified fugacity evolves in spacetime throughout the collision.
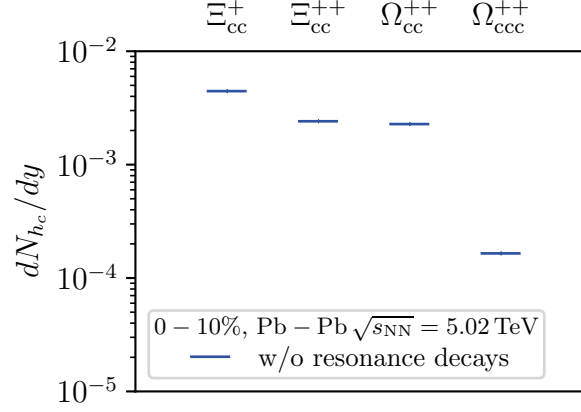
Figure 7.1: Integrated yields of predicted multi-charm states Ξ_{cc}^+, Ξ_{cc}^{++}, Ω_{cc}^{++} and Ω_{ccc}^{++} in Pb–Pb collisions at $\sqrt{s_{NN}} = 5.02$ TeV in the $0 - 10\%$ centrality class.

7.2.5   Multi-charm baryons

Measurements of multi-charm hadrons, such as the Ξ_{cc}^+, Ξ_{cc}^{++}, Ω_{cc}^{++} and Ω_{ccc}^{++} and exotic states such as the newly-discovered T_{cc}^+ (ccud), would provide a direct window on hadron formation from deconfined QGP. In fact, the yields of multi-charm baryons relative to the number of produced charm quarks are predicted to be significantly enhanced in AA relative to pp collisions. The observation and precise quantification of such enhancements would represent a decisive step forward in the study of the properties of deconfined QCD matter.

In Fig. 7.1 we show our predictions for the integrated yields of Ξ_{cc}^+, Ξ_{cc}^{++}, Ω_{cc}^{++} and Ω_{ccc}^{++} in Pb–Pb collisions at $\sqrt{s_{NN}} = 5.02$ TeV in the $0 - 10\%$ centrality class. There is a clear ordering between the 2-charm and 3-charm states stemming from the hadron total mass; the presence of an extra charm quark, in fact, suppresses the integrated yield of Ω_{ccc}^{++} of a factor $\exp(-M_c/T_{FO}) \sim 10^{-4}$ at a freeze-out temperature of 156.5 MeV with respect to the doubly-charmed hadrons. This difference is however partially compensated by the fugacity $\exp(q_i\alpha)$, which scales with the number q_i of charm charge contained in the hadron i. In Fig. 7.2 we show the predictions for the transverse-momentum distributions of Ξ_{cc}^+, Ξ_{cc}^{++}, Ω_{cc}^{++} and Ω_{ccc}^{++} in Pb–Pb collisions at $\sqrt{s_{NN}} = 5.02$ TeV in the $0 - 10\%$ centrality class. The spread in the curves is given by the impact of the spatial diffusion coefficient, as explained in Chapter 6. The comparison of the measured yields to these predictions would provide a very sensitive measure of the degree of equilibration of charm quarks in the medium. Such measurements are expected to be achieved at the LHC, after the major upgrade of the ALICE detector [164].

7.2.6   Limits of thermalization

In this work, we have focused on studying charm hydrodynamization under experimental conditions realized in central Pb–Pb collisions at $\sqrt{s_{NN}} = 5.02$ TeV at the LHC. Hence, the question
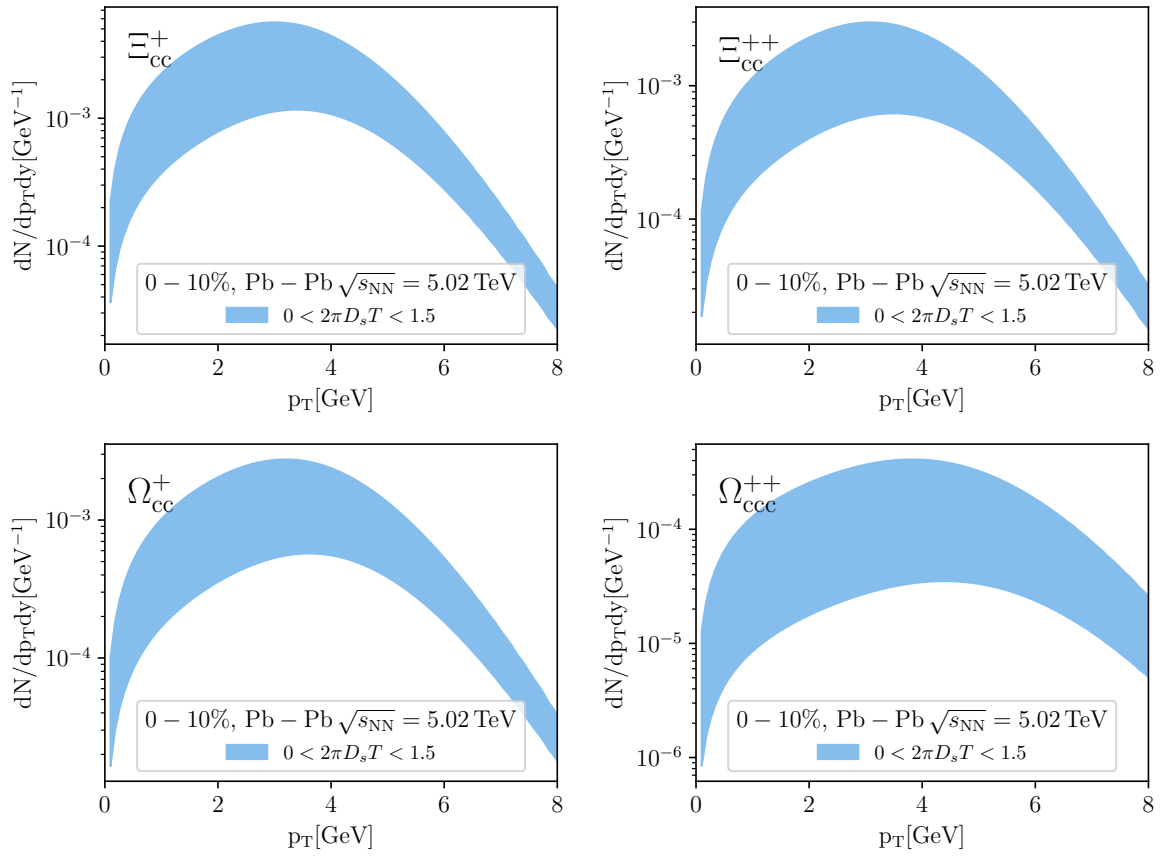
Figure 7.2: Transverse momentum distributions of predicted multi-charm states Ξ_{cc}^+, Ξ_{cc}^{++}, Ω_{cc}^{++} and Ω_{ccc}^{++} in Pb–Pb collisions at $\sqrt{s_{NN}} = 5.02\,\text{TeV}$ in the $0-10\%$ centrality class.
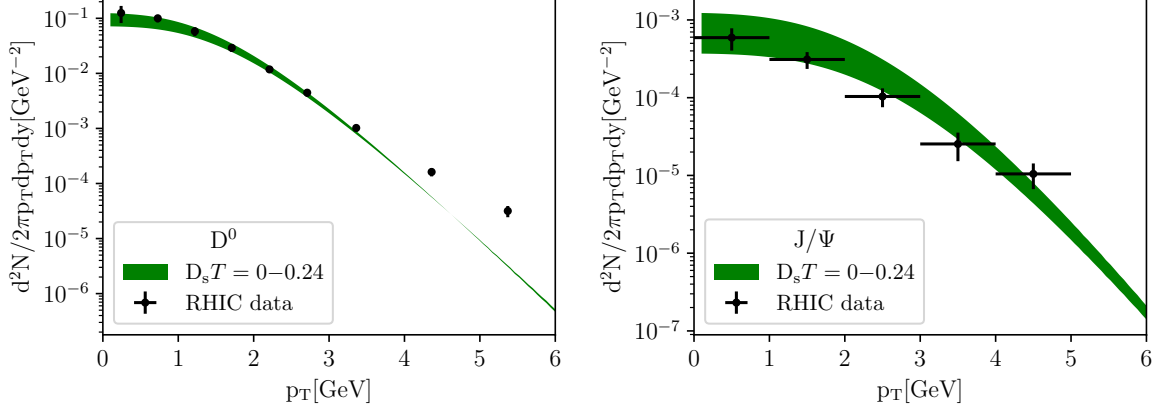
Figure 7.3: Transverse-momentum distributions of D^0 (left panel) and J/ψ (right panel) for Au–Au collisions at $\sqrt{s_{NN}} = 200$ GeV in the $0 - 10\%$ and $0 - 20\%$ centrality class, respectively. Our model results are shown in comparison to experimental data from Refs. [71, 72].

of whether hydrodynamic conditions for charm quarks are realized when moving to more peripheral collisions, lower collision energies, or smaller colliding systems arises naturally. Furthermore, LHC accelerator physicists and the heavy-ion community are currently discussing which ions to collide in Run 5 and Run 6. Smaller ions, such as Xe, In, Kr, Ca, Ar, O, are being considered. Thanks to the unique features of our framework, we will be able to provide quantitative predictions of heavy-flavor observables and their dependence on collision energy and system size.

As a first step in this direction, we have recently started to explore charm thermalization in Au–Au collisions at $\sqrt{s_{NN}} = 200$ GeV. Elliptic flow measurements from the STAR collaboration of D^0 and J/ψ in Au–Au collisions at $\sqrt{s_{NN}} = 200$ GeV at RHIC [69, 165] suggest that charm quarks might reach kinetic equilibration with the medium. The main differences with respect to LHC conditions consist of a lower temperature and energy density – due to the lower collision energy – and a smaller amount of produced $c\bar{c}$ pairs – due to the smaller inelastic cross section for charm quark production and a lower number of binary nucleon-nucleon collisions. With an analog procedure to the one outlined in Chapter 6, we applied our fluid-dynamic model to compute integrated yields and transverse momentum distributions of charm hadrons and compare them with experimental measurements. In Fig. 7.3, we report the results for D^0 and J/ψ, in the $0 - 10\%$ and $0 - 20\%$ centrality class, respectively. Our model results are shown in comparison to experimental data from Refs. [71, 72]. The agreement with the experimental measurements is remarkable, indicating that a fluid-dynamic description for charm quarks can be successfully applied also at RHIC top-energies. In the future, we will investigate whether this approach still holds at lower energies, down to collision energies per nucleon pair of the order of tens of GeV, profiting from the experimental measurements at the Beam Energy Scan (BES). Under these experimental conditions, a validation of the hydrodynamic approach will have to be performed also for the light sector, including the presence of a conserved baryon current and an EoS at finite baryon chemical potential. In this context, however, longitudinal boost invariance is expected to be no longer an effective symmetry of the produced system[2] [170]. Therefore, an extension of

---

[2]The breakdown of Bjorken longitudinal-boost symmetry has already been experimentally observed through rapidity-dependent observables at RHIC [166] and the LHC [167–169]. This effect is expected to be more and more relevant at lower energies such as the ones reached with the BES.

our code to a 3D+1 setup will be pursued to explore the rapidity dependence of anisotropic flow coefficients.

Appendix A

Analytic solutions to fluid-dynamic equations

A.1   Gubser flow

Gubser flow [61] represents a generalization of Bjorken flow allowing for an expansion in the transverse direction. It is invariant under longitudinal Lorentz boosts along the beam axis, and is symmetric under $SO(3)$ transformations in a de-Sitter space obtained from a Weyl rescaling of the metric tensor,

$$g_{\mu\nu} \longrightarrow \hat{g}_{\mu\nu} \equiv \Omega^{-2} g_{\mu\nu} \,. \tag{A.1}$$

The most suitable choice of coordinates is given by

$$\tau = \sqrt{t^2 - z^2} \,, \tag{A.2}$$

$$\eta = \frac{1}{2} \log \left(\frac{t+z}{t-z} \right) \,, \tag{A.3}$$

$$x_\perp = \sqrt{x^2 + y^2} \,, \tag{A.4}$$

$$\phi = \arctan \frac{y}{x} \,. \tag{A.5}$$

Starting from the line element in Minkowski space,

$$ds^2 = -d\tau^2 + dx_\perp^2 + x_\perp^2 \, d\phi^2 + \tau^2 d\eta^2 \,, \tag{A.6}$$

and performing the following Weyl rescaling,

$$d\hat{s}^2 = \frac{ds^2}{\tau^2} = \frac{-d\tau^2 + dx_\perp^2 + x_\perp^2 \, d\phi^2}{\tau^2} + d\eta^2 \tag{A.7}$$

one obtains the metric of $dS_3 \times \mathbf{R}$, where the one-dimensional R is given by the rapidity direction. A change of coordinate,

$$\sinh \rho = -\frac{1 - q^2\tau^2 + q^2 x_\perp^2}{2q\tau} \,, \qquad \tan \theta = \frac{2qx_\perp}{1 + q^2\tau^2 - q^2 x_\perp^2} \,, \tag{A.8}$$

where q is a parameter with the dimensions of an inverse length, leads to

$$d\hat{s}^2 = -d\rho^2 + \cosh^2 \rho \, (d\theta^2 + \sin^2 \theta d\phi^2) + d\eta^2 \, . \tag{A.9}$$

In this new system of coordinates $(\rho, \theta, \phi, \eta)$ a new symmetry becomes manifest: the symmetry under rotations of the sphere parametrized by (θ, ϕ). This symmetry, that was a conformal symmetry in $\mathbf{R}^{3,1}$, is an isometry in $dS_3 \times \mathbf{R}$. In this coordinate system one writes the four-velocity of a fluid at rest:

$$\hat{u}_\rho = -1 \qquad \hat{u}_\theta = \hat{u}_\eta = \hat{u}_\phi = 0 \tag{A.10}$$

It corresponds to a static flow in the new space. When going back to Minkowski space and performing the opportune Weyl rescaling,

$$u_\mu = \tau \frac{\partial \hat{x}^\nu}{\partial x^\mu} \hat{u}_\nu \, , \tag{A.11}$$

where $x^\mu = (\tau, x_\perp, \phi, \eta)$ and $\hat{x}^\mu = (\rho, \theta, \phi, \eta)$, one gets,

$$u_\tau = -\cosh k \, , \tag{A.12}$$

$$u_\perp = \sinh k \, , \tag{A.13}$$

$$u_\eta = u_\phi = 0 \, , \tag{A.14}$$

where we introduced

$$k(\tau, x_\perp) \equiv \operatorname{atanh} \left[\frac{2q^2 \tau x_\perp}{1 + q^2 \tau^2 + q^2 x_\perp^2} \right] . \tag{A.15}$$

In order to find the evolution of the energy density one starts again by working in $dS_3 \times \mathbf{R}$. In this coordinate system the energy density $\hat{\epsilon}$ must depend only on the time-coordinate ρ. Moreover – given the equation of state $\hat{\epsilon} \propto \hat{T}^4$ – the entropy density $\hat{s}$ must be proportional to $\hat{\epsilon}^{3/4}$. At a fixed time ρ the total entropy per unit rapidity is given by $\hat{s}(4\pi \cosh^2 \rho)$, obtained by integrating over the volume of the sphere parametrized by (θ, ϕ). The total entropy in the inviscid case must be constant, thus it must not vary with ρ,

$$\frac{d[\hat{s}(4\pi \cosh^2 \rho)]}{d\rho} = \frac{d[\hat{\epsilon}^{3/4}(4\pi \cosh^2 \rho)]}{d\rho} = 0 \tag{A.16}$$

This leads to the solution,

$$\hat{\epsilon} = \hat{\epsilon}_0 (\cosh \rho)^{-8/3} \tag{A.17}$$

where $\hat{\epsilon}_0$ is an integration constant. By employing the transformation law [1].

$$\epsilon = \frac{\hat{\epsilon}}{\tau^4} \tag{A.18}$$

---

[1]Lengths are scaled by τ in $\mathbf{R}^{3,1}$ with respect to $dS_3 \times \mathbf{R}$, so volumes are scaled by τ^3 and energies by τ^{-1}. Energy densities are scaled then by τ^{-4}

one finds the expression,

$$\epsilon = \frac{\hat{\epsilon}_0}{\tau^{4/3}} \frac{(2q)^{8/3}}{[1 + 2q^2(\tau^2 + x_\perp^2) + q^4(\tau^2 - x_\perp^2)^2]^{4/3}}. \tag{A.19}$$

Using the equation of state, the temperature reads:

$$T = \frac{\hat{T}_0}{\tau^{1/3}} \frac{(2q)^{2/3}}{[1 + 2q^2(\tau^2 + x_\perp^2) + q^4(\tau^2 - x_\perp^2)^2]^{1/3}} \tag{A.20}$$

where one assumes

$$\epsilon = gT^4, \tag{A.21}$$

with g accounting for the relevant degrees of freedom.

Appendix B

Details on fluid-dynamic transport coefficients

B.1 Coefficients of the linear expansion of the off-equilibrium deviation

In this section, we determine the coefficients of the linear expansion of the deviation from equilibrium $\delta f_k^{(r)}$ in terms of its moments, expressed in Eq. (5.22). Each coefficient can be computed by integrating the corresponding moment of the deviation $\delta f_k^{(r)}$. The orthogonality relations between moments given by [45],

$$
\int dK F(k^0) k^{\langle \mu_1 \cdots \mu_n \rangle} k_{\langle \nu_1 \ldots k_{\nu_m} \rangle} = \frac{\delta_n^m m! \Delta_{\nu_1 \ldots \nu_m}^{\mu_1 \ldots \mu_n}}{(2m+1)!!} \int dK F(k^0) (\Delta_{\alpha\beta} k^\alpha k^\beta)^m \,, \tag{B.1}
$$

are employed. The expansion coefficient for the heavy-quark bulk pressure is obtained from the zeroth moment of the deviation as

$$
\begin{aligned}
-\frac{3}{M^2} \Pi_{(r)} = \int dK \delta f_k^{(r)} &= \\
&= -\frac{3}{M^2} \int dK a_0^{(r)} f_0^{(r)} \Pi_{(r)} \\
&\rightarrow a_0^{(r)} = \frac{1}{I_{00}^{(r)}} \,.
\end{aligned} \tag{B.2}
$$

The coefficient for the heavy-quark diffusion current is computed by taking the first moment of the deviation,

$$
\begin{aligned}
\nu_{(r)}^{\langle \sigma \rangle} = \int dK k^{\langle \sigma \rangle} \delta f_k^{(r)} &= \\
&= \int dK f_0^{(r)} a_1^{(r)} k^{\langle \sigma \rangle} k_{\langle \mu \rangle} \nu_{(r)}^\mu = \\
&= -\frac{a_1^{(r)}}{3} \delta_\mu^\sigma \nu_{(r)}^\mu \int dK f_0^{(r)} k^2 \\
&\rightarrow a_1^{(r)} = -\frac{1}{P_{(r)}} \,.
\end{aligned} \tag{B.3}
$$

The coefficient for the heavy-quark shear stress term is obtained by taking the second moment of the deviation,

$$
\begin{aligned}
\pi^{\mu\sigma}_{(r)} &= \int dK k^{\langle\mu} k^{\sigma\rangle} \delta f_k^{(r)} = \\
&= \int dK k^{\langle\mu} k^{\sigma\rangle} k_{\langle\alpha} k_{\beta\rangle} a_2^{(r)} f_0^{(r)} \pi_{\alpha\beta}^{(r)} \\
&= \frac{2}{15} \int dK a_2^{(r)} f_0^{(r)} k^4 \pi_{(r)}^{\mu\sigma} \\
&\rightarrow a_2^{(r)} = \frac{1}{2 I_{42}^{(r)}} \, ,
\end{aligned}
\tag{B.4}
$$

B.2 Transport coefficients

In this section, we report the explicit calculation for the heavy-quark relaxation time and diffusion coefficient leading to the result in Eq. (5.31). The starting point is the Fokker-Planck equation for the heavy (anti)quark distributions (charm, anti-charm, bottom, anti-bottom)

$$
k^\mu \partial_\mu f_k^{(r)} = k_0 \frac{\partial}{\partial k^i} \left\{ A k^i f_k^{(r)} + \delta^{ij} D \frac{\partial}{\partial k^j} f_k^{(r)} \right\} \, ,
\tag{B.5}
$$

where we consider the case of a isotropic momentum broadening, i.e. $D = B_0 = B_1$.

The zeroth moment of the Fokker-Planck equation gives the continuity equation in the LRF of the fluid,

$$
\partial_t n_{(r)} + \partial_i \nu_{(r)}^i = 0 \quad \longrightarrow \quad \partial_t n_+ + \partial_i \nu_+^i = 0 \, .
\tag{B.6}
$$

Notice that the RHS of Eq. (B.5) provides a vanishing contribution when taking its zeroth moment. This can be verified by doing the integration by parts.

The first moment of the Fokker-Planck equation gives

$$
\partial_t \int dK k_0 k^l f_k^{(r)} + \partial_i \int dK k^l k^i f_k^{(r)} = \int dK k_0 k^l \frac{\partial}{\partial k^i} \left(A k^i f_k^{(r)} \right)
\tag{B.7}
$$

As we will show below, this will lead to the equation of motion for the diffusion current in the LRF of the fluid. Notice that the term proportional to the momentum-broadening coefficient vanishes when taking the first moment of the Fokker-Planck equation. In fact, since it is proportional to a second-order derivative it vanishes after integration by parts. Let us now analyze all the terms involved in Eq. (B.7) separately.

1st term. Here we compute the term containing the time derivative of the distribution function,

$$
\partial_t \int dK k_0 k^l f_k^{(r)} \, .
\tag{B.8}
$$

Due to the symmetry properties of the distribution function at equilibrium (it depends only on the particle energy in the LRF of the fluid), the first moment of $f_{0k}^{(r)}$ vanishes. The only

contribution comes from the off-equilibrium deviation $\delta f_k^{(r)}$, which we expand in terms of the diffusion current,

$$\partial_t \int dK k_0 k^l f_0^{(r)} \left(-\frac{1}{P_{(r)}} k_{\langle \mu \rangle} \nu^{\langle \mu \rangle} \right) . \tag{B.9}$$

We then employ the orthogonality relation in Eq. (B.1)

$$\partial_t \int dK \frac{k^2}{3} k_0 f_0^{(r)} \left(\frac{1}{P_{(r)}} \right) \nu^l , \tag{B.10}$$

and, rewriting in terms of the thermodynamic integrals introduced in the text, we get

$$\frac{I_{31}^{(r)}}{P_{(r)}} \partial_t \nu_{(r)}^l \quad \longrightarrow \quad \frac{I_{31}}{P_0} \partial_t \nu_+^l , \tag{B.11}$$

where

$$I_{31}^{(r)} = \frac{1}{3} \langle k_0 k^2 \rangle_{0,r} . \tag{B.12}$$

Notice that $I_{31} \sim M P_0$ in the non-relativistic limit, reducing the computed term to $M \partial_t \nu_+^l$.

2nd term. Here we compute the term containing the spatial derivative of the distribution function,

$$\partial_i \int dK k^l k^i f_k^{(r)} . \tag{B.13}$$

We use the decomposition for the distribution function to get

$$\partial_i \delta^{il} \int dK \frac{k^2}{3} f_0^{(r)} + \partial_i \int dK k^i k^l \delta f_k^{(r)} . \tag{B.14}$$

Exploiting the orthogonality conditions and the definition of the pressure, we get

$$\delta^{il} \partial_i P_{(r)} + O(\delta^{il} \partial_i \Pi) + O(\partial_i \pi^{il})$$
$$= T n_{(r)} \delta^{il} \partial_i \left(\frac{\mu_r}{T} \right) + \text{corr} \tag{B.15}$$

where in the last passage we used $\partial_i P_0 = T n_0 \partial_i (\mu_r / T)$ and the neglected terms, involving derivatives of the bulk pressure and of the shear stress, are at least of second order in the gradients.

3rd term. Here we compute the RHS of the equation. Notice that the term containing the momentum-diffusion coefficient doesn't contribute. In fact, it is proportional to a second order

derivative, thus its first moment vanishes. Hence, one has simply to compute

$$
\int dK k^l k_0 \frac{\partial}{\partial k^i} \left(A k^i f^{(r)} \right)
$$

$$
= \int \frac{d^3 k}{(2\pi)^3} k^l \left[\frac{\partial k^i}{\partial k^i} \left(A f^{(r)} \right) + \frac{\partial A f^{(r)}}{\partial k^i} k^i \right]
$$

$$
\overset{\text{IBP}}{=} \int \frac{d^3 k}{(2\pi)^3} \left[3 \left(A f^{(r)} \right) k^l - \frac{\partial (k^i k^l)}{\partial k^i} A f^{(r)} \right] \tag{B.16}
$$

$$
= \int \frac{d^3 k}{(2\pi)^3} \left[3 \left(A f^{(r)} \right) k^l - 3 \left(A f^{(r)} \right) k^l + \right.
$$

$$
\left. - k^l A f^{(r)} \right] = \int \frac{d^3 k}{(2\pi)^3} \left[-k^l A f^{(r)} \right]
$$

where IBP means we performed the integration by parts. Now we exploit the decomposition of the distribution function. Due to symmetry constraints, the equilibrium part of the distribution doesn't contribute since its first moment is zero. Thus we have

$$
\int dK k^0 k^l A f_0^{(r)} \frac{k_{\langle \mu \rangle} \nu^\mu}{P_{(r)}} \,. \tag{B.17}
$$

By exploiting the orthogonality relation, one obtains

$$
-\frac{1}{3 P_{(r)}} \int dK k^0 k^2 A f_0^{(r)} \nu^l
$$

$$
= -\frac{1}{P_{(r)}} \frac{1}{3} \int dK k^0 k^2 \left(\frac{D}{k^0 T} \right) f_0^{(r)} \nu^l \tag{B.18}
$$

$$
= \frac{D}{P_{(r)} T} \left[\frac{1}{3} \int dK k^2 f_0^{(r)} \right] \nu^l
$$

$$
= -\frac{D}{T} \nu_{(r)}^l \,,
$$

where we made use of the Einstein fluctuation-dissipation relation to express A in terms of the momentum-diffusion coefficient D.

Putting all blocks together. We now combine the three terms to obtain the equation for the diffusion current:

$$
\frac{T}{D} \frac{I_{31}}{P_0} \partial_t \nu_{(r)}^l + \nu_{(r)}^l = -\frac{T^2}{D} n_{(r)} \partial^l \left(\frac{\mu_r}{T} \right) \,. \tag{B.19}
$$

This is a relaxation-type equation for the diffusion current $\nu_{(r)}^\mu$. Thus, we can identify the corresponding relaxation time and diffusion coefficient,

$$
\tau_n = \frac{T I_{31}}{D P_0} \,, \tag{B.20}
$$

$$
\kappa_n^{(r)} = \frac{T^2}{D} n_{(r)} \equiv D_s n_{(r)} \,. \tag{B.21}
$$

We find that the relation $D_s = T^2/D$ between the spatial (D_s) and momentum (D) diffusion coefficients, usually found in studying the non-relativistic Brownian motion, arises naturally and holds also in this case in which the heavy particle undergoes a relativistic dynamics, with

$E_k = \sqrt{k^2 + M^2}$. This is a non-trivial result, valid as long as the momentum dependence of D can be neglected.

Bibliography

[1] G. Giacalone, "A matter of shape: seeing the deformation of atomic nuclei at high-energy colliders," Ph.D. dissertation, U. Paris-Saclay, 2020. arXiv: `2101.00168` `[nucl-th]`.

[2] "The ALICE experiment – A journey through QCD," Nov. 2022. arXiv: `2211.04384` `[nucl-ex]`.

[3] A. Jaiswal and V. Roy, "Relativistic hydrodynamics in heavy-ion collisions: general aspects and recent developments," *Adv. High Energy Phys.*, vol. 2016, p. 9 623 034, 2016. DOI: `10.1155/2016/9623034`. arXiv: `1605.08694` `[nucl-th]`.

[4] R. Baier, A. H. Mueller, D. Schiff, and D. T. Son, "'Bottom up' thermalization in heavy ion collisions," *Phys. Lett. B*, vol. 502, pp. 51–58, 2001. DOI: `10.1016/S0370-2693(01)00191-5`. arXiv: `hep-ph/0009237`.

[5] T. Epelbaum and F. Gelis, "Pressure isotropization in high energy heavy ion collisions," *Phys. Rev. Lett.*, vol. 111, p. 232 301, 2013. DOI: `10.1103/PhysRevLett.111.232301`. arXiv: `1307.2214` `[hep-ph]`.

[6] J. Berges, K. Boguslavski, S. Schlichting, and R. Venugopalan, "Universal attractor in a highly occupied non-Abelian plasma," *Phys. Rev. D*, vol. 89, no. 11, p. 114 007, 2014. DOI: `10.1103/PhysRevD.89.114007`. arXiv: `1311.3005` `[hep-ph]`.

[7] S. Schlichting and D. Teaney, "The First fm/c of Heavy-Ion Collisions," *Ann. Rev. Nucl. Part. Sci.*, vol. 69, pp. 447–476, 2019. DOI: `10.1146/annurev-nucl-101918-023825`. arXiv: `1908.02113` `[nucl-th]`.

[8] J. L. Nagle and W. A. Zajc, "Small System Collectivity in Relativistic Hadronic and Nuclear Collisions," *Ann. Rev. Nucl. Part. Sci.*, vol. 68, pp. 211–235, 2018. DOI: `10.1146/annurev-nucl-101916-123209`. arXiv: `1801.03477` `[nucl-ex]`.

[9] M. Strickland, "Small system studies: A theory overview," *Nuclear Physics A*, vol. 982, pp. 92–98, 2019, ISSN: 0375-9474. DOI: `https://doi.org/10.1016/j.nuclphysa.2018.09.071`. [Online]. Available: `https://www.sciencedirect.com/science/article/pii/S0375947418302598`.

[10] J. Jia, G. Giacalone, and C. Zhang, "Separating the Impact of Nuclear Skin and Nuclear Deformation in High-Energy Isobar Collisions," *Phys. Rev. Lett.*, vol. 131, no. 2, p. 022 301, 2023. DOI: `10.1103/PhysRevLett.131.022301`. arXiv: `2206.10449` `[nucl-th]`.

[11] W. Ryssens, G. Giacalone, B. Schenke, and C. Shen, "Evidence of Hexadecapole Deformation in Uranium-238 at the Relativistic Heavy Ion Collider," *Phys. Rev. Lett.*, vol. 130, no. 21, p. 212 302, 2023. DOI: `10.1103/PhysRevLett.130.212302`. arXiv: `2302.13617` `[nucl-th]`.

[12] G. Giacalone, G. Nijs, and W. van der Schee, "Determination of the Neutron Skin of Pb208 from Ultrarelativistic Nuclear Collisions," *Phys. Rev. Lett.*, vol. 131, no. 20, p. 202 302, 2023. DOI: `10.1103/PhysRevLett.131.202302`. arXiv: `2305.00015` [`nucl-th`].

[13] S. Floerchinger, G. Giacalone, L. H. Heyen, and L. Tharwat, "Qualifying collective behavior in expanding ultracold gases as a function of particle number," *Phys. Rev. C*, vol. 105, no. 4, p. 044 908, 2022. DOI: `10.1103/PhysRevC.105.044908`. arXiv: `2111.13591` [`cond-mat.quant-gas`].

[14] S. Brandstetter *et al.*, "Emergent hydrodynamic behaviour of few strongly interacting fermions," Aug. 2023. arXiv: `2308.09699` [`cond-mat.quant-gas`].

[15] A. Bazavov *et al.*, "Equation of state in (2+1)-flavor QCD," *Phys. Rev. D*, vol. 90, p. 094 503, 2014. DOI: `10.1103/PhysRevD.90.094503`. arXiv: `1407.6387` [`hep-lat`].

[16] S. Borsanyi *et al.*, "Calculation of the axion mass based on high-temperature lattice quantum chromodynamics," *Nature*, vol. 539, no. 7627, pp. 69–71, 2016. DOI: `10.1038/nature20115`. arXiv: `1606.07494` [`hep-lat`].

[17] R.-A. Tripolt, J. Weyrich, L. von Smekal, and J. Wambach, "Fermionic spectral functions with the Functional Renormalization Group," *Phys. Rev. D*, vol. 98, no. 9, p. 094 002, 2018. DOI: `10.1103/PhysRevD.98.094002`. arXiv: `1807.11708` [`hep-ph`].

[18] R. Alkofer, A. Maas, W. A. Mian, M. Mitter, J. Parıs-López, J. M. Pawlowski, and N. Wink, "Bound state properties from the functional renormalization group," *Phys. Rev. D*, vol. 99, no. 5, p. 054 029, 2019. DOI: `10.1103/PhysRevD.99.054029`. arXiv: `1810.07955` [`hep-ph`].

[19] K. Fukushima and T. Hatsuda, "The phase diagram of dense QCD," *Rept. Prog. Phys.*, vol. 74, p. 014 001, 2011. DOI: `10.1088/0034-4885/74/1/014001`. arXiv: `1005.4814` [`hep-ph`].

[20] J. N. Guenther, "Overview of the QCD phase diagram: Recent progress from the lattice," *Eur. Phys. J. A*, vol. 57, no. 4, p. 136, 2021. DOI: `10.1140/epja/s10050-021-00354-6`. arXiv: `2010.15503` [`hep-lat`].

[21] M. G. Alford, A. Schmitt, K. Rajagopal, and T. Schäfer, "Color superconductivity in dense quark matter," *Rev. Mod. Phys.*, vol. 80, pp. 1455–1515, 2008. DOI: `10.1103/RevModPhys.80.1455`. arXiv: `0709.4635` [`hep-ph`].

[22] E. Iancu and R. Venugopalan, "Color glass condensate and small x physics: 4 lectures," *Proceedings of the Theoretical Advanced Study Institute in Elementary Particle Physics (TASI 2002)*, 2003. eprint: `hep-ph/0303204`.

[23] F. Gelis and R. Venugopalan, "Particle production in field theories coupled to strong external sources," *Physical Review D*, vol. 78, no. 5, p. 054 019, 2008. eprint: `arXiv:0710.4273`.

[24] L. D. McLerran and R. Venugopalan, "Computing quark and gluon distribution functions for very large nuclei," *Physical Review D*, vol. 49, no. 5, p. 2233, 1994. eprint: `hep-ph/9309289`.

[25] R. Venugopalan, "Classical fields, quantum fields and the onset of hydrodynamics at rhic," *Acta Physica Polonica B*, vol. 32, no. 4, p. 1273, 2001. eprint: `hep-ph/0105317`.

[26] F. Gelis, T. Lappi, and L. McLerran, "Glasma flux tubes and the near side ridge phenomenon at rhic," *Nuclear Physics A*, vol. 828, p. 149, 2009. eprint: `arXiv: 0809.3080`.

[27] F. Gelis, T. Lappi, and L. McLerran, "Color charge dependence of glasma fluctuations in high energy nuclear collisions," *Nuclear Physics A*, vol. 828, p. 149, 2009. eprint: `arXiv:0809.3130`.

[28] F. Gelis, E. Iancu, J. Jalilian-Marian, and R. Venugopalan, "Exploring the glasma with di-hadron correlations in nuclear collisions," *Journal of High Energy Physics*, vol. 04, p. 048, 2010. eprint: `arXiv:1002.0333`.

[29] L. McLerran, M. Praszalowicz, and B. Schenke, "Initial conditions for space-time evolution of nuclear collisions at rhic," *Acta Physica Polonica B*, vol. 42, p. 99, 2011. eprint: `arXiv:1009.2283`.

[30] M. L. Miller, K. Reygers, S. J. Sanders, and P. Steinberg, "Glauber modeling in high energy nuclear collisions," *Ann. Rev. Nucl. Part. Sci.*, vol. 57, pp. 205–243, 2007. DOI: `10.1146/annurev.nucl.57.090506.123020`. arXiv: `nucl-ex/0701025`.

[31] J. S. Moreland, J. E. Bernhard, and S. A. Bass, "Alternative ansatz to wounded nucleon and binary collision scaling in high-energy nuclear collisions," *Phys. Rev. C*, vol. 92, no. 1, p. 011 901, 2015. DOI: `10.1103/PhysRevC.92.011901`. arXiv: `1412.4708 [nucl-th]`.

[32] J. Liu, C. Shen, and U. Heinz, "Pre-equilibrium evolution effects on heavy-ion collision observables," *Phys. Rev. C*, vol. 91, no. 6, p. 064 906, 2015, [Erratum: Phys.Rev.C 92, 049904 (2015)]. DOI: `10.1103/PhysRevC.91.064906`. arXiv: `1504. 02160 [nucl-th]`.

[33] W. Broniowski, W. Florkowski, M. Chojnacki, and A. Kisiel, "Free-streaming approximation in early dynamics of relativistic heavy-ion collisions," *Phys. Rev. C*, vol. 80, p. 034 902, 2009. DOI: `10.1103/PhysRevC.80.034902`. arXiv: `0812.3393 [nucl-th]`.

[34] G. Nijs, W. van der Schee, U. Gürsoy, and R. Snellings, "Bayesian analysis of heavy ion collisions with the heavy ion computational framework Trajectum," *Phys. Rev. C*, vol. 103, no. 5, p. 054 909, 2021. DOI: `10.1103/PhysRevC.103.054909`. arXiv: `2010.15134 [nucl-th]`.

[35] B. Schenke, S. Jeon, and C. Gale, "(3+1)D hydrodynamic simulation of relativistic heavy-ion collisions," *Phys. Rev. C*, vol. 82, p. 014 903, 2010. DOI: `10.1103/ PhysRevC.82.014903`. arXiv: `1004.1408 [hep-ph]`.

[36] S. Floerchinger, E. Grossi, and J. Lion, "Fluid dynamics of heavy ion collisions with mode expansion," *Phys. Rev. C*, vol. 100, no. 1, p. 014 905, 2019. DOI: `10. 1103/PhysRevC.100.014905`. arXiv: `1811.01870 [nucl-th]`.

[37] F. Cooper and G. Frye, "Single-particle distribution in the hydrodynamic and statistical thermodynamic models of multiparticle production," *Phys. Rev. D*, vol. 10, 1 1974.

[38] L. Vermunt, Y. Seemann, A. Dubla, S. Floerchinger, E. Grossi, A. Kirchner, S. Masciocchi, and I. Selyuzhenkov, "Mapping QGP properties in Pb–Pb and Xe–Xe collisions at the LHC," Aug. 2023. arXiv: `2308.16722 [hep-ph]`.

[39] P. Huovinen, "Chemical freeze-out temperature in hydrodynamical description of Au+Au collisions at s(NN)**(1/2) = 200-GeV," *Eur. Phys. J. A*, vol. 37, pp. 121–128, 2008. DOI: `10.1140/epja/i2007-10611-3`. arXiv: `0710.4379 [nucl-th]`.

[40] J. .-. Rose, J. M. Torres-Rincon, A. Schäfer, D. R. Oliinychenko, and H. Petersen, "Shear viscosity of a hadron gas and influence of resonance lifetimes on relaxation time," *Phys. Rev. C*, vol. 97, no. 5, p. 055 204, 2018. DOI: `10.1103/PhysRevC.97.055204`. arXiv: `1709.03826 [nucl-th]`.

[41] N. Demir and S. A. Bass, "Shear-Viscosity to Entropy-Density Ratio of a Relativistic Hadron Gas," *Phys. Rev. Lett.*, vol. 102, p. 172 302, 2009. DOI: `10.1103/PhysRevLett.102.172302`. arXiv: `0812.2422 [nucl-th]`.

[42] A. Mazeliauskas, S. Floerchinger, E. Grossi, and D. Teaney, "Fast resonance decays in nuclear collisions," *Eur. Phys. J. C*, vol. 79, no. 3, p. 284, 2019. DOI: `10.1140/epjc/s10052-019-6791-7`. arXiv: `1809.11049 [nucl-th]`.

[43] P. Romatschke and U. Romatschke, *Relativistic Fluid Dynamics In and Out of Equilibrium* (Cambridge Monographs on Mathematical Physics). Cambridge University Press, May 2019, ISBN: 978-1-108-48368-1, 978-1-108-75002-8. DOI: `10.1017/9781108651998`. arXiv: `1712.05815 [nucl-th]`.

[44] L. Rezzolla and O. Zanotti, *Relativistic Hydrodynamics*. Sep. 2013, ISBN: 978-0198528906. DOI: `https://doi.org/10.1093/acprof:oso/9780198528906.002.0002`.

[45] G. S. Denicol, H. Niemi, E. Molnar, and D. H. Rischke, "Derivation of transient relativistic fluid dynamics from the Boltzmann equation," *Phys. Rev. D*, vol. 85, p. 114 047, 2012, [Erratum: Phys.Rev.D 91, 039902 (2015)]. DOI: `10.1103/PhysRevD.85.114047`. arXiv: `1202.4551 [nucl-th]`.

[46] P. Huovinen and P. V. Ruuskanen, "Hydrodynamic Models for Heavy Ion Collisions," *Ann. Rev. Nucl. Part. Sci.*, vol. 56, pp. 163–206, 2006. DOI: `10.1146/annurev.nucl.54.070103.181236`. arXiv: `nucl-th/0605008`.

[47] S. Kato and J. Fukue, *Fundamentals of Astrophysical Fluid Dynamics: Hydrodynamics, Magnetohydrodynamics, and Radiation Hydrodynamics*. Jan. 2020, ISBN: 978-981-15-4173-5. DOI: `10.1007/978-981-15-4174-2`.

[48] J. M. Maldacena, "The Large N limit of superconformal field theories and supergravity," *Adv. Theor. Math. Phys.*, vol. 2, pp. 231–252, 1998. DOI: `10.4310/ATMP.1998.v2.n2.a1`. arXiv: `hep-th/9711200`.

[49] L. D. Landau and E. M. Lifshitz, *Fluid Mechanics, Second Edition: Volume 6 (Course of Theoretical Physics)* (Course of theoretical physics / by L. D. Landau and E. M. Lifshitz, Vol. 6). Butterworth-Heinemann, 1987. [Online]. Available: `http://www.worldcat.org/isbn/0750627670`.

[50] C. Eckart, "The Thermodynamics of irreversible processes. 3.. Relativistic theory of the simple fluid," *Phys. Rev.*, vol. 58, pp. 919–924, 1940. DOI: `10.1103/PhysRev.58.919`.

[51] P. Kovtun, "First-order relativistic hydrodynamics is stable," *JHEP*, vol. 10, p. 034, 2019. DOI: `10.1007/JHEP10(2019)034`. arXiv: `1907.08191 [hep-th]`.

[52] W. A. Hiscock and L. Lindblom, "Generic instabilities in first-order dissipative relativistic fluid theories," *Phys. Rev. D*, vol. 31, pp. 725–733, 4 Feb. 1985. DOI: `10.1103/PhysRevD.31.725`. [Online]. Available: `https://link.aps.org/doi/10.1103/PhysRevD.31.725`.

[53] W. A. Hiscock and L. Lindblom, "Linear plane waves in dissipative relativistic fluids," *Phys. Rev. D*, vol. 35, pp. 3723–3732, 12 Jun. 1987. DOI: `10.1103/PhysRevD.35.3723`. [Online]. Available: `https://link.aps.org/doi/10.1103/PhysRevD.35.3723`.

[54] S. Floerchinger and E. Grossi, "Causality of fluid dynamics for high-energy nuclear collisions," *JHEP*, vol. 08, p. 186, 2018. DOI: `10.1007/JHEP08(2018)186`. arXiv: `1711.06687 [nucl-th]`.

[55] I. Müller, "Zum Paradoxon der Wärmeleitungstheorie," *Zeitschrift für Physik*, vol. 198, no. 329, 1967.

[56] W. Israel and J. M. Stewart, "Transient relativistic thermodynamics and kinetic theory," *Annals of Physics*, vol. 118, no. 2, pp. 341–372, Apr. 1979. DOI: `10.1016/0003-4916(79)90130-1`.

[57] R. Baier, P. Romatschke, D. T. Son, A. O. Starinets, and M. A. Stephanov, "Relativistic viscous hydrodynamics, conformal invariance, and holography," *JHEP*, vol. 04, p. 100, 2008. DOI: `10.1088/1126-6708/2008/04/100`. arXiv: `0712.2451 [hep-th]`.

[58] P. Romatschke, "Relativistic Viscous Fluid Dynamics and Non-Equilibrium Entropy," *Class. Quant. Grav.*, vol. 27, p. 025 006, 2010. DOI: `10.1088/0264-9381/27/2/025006`. arXiv: `0906.4787 [hep-th]`.

[59] H. Grad, "About kinetic theory of rarefied gases, communications on pure and applied mathematics," vol. 2, no. 4, pp. 331–407, 1949. DOI: `10.1002/cpa.3160020403`.

[60] J. D. Bjorken, "Highly relativistic nucleus-nucleus collisions: The central rapidity region," *Phys. Rev. D*, vol. 27, 1 1983.

[61] S. S. Gubser and A. Yarom, "Conformal hydrodynamics in Minkowski and de Sitter spacetimes," *Nucl. Phys. B*, vol. 846, pp. 469–511, 2011. DOI: `10.1016/j.nuclphysb.2011.01.012`. arXiv: `1012.1314 [hep-th]`.

[62] A. Beraudo *et al.*, "Extraction of Heavy-Flavor Transport Coefficients in QCD Matter," *Nucl. Phys. A*, vol. 979, R. Rapp, P. B. Gossiaux, A. Andronic, R. Averbeck, and S. Masciocchi, Eds., pp. 21–86, 2018. DOI: `10.1016/j.nuclphysa.2018.09.002`. arXiv: `1803.03824 [nucl-th]`.

[63] J. Dunkel and P. Hänggi, "Relativistic brownian motion," *Physics Reports*, vol. 471, no. 1, pp. 1–73, Feb. 2009, ISSN: 0370-1573. DOI: `10.1016/j.physrep.2008.12.001`. [Online]. Available: `http://dx.doi.org/10.1016/j.physrep.2008.12.001`.

[64] S. Acharya *et al.*, "Measurement of prompt D_s^+-meson production and azimuthal anisotropy in Pb–Pb collisions at $\sqrt{s_{NN}}$=5.02TeV," *Phys. Lett. B*, vol. 827, p. 136 986, 2022. DOI: `10.1016/j.physletb.2022.136986`. arXiv: `2110.10006 [nucl-ex]`.

[65] S. Acharya *et al.*, "Prompt D^0, D^+, and D^{*+} production in Pb –Pb collisions at $\sqrt{s_{NN}} = 5.02$ TeV," *JHEP*, vol. 01, p. 174, 2022. DOI: `10.1007/JHEP01(2022)174`. arXiv: `2110.09420 [nucl-ex]`.

[66] S. Acharya *et al.*, "Measurements of inclusive J/ψ production at midrapidity and forward rapidity in Pb−Pb collisions at $\sqrt{s_{\mathrm{NN}}}$ = 5.02 TeV," Mar. 2023. arXiv: `2303.13361` `[nucl-ex]`.

[67] S. Acharya *et al.*, "Constraining hadronization mechanisms with Λc+/D0 production ratios in Pb–Pb collisions at sNN=5.02 TeV," *Phys. Lett. B*, vol. 839, p. 137 796, 2023. DOI: `10.1016/j.physletb.2023.137796`. arXiv: `2112.08156` `[nucl-ex]`.

[68] S. Acharya *et al.*, "Transverse-momentum and event-shape dependence of D-meson flow harmonics in Pb–Pb collisions at $\sqrt{s_{NN}}$ = 5.02 TeV," *Phys. Lett. B*, vol. 813, p. 136 054, 2021. DOI: `10.1016/j.physletb.2020.136054`. arXiv: `2005.11131` `[nucl-ex]`.

[69] L. Adamczyk *et al.*, "Measurement of D^0 Azimuthal Anisotropy at Midrapidity in Au+Au Collisions at $\sqrt{s_{NN}}$=200 GeV," *Phys. Rev. Lett.*, vol. 118, no. 21, p. 212 301, 2017. DOI: `10.1103/PhysRevLett.118.212301`. arXiv: `1701.06060` `[nucl-ex]`.

[70] L. Adamczyk *et al.*, "Measurements of D^0 and D^* Production in $p+p$ Collisions at $\sqrt{s}$ = 200 GeV," *Phys. Rev. D*, vol. 86, p. 072 013, 2012. DOI: `10.1103/PhysRevD.86.072013`. arXiv: `1204.4244` `[nucl-ex]`.

[71] J. Adam *et al.*, "Centrality and transverse momentum dependence of D^0-meson production at mid-rapidity in Au+Au collisions at $\sqrt{s_{\mathrm{NN}}}$ = 200 GeV," *Phys. Rev. C*, vol. 99, no. 3, p. 034 908, 2019. DOI: `10.1103/PhysRevC.99.034908`. arXiv: `1812.10224` `[nucl-ex]`.

[72] L. Adamczyk *et al.*, "Energy dependence of J/ψ production in Au+Au collisions at $\sqrt{s_{NN}}$ = 39, 62.4 and 200 GeV," *Phys. Lett. B*, vol. 771, pp. 13–20, 2017. DOI: `10.1016/j.physletb.2017.04.078`. arXiv: `1607.07517` `[hep-ex]`.

[73] S. Acharya *et al.*, "J/ψ elliptic and triangular flow in Pb-Pb collisions at $\sqrt{s_{NN}}$ = 5.02 TeV," *JHEP*, vol. 10, p. 141, 2020. DOI: `10.1007/JHEP10(2020)141`. arXiv: `2005.14518` `[nucl-ex]`.

[74] S. Acharya *et al.*, "Υ production and nuclear modification at forward rapidity in Pb–Pb collisions at $\sqrt{s_{NN}}$ = 5.02 TeV," *Phys. Lett. B*, vol. 822, p. 136 579, 2021. DOI: `10.1016/j.physletb.2021.136579`. arXiv: `2011.05758` `[nucl-ex]`.

[75] S. Acharya *et al.*, "Transverse-momentum and event-shape dependence of D-meson flow harmonics in Pb–Pb collisions at $\sqrt{s_{NN}}$ = 5.02 TeV," *Phys. Lett. B*, vol. 813, p. 136 054, 2021. DOI: `10.1016/j.physletb.2020.136054`. arXiv: `2005.11131` `[nucl-ex]`.

[76] S. Frixione, P. Nason, and G. Ridolfi, "A Positive-weight next-to-leading-order Monte Carlo for heavy flavour hadroproduction," *JHEP*, vol. 09, p. 126, 2007. DOI: `10.1088/1126-6708/2007/09/126`. arXiv: `0707.3088` `[hep-ph]`.

[77] T. Sjöstrand, S. Ask, J. R. Christiansen, R. Corke, N. Desai, P. Ilten, S. Mrenna, S. Prestel, C. O. Rasmussen, and P. Z. Skands, "An introduction to PYTHIA 8.2," *Comput. Phys. Commun.*, vol. 191, pp. 159–177, 2015. DOI: `10.1016/j.cpc.2015.01.024`. arXiv: `1410.3012` `[hep-ph]`.

[78] M. Cacciari, M. Greco, and P. Nason, "The p_{T} spectrum in heavy flavor hadroproduction," *JHEP*, vol. 05, p. 007, 1998. DOI: `10.1088/1126-6708/1998/05/007`. arXiv: `hep-ph/9803400`.

[79] M. Cacciari, S. Frixione, and P. Nason, "The p_T spectrum in heavy flavor photo-production," *JHEP*, vol. 03, p. 006, 2001. DOI: 10.1088/1126-6708/2001/03/006. arXiv: hep-ph/0102134.

[80] K. J. Eskola, P. Paakkinen, H. Paukkunen, and C. A. Salgado, "EPPS16: Nuclear parton distributions with LHC data," *Eur. Phys. J. C*, vol. 77, no. 3, p. 163, 2017. DOI: 10.1140/epjc/s10052-017-4725-9. arXiv: 1612.05741 [hep-ph].

[81] K. Kovarik *et al.*, "nCTEQ15 - Global analysis of nuclear parton distributions with uncertainties in the CTEQ framework," *Phys. Rev. D*, vol. 93, no. 8, p. 085 037, 2016. DOI: 10.1103/PhysRevD.93.085037. arXiv: 1509.00792 [hep-ph].

[82] B. Abelev *et al.*, "Measurement of charm production at central rapidity in proton-proton collisions at $\sqrt{s} = 2.76$ TeV," *JHEP*, vol. 07, p. 191, 2012. DOI: 10.1007/JHEP07(2012)191. arXiv: 1205.4007 [hep-ex].

[83] S. Caron-Huot, M. Laine, and G. D. Moore, "A Way to estimate the heavy quark thermalization rate from the lattice," *JHEP*, vol. 04, p. 053, 2009. DOI: 10.1088/1126-6708/2009/04/053. arXiv: 0901.1195 [hep-lat].

[84] J. Casalderrey-Solana and D. Teaney, "Heavy quark diffusion in strongly coupled N=4 Yang-Mills," *Phys. Rev. D*, vol. 74, p. 085 012, 2006. DOI: 10.1103/PhysRevD.74.085012. arXiv: hep-ph/0605199.

[85] L. Altenkort, D. de la Cruz, O. Kaczmarek, R. Larsen, G. D. Moore, S. Mukherjee, P. Petreczky, H.-T. Shu, and S. Stendebach, "Quark Mass Dependence of Heavy Quark Diffusion Coefficient from Lattice QCD," *Phys. Rev. Lett.*, vol. 132, no. 5, p. 051 902, 2024. DOI: 10.1103/PhysRevLett.132.051902. arXiv: 2311.01525 [hep-lat].

[86] H. van Hees, "Introduction to relativistic transport theory," 2016. [Online]. Available: https://api.semanticscholar.org/CorpusID:14454988.

[87] S. Cao *et al.*, "Toward the determination of heavy-quark transport coefficients in quark-gluon plasma," *Phys. Rev. C*, vol. 99, no. 5, p. 054 907, 2019. DOI: 10.1103/PhysRevC.99.054907. arXiv: 1809.07894 [nucl-th].

[88] S. Batsouli, S. Kelly, M. Gyulassy, and J. L. Nagle, "Does the charm flow at RHIC?" *Phys. Lett. B*, vol. 557, pp. 26–32, 2003. DOI: 10.1016/S0370-2693(03)00175-8. arXiv: nucl-th/0212068.

[89] H. van Hees, V. Greco, and R. Rapp, "Heavy-quark probes of the quark-gluon plasma at RHIC," *Phys. Rev. C*, vol. 73, p. 034 913, 2006. DOI: 10.1103/PhysRevC.73.034913. arXiv: nucl-th/0508055.

[90] G. D. Moore and D. Teaney, "How much do heavy quarks thermalize in a heavy ion collision?" *Phys. Rev. C*, vol. 71, p. 064 904, 6 Jun. 2005. DOI: 10.1103/PhysRevC.71.064904. [Online]. Available: https://link.aps.org/doi/10.1103/PhysRevC.71.064904.

[91] P. B. Gossiaux, V. Guiho, and J. Aichelin, "Heavy quarks thermalization in heavy-ion ultrarelativistic collisions: Elastic or radiative?" *J. Phys. G*, vol. 32, S359–S364, 2006. DOI: 10.1088/0954-3899/32/12/S44.

[92] S. Cao and S. A. Bass, "Thermalization of charm quarks in infinite and finite QGP matter," *Phys. Rev. C*, vol. 84, p. 064 902, 2011. DOI: 10.1103/PhysRevC.84.064902. arXiv: 1108.5101 [nucl-th].

[93] S. S. Adler *et al.*, "Measurement of single electron event anisotropy in Au+Au collisions at s(NN)**(1/2) = 200-GeV," *Phys. Rev. C*, vol. 72, p. 024 901, 2005. DOI: 10.1103/PhysRevC.72.024901. arXiv: nucl-ex/0502009.

[94] A. Andronic, P. Braun-Munzinger, M. K. Köhler, A. Mazeliauskas, K. Redlich, J. Stachel, and V. Vislavicius, "The multiple-charm hierarchy in the statistical hadronization model," *JHEP*, vol. 07, p. 035, 2021. DOI: 10.1007/JHEP07(2021)035. arXiv: 2104.12754 [hep-ph].

[95] L. Altenkort, O. Kaczmarek, R. Larsen, S. Mukherjee, P. Petreczky, H.-T. Shu, and S. Stendebach, "Heavy Quark Diffusion from 2+1 Flavor Lattice QCD with 320 MeV Pion Mass," *Phys. Rev. Lett.*, vol. 130, no. 23, p. 231 902, 2023. DOI: 10.1103/PhysRevLett.130.231902. arXiv: 2302.08501 [hep-lat].

[96] S. Acharya *et al.*, "J/ψ elliptic and triangular flow in Pb-Pb collisions at $\sqrt{s_{\mathrm{NN}}} = 5.02$ TeV," *JHEP*, vol. 10, p. 141, 2020. DOI: 10.1007/JHEP10(2020)141. arXiv: 2005.14518 [nucl-ex].

[97] A. Adare *et al.*, "Detailed measurement of the e^+e^- pair continuum in $p+p$ and Au+Au collisions at $\sqrt{s_{NN}} = 200$ GeV and implications for direct photon production," *Phys. Rev. C*, vol. 81, p. 034 911, 2010. DOI: 10.1103/PhysRevC.81.034911. arXiv: 0912.0244 [nucl-ex].

[98] A. Beraudo, A. De Pace, M. Monteno, M. Nardi, and F. Prino, "Development of heavy-flavour flow-harmonics in high-energy nuclear collisions," *JHEP*, vol. 02, p. 043, 2018. DOI: 10.1007/JHEP02(2018)043. arXiv: 1712.00588 [hep-ph].

[99] E. A. Calzetta and B.-L. B. Hu, *Nonequilibrium Quantum Field Theory* (Cambridge Monographs on Mathematical Physics). Cambridge University Press, 2008. DOI: 10.1017/CBO9780511535123.

[100] D. Bodeker and M. Laine, "Heavy quark chemical equilibration rate as a transport coefficient," *JHEP*, vol. 07, p. 130, 2012. DOI: 10.1007/JHEP07(2012)130. arXiv: 1205.4987 [hep-ph].

[101] G. S. Denicol, J. Noronha, H. Niemi, and D. H. Rischke, "Origin of the Relaxation Time in Dissipative Fluid Dynamics," *Phys. Rev. D*, vol. 83, p. 074 019, 2011. DOI: 10.1103/PhysRevD.83.074019. arXiv: 1102.4780 [hep-th].

[102] W. Florkowski, M. P. Heller, and M. Spalinski, "New theories of relativistic hydrodynamics in the LHC era," *Rept. Prog. Phys.*, vol. 81, no. 4, p. 046 001, 2018. DOI: 10.1088/1361-6633/aaa091. arXiv: 1707.02282 [hep-ph].

[103] J.-P. Blaizot and E. Iancu, "The Quark gluon plasma: Collective dynamics and hard thermal loops," *Phys. Rept.*, vol. 359, pp. 355–528, 2002. DOI: 10.1016/S0370-1573(01)00061-8. arXiv: hep-ph/0101103.

[104] D. Banerjee, S. Datta, R. Gavai, and P. Majumdar, "Heavy Quark Momentum Diffusion Coefficient from Lattice QCD," *Phys. Rev. D*, vol. 85, p. 014 510, 2012. DOI: 10.1103/PhysRevD.85.014510. arXiv: 1109.5738 [hep-lat].

[105] A. Andronic, P. Braun-Munzinger, K. Redlich, and J. Stachel, "Decoding the phase structure of QCD via particle production at high energy," *Nature*, vol. 561, no. 7723, pp. 321–330, 2018. DOI: 10.1038/s41586-018-0491-6. arXiv: 1710.09425 [nucl-th].

[106] M. He and R. Rapp, "Charm-Baryon Production in Proton-Proton Collisions," *Phys. Lett. B*, vol. 795, pp. 117–121, 2019. DOI: 10.1016/j.physletb.2019.06.004. arXiv: 1902.08889 [nucl-th].

[107] M. He and R. Rapp, "Hadronization and Charm-Hadron Ratios in Heavy-Ion Collisions," *Phys. Rev. Lett.*, vol. 124, no. 4, p. 042301, 2020. DOI: 10.1103/PhysRevLett.124.042301. arXiv: 1905.09216 [nucl-th].

[108] A. Andronic, P. Braun-Munzinger, M. K. Köhler, A. Mazeliauskas, K. Redlich, J. Stachel, and V. Vislavicius, "The multiple-charm hierarchy in the statistical hadronization model," *JHEP*, vol. 07, p. 035, 2021. DOI: 10.1007/JHEP07(2021)035. arXiv: 2104.12754 [hep-ph].

[109] A. Beraudo, A. De Pace, M. Monteno, M. Nardi, and F. Prino, "In-medium hadronization of heavy quarks and its effect on charmed meson and baryon distributions in heavy-ion collisions," *Eur. Phys. J. C*, vol. 82, no. 7, p. 607, 2022. DOI: 10.1140/epjc/s10052-022-10482-y. arXiv: 2202.08732 [hep-ph].

[110] S. Plumari, V. Minissale, S. K. Das, G. Coci, and V. Greco, "Charmed Hadrons from Coalescence plus Fragmentation in relativistic nucleus-nucleus collisions at RHIC and LHC," *Eur. Phys. J. C*, vol. 78, no. 4, p. 348, 2018. DOI: 10.1140/epjc/s10052-018-5828-7. arXiv: 1712.00730 [hep-ph].

[111] Y. Xu, J. E. Bernhard, S. A. Bass, M. Nahrgang, and S. Cao, "Data-driven analysis for the temperature and momentum dependence of the heavy-quark diffusion coefficient in relativistic heavy-ion collisions," *Physical Review C*, vol. 97, no. 1, Jan. 2018, ISSN: 2469-9993. DOI: 10.1103/physrevc.97.014907. [Online]. Available: http://dx.doi.org/10.1103/PhysRevC.97.014907.

[112] M. L. Sambataro, V. Minissale, S. Plumari, and V. Greco, "B meson production in Pb+Pb at 5.02 ATeV at LHC: estimating the diffusion coefficient in the infinite mass limit," Apr. 2023. arXiv: 2304.02953 [hep-ph].

[113] A. Francis, O. Kaczmarek, M. Laine, T. Neuhaus, and H. Ohno, "Nonperturbative estimate of the heavy quark momentum diffusion coefficient," *Phys. Rev. D*, vol. 92, no. 11, p. 116003, 2015. DOI: 10.1103/PhysRevD.92.116003. arXiv: 1508.04543 [hep-lat].

[114] L. Altenkort, A. M. Eller, O. Kaczmarek, L. Mazur, G. D. Moore, and H. Shu, "Spectral reconstruction details of a gradient-flowed color-electric correlator," *EPJ Web Conf.*, vol. 259, p. 10004, 2022. DOI: 10.1051/epjconf/202225910004. arXiv: 2109.11303 [hep-lat].

[115] H. Ding, O. Kaczmarek, A. Lorenz, H. Ohno, H. Sandmeyer, and H. Shu, "Charm and beauty in the deconfined plasma from quenched lattice QCD," *Phys. Rev. D*, vol. 104, no. 11, p. 114508, 2021. DOI: 10.1103/PhysRevD.104.114508. arXiv: 2108.13693 [hep-lat].

[116] L. Altenkort, A. M. Eller, O. Kaczmarek, L. Mazur, G. D. Moore, and H. Shu, "Heavy quark momentum diffusion from the lattice using gradient flow," *Phys. Rev. D*, vol. 103, no. 1, p. 014511, 2021. DOI: 10.1103/PhysRevD.103.014511. arXiv: 2009.13553 [hep-lat].

[117] N. Brambilla, V. Leino, P. Petreczky, and A. Vairo, "Lattice QCD constraints on the heavy quark diffusion coefficient," *Phys. Rev. D*, vol. 102, no. 7, p. 074503, 2020. DOI: 10.1103/PhysRevD.102.074503. arXiv: 2007.10078 [hep-lat].

[118]   Z. Tang, S. Mukherjee, P. Petreczky, and R. Rapp, "T-matrix Analysis of Static Wilson Line Correlators from Lattice QCD at Finite Temperature," Oct. 2023. arXiv: 2310.18864 [hep-lat].

[119]   S. K. Das, F. Scardina, S. Plumari, and V. Greco, "Heavy-flavor in-medium momentum evolution: Langevin versus Boltzmann approach," *Phys. Rev. C*, vol. 90, p. 044 901, 2014. DOI: 10.1103/PhysRevC.90.044901. arXiv: 1312.6857 [nucl-th].

[120]   A. Andronic, P. Braun-Munzinger, K. Redlich, and J. Stachel, "Statistical Hadronization of b-quarks in Pb–Pb Collisions at LHC Energy: A Case for Partial Equilibration of b-quarks?" *Acta Phys. Polon. Supp.*, vol. 16, no. 1, p. 107, 2023. DOI: 10.5506/APhysPolBSupp.16.1-A107. arXiv: 2209.14562 [hep-ph].

[121]   A. M. Sirunyan *et al.*, "Suppression of Excited Υ States Relative to the Ground State in Pb-Pb Collisions at $\sqrt{s_{\mathrm{NN}}}$=5.02 TeV," *Phys. Rev. Lett.*, vol. 120, no. 14, p. 142 301, 2018. DOI: 10.1103/PhysRevLett.120.142301. arXiv: 1706.05984 [hep-ex].

[122]   S. Lee, "Bottomonium production in Pb + Pb collisions with ATLAS," *Nucl. Phys. A*, vol. 1005, F. Liu, E. Wang, X.-N. Wang, N. Xu, and B.-W. Zhang, Eds., p. 121 860, 2021. DOI: 10.1016/j.nuclphysa.2020.121860.

[123]   A. M. Sirunyan *et al.*, "Measurement of the azimuthal anisotropy of Υ(1S) and Υ(2S) mesons in PbPb collisions at sNN=5.02TeV," *Phys. Lett. B*, vol. 819, p. 136 385, 2021. DOI: 10.1016/j.physletb.2021.136385. arXiv: 2006.07707 [hep-ex].

[124]   F. Capellino, A. Beraudo, A. Dubla, S. Floerchinger, S. Masciocchi, J. Pawlowski, and I. Selyuzhenkov, "Fluid-dynamic approach to heavy-quark diffusion in the quark-gluon plasma," *Phys. Rev. D*, vol. 106, no. 3, p. 034 021, 2022. DOI: 10.1103/PhysRevD.106.034021. arXiv: 2205.07692 [nucl-th].

[125]   A. Andronic, P. Braun-Munzinger, K. Redlich, and J. Stachel, "Statistical hadronization of heavy quarks in ultra-relativistic nucleus-nucleus collisions," *Nucl. Phys. A*, vol. 789, pp. 334–356, 2007. DOI: 10.1016/j.nuclphysa.2007.02.013. arXiv: nucl-th/0611023.

[126]   A. Andronic, P. Braun-Munzinger, M. K. Köhler, K. Redlich, and J. Stachel, "Transverse momentum distributions of charmonium states with the statistical hadronization model," *Phys. Lett. B*, vol. 797, p. 134 836, 2019. DOI: 10.1016/j.physletb.2019.134836. arXiv: 1901.09200 [nucl-th].

[127]   P. Braun-Munzinger and J. Stachel, "(Non)thermal aspects of charmonium production and a new look at J/ψ suppression," *Phys. Lett. B*, vol. 490, pp. 196–202, 2000. DOI: 10.1016/S0370-2693(00)00991-6. arXiv: nucl-th/0007059.

[128]   P. Braun-Munzinger, "Quarkonium production in ultra-relativistic nuclear collisions: Suppression versus enhancement," *J. Phys. G*, vol. 34, Y.-G. Ma, Z.-Y. Zhu, E.-K. Wang, X. Cai, H.-Z. Huang, and X.-N. Wang, Eds., S471–478, 2007. DOI: 10.1088/0954-3899/34/8/S36. arXiv: nucl-th/0701093.

[129]   S. K. Das, S. Plumari, S. Chatterjee, J. Alam, F. Scardina, and V. Greco, "Directed Flow of Charm Quarks as a Witness of the Initial Strong Magnetic Field in Ultra-Relativistic Heavy Ion Collisions," *Phys. Lett. B*, vol. 768, pp. 260–264, 2017. DOI: 10.1016/j.physletb.2017.02.046. arXiv: 1608.02231 [nucl-th].

[130]   S. R. De Groot, *Relativistic Kinetic Theory. Principles and Applications*, W. A. Van Leeuwen and C. G. Van Weert, Eds. 1980.

[131] W. M. Alberico, A. Beraudo, A. De Pace, A. Molinari, M. Monteno, M. Nardi, and F. Prino, "Heavy-flavour spectra in high energy nucleus-nucleus collisions," *Eur. Phys. J. C*, vol. 71, p. 1666, 2011. DOI: `10.1140/epjc/s10052-011-1666-6`. arXiv: `1101.6008 [hep-ph]`.

[132] G. Kaniadakis and P. Quarati, "Classical model of bosons and fermions," *Phys. Rev. E*, vol. 49, pp. 5103–5110, 6 Jun. 1994. DOI: `10.1103/PhysRevE.49.5103`. [Online]. Available: `https://link.aps.org/doi/10.1103/PhysRevE.49.5103`.

[133] F. Capellino, A. Dubla, S. Floerchinger, E. Grossi, A. Kirchner, and S. Masciocchi, "Fluid dynamics of charm quarks in the quark-gluon plasma," *Phys. Rev. D*, vol. 108, no. 11, p. 116 011, 2023. DOI: `10.1103/PhysRevD.108.116011`. arXiv: `2307.14449 [hep-ph]`.

[134] D. Devetak, A. Dubla, S. Floerchinger, E. Grossi, S. Masciocchi, A. Mazeliauskas, and I. Selyuzhenkov, "Global fluid fits to identified particle transverse momentum spectra from heavy-ion collisions at the Large Hadron Collider," *JHEP*, vol. 06, p. 044, 2020. DOI: `10.1007/JHEP06(2020)044`. arXiv: `1909.10485 [hep-ph]`.

[135] J. P. Boris and D. L. Book, "Flux-corrected transport. I. SHASTA, a fluid transport algorithm that works," *J. Comput. Phys.*, vol. 11, no. 1, pp. 38–69, 1973. DOI: `10.1016/0021-9991(73)90147-2`.

[136] A. Kurganov and E. Tadmor, "New high-resolution central schemes for nonlinear conservation laws and convection–diffusion equations," *Journal of computational physics*, vol. 160, no. 1, pp. 241–282, 2000.

[137] S. Osher and F. Solomon, "Upwind difference schemes for hyperbolic systems of conservation laws," *Mathematics of computation*, vol. 38, no. 158, pp. 339–374, 1982.

[138] J. Yan and S. Osher, "A local discontinuous galerkin method for directly solving hamilton–jacobi equations," *Journal of Computational Physics*, vol. 230, no. 1, pp. 232–244, 2011.

[139] M. Castro, T. Morales de Luna, and C. Madroñal, "Well-balanced schemes and path-conservative numerical methods," in Dec. 2016. DOI: `10.1016/bs.hna.2016.10.002`.

[140] M. J. Castro, J. Gallardo, and A. Marquina, "A class of incomplete riemann solvers based on uniform rational approximations to the absolute value function," *Journal of Scientific Computing*, vol. 60, no. 2, pp. 363–389, 2014. DOI: `10.1007/s10915-013-9800-2`. [Online]. Available: `https://doi.org/10.1007/s10915-013-9800-2`.

[141] J. Bezanson, A. Edelman, S. Karpinski, and V. B. Shah, "Julia: A fresh approach to numerical computing," *SIAM Review*, vol. 59, no. 1, pp. 65–98, 2017. DOI: `10.1137/141000671`. [Online]. Available: `https://epubs.siam.org/doi/10.1137/141000671`.

[142] C. Rackauckas and Q. Nie, "Differentialequations.jl–a performant and feature-rich ecosystem for solving differential equations in julia," *Journal of Open Research Software*, vol. 5, no. 1, p. 15, 2017.

[143] G. Söderlind, "Digital filters in adaptive time-stepping," *ACM Trans. Math. Softw.*, vol. 29, no. 1, pp. 1–26, Mar. 2003, ISSN: 0098-3500. DOI: `10.1145/641876.641877`. [Online]. Available: `https://doi.org/10.1145/641876.641877`.

[144]   G. Söderlind and L. Wang, "Adaptive time-stepping and computational stability,"
        Journal of Computational and Applied Mathematics, vol. 185, no. 2, pp. 225–243,
        2006.

[145]   H. Ranocha, L. Dalcin, M. Parsani, and D. I. Ketcheson, "Optimized runge-kutta
        methods with automatic step size control for compressible computational fluid
        dynamics," *Communications on Applied Mathematics and Computation*, vol. 4,
        no. 4, pp. 1191–1228, 2022.

[146]   S. G. Johnson, *The HCubature.jl package for multi-dimensional adaptive integra-
        tion in Julia*, `https://github.com/JuliaMath/HCubature.jl`, 2017.

[147]   A. C. Genz and A. A. Malik, "Remarks on algorithm 006: An adaptive algorithm
        for numerical integration over an N-dimensional rectangular region," *Journal of
        Computational and Applied Mathematics*, vol. 6, pp. 295–302, 1980. DOI: `10.1016/
        0771-050x(80)90039-x`.

[148]   S. G. Johnson, *QuadGK.jl: Gauss–Kronrod integration in Julia*, `https://github.
        com/JuliaMath/QuadGK.jl`, 2013.

[149]   S. Olver and A. Townsend, "A practical framework for infinite-dimensional linear
        algebra," in *Proceedings of the 1st Workshop for High Performance Technical Com-
        puting in Dynamic Languages – HPTCDL '14*, IEEE, 2014.

[150]   G. Giacalone, "There and Sharp Again: The Circle Journey of Nucleons and Energy
        Deposition," Aug. 2022. arXiv: `2208.06839 [nucl-th]`.

[151]   G. Nijs, W. van der Schee, U. Gürsoy, and R. Snellings, "Transverse Momentum
        Differential Global Analysis of Heavy-Ion Collisions," *Phys. Rev. Lett.*, vol. 126,
        no. 20, p. 202 301, 2021. DOI: `10.1103/PhysRevLett.126.202301`. arXiv: `2010.
        15130 [nucl-th]`.

[152]   "ALICE luminosity determination for Pb−Pb collisions at $\sqrt{s_{NN}} = 5.02$ TeV," Apr.
        2022. arXiv: `2204.10148 [nucl-ex]`.

[153]   "Production of charged pions, kaons, and (anti-)protons in pb-pb and inelastic *pp*
        collisions at $\sqrt{s_{NN}} = 5.02$ tev," *Phys. Rev. C*, vol. 101, p. 044 907, 4 Apr. 2020.
        DOI: `10.1103/PhysRevC.101.044907`. [Online]. Available: `https://link.aps.
        org/doi/10.1103/PhysRevC.101.044907`.

[154]   S. Floerchinger, E. Grossi, and J. Lion, "Fluid dynamics of heavy ion collisions
        with mode expansion," *Phys. Rev. C*, vol. 100, no. 1, p. 014 905, 2019. DOI: `10.
        1103/PhysRevC.100.014905`. arXiv: `1811.01870 [nucl-th]`.

[155]   R. L. Workman *et al.*, "Review of Particle Physics," *PTEP*, vol. 2022, p. 083C01,
        2022. DOI: `10.1093/ptep/ptac097`.

[156]   V. Minissale, S. Plumari, and V. Greco, "Charm hadrons in pp collisions at LHC
        energy within a coalescence plus fragmentation approach," *Phys. Lett. B*, vol. 821,
        p. 136 622, 2021. DOI: `10.1016/j.physletb.2021.136622`. arXiv: `2012.12001
        [hep-ph]`.

[157]   A. Beraudo, A. De Pace, D. Pablos, F. Prino, M. Monteno, and M. Nardi, "Heavy-
        flavor transport and hadronization in pp collisions," Jun. 2023. arXiv: `2306.02152
        [hep-ph]`.

[158] X. Zhao and R. Rapp, "Transverse Momentum Spectra of J/ψ in Heavy-Ion Collisions," *Phys. Lett. B*, vol. 664, pp. 253–257, 2008. DOI: 10.1016/j.physletb.2008.03.068. arXiv: 0712.2407 [hep-ph].

[159] M. He, B. Wu, and R. Rapp, "Collectivity of J/ψ Mesons in Heavy-Ion Collisions," *Phys. Rev. Lett.*, vol. 128, no. 16, p. 162 301, 2022. DOI: 10.1103/PhysRevLett.128.162301. arXiv: 2111.13528 [nucl-th].

[160] T. Song, J. Aichelin, and E. Bratkovskaya, "Production of primordial J/ψ in relativistic $p + p$ and heavy-ion collisions," *Phys. Rev. C*, vol. 96, no. 1, p. 014 907, 2017. DOI: 10.1103/PhysRevC.96.014907. arXiv: 1705.00046 [nucl-th].

[161] J. A. Fotakis, M. Greif, C. Greiner, G. S. Denicol, and H. Niemi, "Diffusion processes involving multiple conserved charges: A study from kinetic theory and implications to the fluid-dynamical modeling of heavy ion collisions," *Phys. Rev. D*, vol. 101, no. 7, p. 076 007, 2020. DOI: 10.1103/PhysRevD.101.076007. arXiv: 1912.09103 [hep-ph].

[162] J. A. Fotakis, M. Greif, H. Niemi, G. S. Denicol, and C. Greiner, "Longitudinal dynamics of multiple conserved charges," *Nucl. Phys. A*, vol. 1005, F. Liu, E. Wang, X.-N. Wang, N. Xu, and B.-W. Zhang, Eds., p. 121 899, 2021. DOI: 10.1016/j.nuclphysa.2020.121899.

[163] C. Chattopadhyay, U. Heinz, and T. Schaefer, "Fluid dynamics from the Boltzmann equation using a maximum entropy distribution," *Phys. Rev. C*, vol. 108, no. 3, p. 034 907, 2023. DOI: 10.1103/PhysRevC.108.034907. arXiv: 2307.10769 [hep-ph].

[164] "Letter of intent for ALICE 3: A next-generation heavy-ion experiment at the LHC," Nov. 2022. arXiv: 2211.02491 [physics.ins-det].

[165] L. Adamczyk *et al.*, "Measurement of J/ψ azimuthal anisotropy in Au+Au collisions at $\sqrt{s_{NN}}$=200 GeV," *Phys. Rev. Lett.*, vol. 111, p. 052 301, 5 Jul. 2013. DOI: 10.1103/PhysRevLett.111.052301. [Online]. Available: https://link.aps.org/doi/10.1103/PhysRevLett.111.052301.

[166] J. Adam *et al.*, "First Observation of the Directed Flow of D^0 and $\overline{D^0}$ in Au+Au Collisions at $\sqrt{s_{\mathrm{NN}}} = 200$ GeV," *Phys. Rev. Lett.*, vol. 123, no. 16, p. 162 301, 2019. DOI: 10.1103/PhysRevLett.123.162301. arXiv: 1905.02052 [nucl-ex].

[167] V. Khachatryan *et al.*, "Evidence for transverse momentum and pseudorapidity dependent event plane fluctuations in PbPb and pPb collisions," *Phys. Rev. C*, vol. 92, no. 3, p. 034 911, 2015. DOI: 10.1103/PhysRevC.92.034911. arXiv: 1503.01692 [nucl-ex].

[168] G. Aad *et al.*, "Measurement of the centrality and pseudorapidity dependence of the integrated elliptic flow in lead-lead collisions at $\sqrt{s_{\mathrm{NN}}} = 2.76$ TeV with the ATLAS detector," *Eur. Phys. J. C*, vol. 74, no. 8, p. 2982, 2014. DOI: 10.1140/epjc/s10052-014-2982-4. arXiv: 1405.3936 [hep-ex].

[169] J. Adam *et al.*, "Pseudorapidity dependence of the anisotropic flow of charged particles in Pb-Pb collisions at $\sqrt{s_{\mathrm{NN}}} = 2.76$ TeV," *Phys. Lett. B*, vol. 762, pp. 376–388, 2016. DOI: 10.1016/j.physletb.2016.07.017. arXiv: 1605.02035 [nucl-ex].

[170] L. Du and U. Heinz, "(3+1)-dimensional dissipative relativistic fluid dynamics at non-zero net baryon density," *Comput. Phys. Commun.*, vol. 251, p. 107 090, 2020. DOI: 10.1016/j.cpc.2019.107090. arXiv: 1906.11181 [nucl-th].

Acknowledgments

This is the section I was most looking forward to writing. This PhD was a life-changing experience, and without the presence and support of all the following people I would have probably not reached the end of it.

First of all I would like to thank Silvia Masciocchi for offering me the possibility to work in this wonderful place that is GSI. I never would have expected to find here such a friendly and welcoming environment. Thank you for giving me the challenge of being a theorist among experimentalists, it has been a lot of fun and I have certainly learnt a lot.

Secondly, I would like to thank Stefan Floerchinger for following my work and always providing brilliant suggestions. Discussing with you is always enlightening, I hope we will continue to collaborate in the future.

Thank you to the whole ALICE@GSI/Heidelberg group for all the physics discussions, group retreats, Ugly Olympics, conferences, beers and songs around the fire. Anyone having the chance to be part of this group at some point is a very lucky person.

Among my GSI colleagues and friends, a special thanks (with related to-be-built statues) goes to Andrea Dubla. Thank you for this wonderful collaboration and friendship that we developed, you will never get rid of me.

A big big thank you goes to Eduardo Grossi. Thanks for sharing with me (a lot) of your time and all of your passion for physics (and for Julia, of course). You have a way of explaining things and valuing others' opinion (even if they're just a PhD student) that makes it always exciting to work with you.

To the whole phenomenology team: Thank you Andreas for sharing your PhD journey, dubious Mathematica licenses and German dishes' recipes with me. Thank you Rafet and Rossana for your enthusiasm (and patience), it's great working with you.

Before getting emotional, I would like to thank Paolo Nutini, Florence and The Machine, Bruce Springsteen and, what the hell, Taylor Swift for being a constant presence during my coding and writing times.

Now I will get emotional.

One (or five) of the reasons why this PhD has been such a beautiful experience is the people I've met down the road. Lucky for me, I've met these ones pretty early. T-square, thank you for being as sweet as your name says, and for all the amazing dinners, marathons and ripe watermelons we had together. Malu, thank you for all the sleepovers, wine nights, "I can't see properly", and avocado toasts in the morning. JJ, thank you for understanding the god-like nature of Florence and Paolo just like I do, and for dancing and screaming in the night with me. We are free. GG, thanks for not having an accent, for our climbing-coffee-beer-venting sessions, and for stealing a born-to-die rosemary plant with me. Luuk, thank you for compromising your physical shape, for German-Russian karaokes, for beers and benches and for being the best conference buddy and CHB I'll ever meet. As T-square said, when you are abroad your friends become your family. You guys truly did and for this I will never thank you enough.

Thank you to Carlo, Chiara, Cri and Marty, for being my Italian home in Darmstadt. I'm thankful for all of Carlo's dinners, for cutting the salad badly, for the Moscow Mules, for the Masterchef's season we've never finished and for the four fingers (not bad). Thanks for always being there for me.

Thank you to Martin and Hrishi, the best roommates I could ask for. Thank you Martin for cooking for us, Hrishi for watching (your sitting skills are remarkable), and for teaching me Internet words I have probably already forgotten.

Thank you Seb for being my spiritual guide through my first half-marathon, geteiltes Leid is indeed halbes Leid.

I would like to thank my Stuggi friends for being so nice (or not, see Steffi) and helping me to find my place in Stuttgart. That place has a name and it is 7Grad. In particular, I want to thank my climbing coaches, Henrik and Sida, for helping me realize one of the dreams I didn't know I'd ever have, i.e. closing a blue route.

Non posso scordarmi di ringraziare Dario, Ele, Fabri, La Rebi, Lalau, Mauri, Nic e Vincé, i Los Nueves. Il cammino che abbiamo condiviso mi ha aiutato in un modo che riesco a malapena a descrivere. Siete il mio Chilometro 0.

Un grazie alle persone di sempre. Alu e Carbo che mi aiutano ad affrontare La Vita. Bongi e Risso e il pianto al castello di Heidelberg. Eli e le notti d'Oriente. Vero e i suoi Spritz. Eli Garabs che prende un aereo per venirmi a trovare il weekend a Seattle. Andre, Jappi e Lollo che vedervi insieme è stato come ritornare a Fisica Beach per un giorno. Miss, Emis Villa e Giudibirra, il nostro trash manda avanti le mie giornate.

Un grazie infinito va a mia mamma, mio papà e mio fratello. Grazie per avermi supportato

nella scelta di fare il dottorato anche se era molto lontano da casa. Grazie per aver sempre trovato il tempo di telefonarmi e di stare con me quando tornavo. Vi voglio bene.

Un grazie speciale va al mio Raffo. Dal gelo di Busnau alla cima della Tour Eiffel, in dieta o in carbonara, grazie per esserci sempre.